Photonuclear reaction data measurements and interpretation

Toshiyuki Shizuma

Japan Atomic Energy Agency

1.1. Introduction; Photonuclear Reaction

- Absorption of photons (γ) by atomic nuclei and subsequent ejection of photons (γ'), protons (p), neutrons (n), or heavier particles from nuclei
- Different threshold energy for each particle emission
- Below the particle separation energy, elastic (γ,γ) and inelastic (γ,γ') photon scatterings take place. Low level density → Sharp resonance
- With increasing the incident photon energy, the nucleus starts to emit a neutron and/or a proton, and the cross section gradually increases.

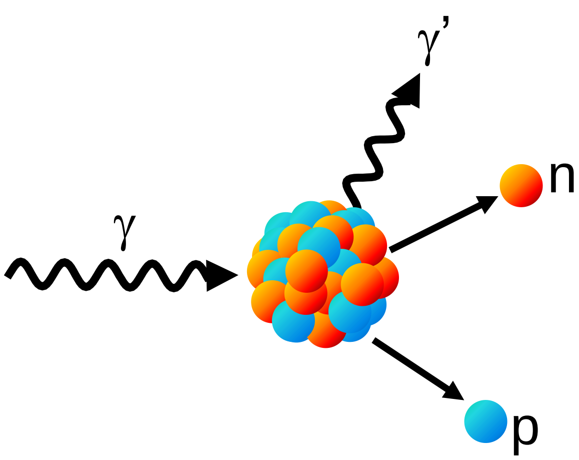

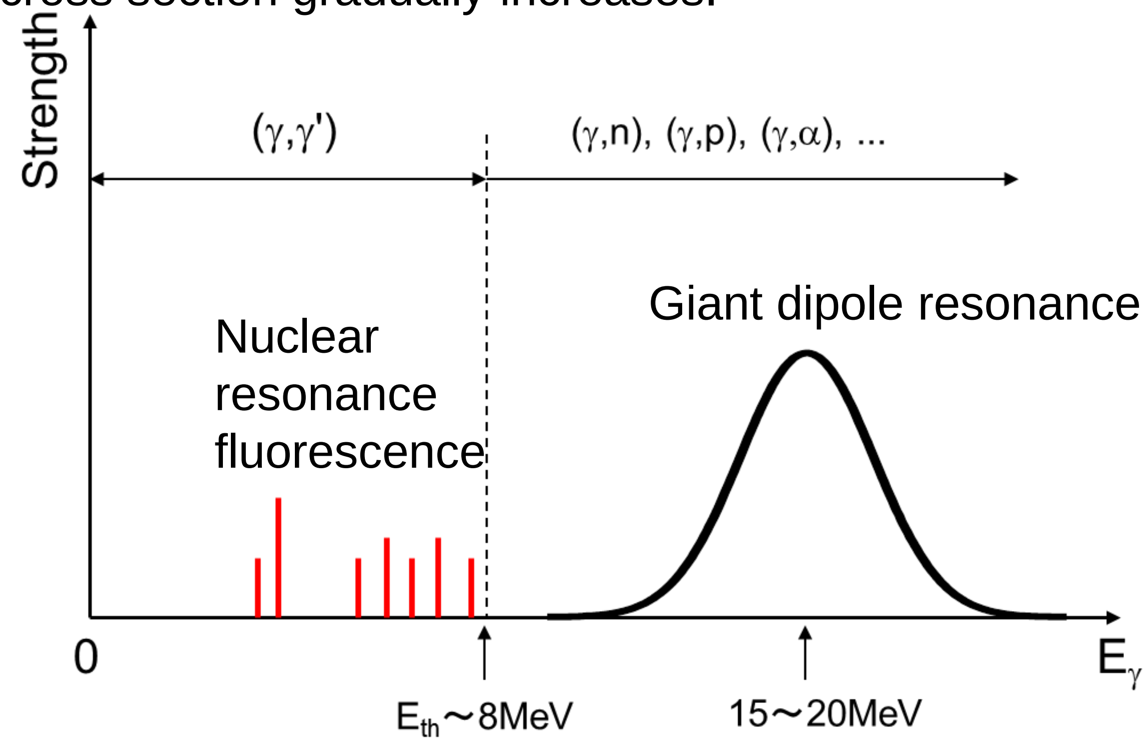

Photonuclear Reaction Data

Cross section, photoneutron yield, angular distribution data etc. for photo-induced reactions such as (γ,γ'), (γ,n), $(\gamma,2n)$,$\cdots$, (γ,p),$\cdots$, (γ,α),$\cdots$, (γ,F) etc.

Cross sections of each reaction

$$\sigma(\gamma,n),\ \sigma(\gamma,2n),\cdots,\ \sigma(\gamma,p),\cdots,\ \sigma(\gamma,\alpha),\cdots,\ \sigma(\gamma,F)$$

Total photoneutron cross section: Neutron emission channels

$$\sigma(\gamma,sn)=\sigma(\gamma,n)+\sigma(\gamma,np)+\sigma(\gamma,n2p)+\cdots$$
$$+\sigma(\gamma,2n)+\sigma(\gamma,2np)+\cdots+\sigma(\gamma,3n)+\cdots+\sigma(\gamma,F)$$

Photoabsorption cross section

$$\sigma(\gamma,abs)=\sigma(\gamma,sn)+\sigma(\gamma,p)+\sigma(\gamma,2p)+\cdots$$
$$+\sigma(\gamma,d)+\sigma(\gamma,dp)+\cdots+\sigma(\gamma,\alpha)+\cdots$$

- Strong Coulomb force for heavy nuclei
  small σ for charged particle emission
  $\rightarrow \sigma(\gamma,abs)\approx\sigma(\gamma,sn)$
- Weak Coulomb force for light nuclei
  large σ for charged particle emission
  $\rightarrow \sigma(\gamma,abs)>\sigma(\gamma,sn)$

Photoneutron production cross section

$$\sigma(\gamma,xn)=\sigma(\gamma,n)+\sigma(\gamma,np)+\sigma(\gamma,n2p)+\cdots$$
$$+2\sigma(\gamma,2n)+2\sigma(\gamma,2np)+\cdots+3\sigma(\gamma,3n)+\cdots+\nu\sigma(\gamma,F)$$

ν: average multiplicity of photofission neutrons

Applications of Photonuclear Reaction Data

- Radiation shielding design and radiation transport analyses
- Calculations of absorbed dose in the human body during radiotherapy
- Physics and technology of fission and fusion reactors
- Activation analysis, safeguards and inspection technologies
- Nuclear waste transmutation
- Nuclear Astrophysics

Handbook on photonuclear data for applications

IAEA-TECDOC 1178 (2000)

1.2. Photon Sources

In the past photonuclear reaction measurements, several kinds of photon sources were used, particularly for systematic studies on giant dipole resonance.

I. Discrete γ rays produced by thermal neutron capture
II. Bremsstrahlung radiation
III. Positron annihilation in flight
IV. Bremsstrahlung tagged photon

I. Discrete γ-Rays from Thermal Neutron Capture

Pennsylvania State University

Neutron source: 200 kW, pool-type reactor

Source targets: Al, Cu, Cl, N, Ni, Cr, Fe, Pb, S, Ti, Mg, Zn, etc. with weight of a few kg

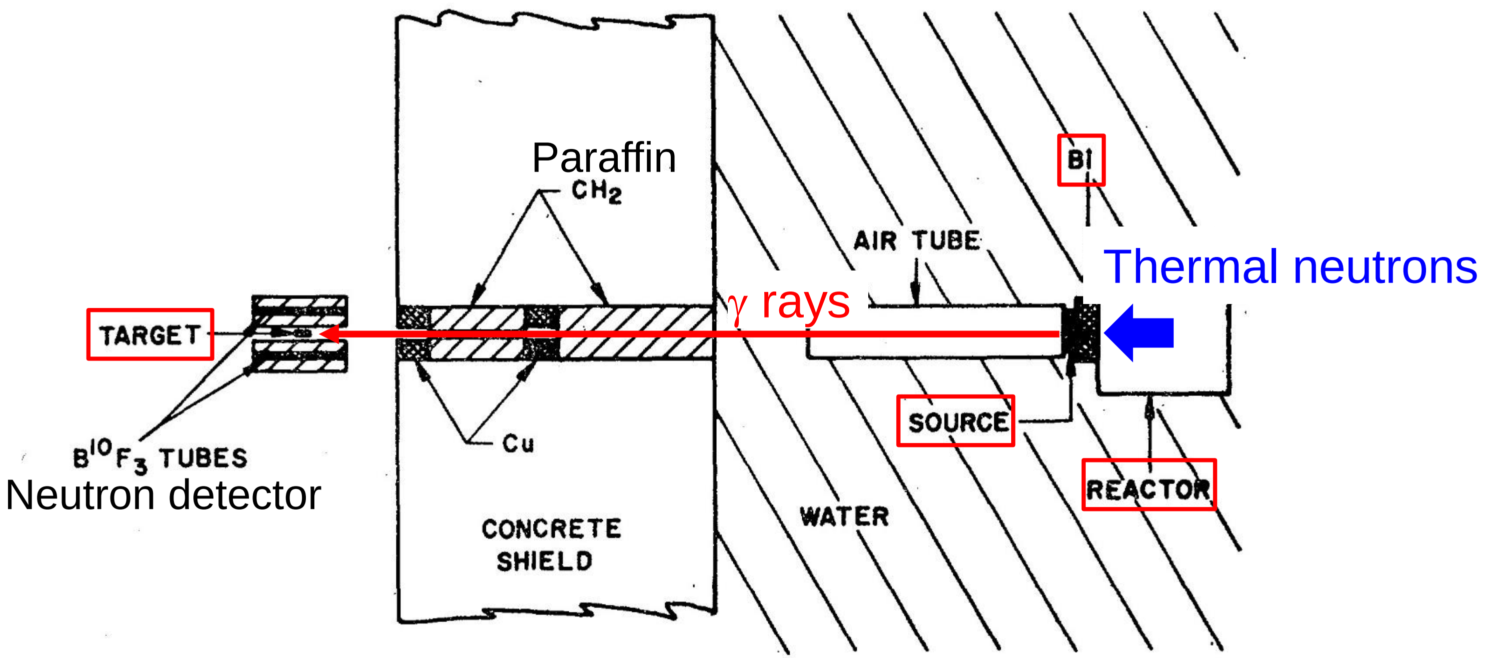

FIG. 1. Neutron counter and source arrangement.

Green and Donahue, PR 135, B701 (1964)

γ-Ray Energy and Intensity

TABLE I. Measured gamma-ray intensities.

Source	Energy[a] (MeV)	Intensity $\times 10^{-4}$ (γ rays/cm²-sec)
Aluminum	7.72	8.1 ±0.7
Copper	7.91	14.0 ±1.4
	7.63	6.4 ±0.6
Chlorine	8.56	2.3 ±0.3
	7.77	6.0 ±0.7
	7.42	6.9 ±0.8
Nitrogen	10.83	0.49±0.03
	8.31	0.10±0.03
Nickel	9.00	19.8 ±2.1
	8.53	9.1 ±0.9
Chromium	9.72	2.5 ±0.4
	8.88	6.2 ±0.9
Iron	7.64	22.0 ±2.8
	9.30	1.9 ±0.2
	6.03+5.92	11.3 ±1.5
Lead	7.38	1.9 ±0.3
Sulphur	5.43	10.2 ±1.4
	8.64	0.6 ±0.1
	7.78	0.8 ±0.2
Titanium	6.75	18.9 ±2.2
	6.41	12.5 ±1.5
	6.61[b]	33.7 ±2.7
Manganese	7.16[c]	19.0 ±1.7
Zinc	7.88	4.5 ±0.5

[a] Energies taken from Refs. 4 and 5.
[b] Weighted average of 6.75-, 6.55-, and 6.41-MeV γ rays.
[c] Weighted average of 7.26-, 7.15-, and 7.05-MeV γ rays.

E_γ: Discrete, 5.4-10.8 MeV

I_γ: 10^3-10^5 photons/cm^2/s

Relative intensity depends on the thermal neutron capture cross sections for each source target.

Green and Donahue, PR 135, B701 (1964)

Measured Cross Sections

TABLE II. Summary of measured cross sections (millibarns).

Source	Energy[a] (MeV)	Targets Ta^{181}	Li^7	Li^6	C^{13}	B^{10}
Aluminum	7.72	4.1± 0.4	0.06 ±0.01	1.13±0.12	1.7 ±0.2	...
Copper	7.91	10.8±1.0	0.07 ±0.01	1.1 ±0.2	0.97±0.13	...
Chlorine	8.56	29 ± 6	0.17 ±0.12	...	...	...
Nickel	9.00	44 ± 6	0.16 ±0.06	1.6 ±0.3	0.6 ±0.1	0.11±0.01
Nitrogen	10.83	121 ±12	1.07 ±0.25	...	4 ±2	0.9 ±0.2
Chromium	9.72	84 ±25	0.55 ±0.25	...	...	0.23±0.05
Iron	7.64	0.0± 0.9	0.079±0.014	1.3 ±0.2	0.23±0.05	...
Iron	9.30	...	...	...	...	0.09±0.03
Lead	7.38	...	0.068±0.035	1.2 ±0.2	0.3 ±0.3	...
Sulphur	5.43	...	...	0.42±0.07		
Sodium	6.41	...	...	0.6 ±0.1		
Titanium	6.75	...	...	1.3 ±0.2	...	...
Titanium	6.61[b]	...	...	...	0.32±0.04	...
Manganese	7.16[c]	...	...	0.9 ±0.1	0.4 ±0.1	
Zinc	7.88	...	...	1.0 ±0.2	1.2 ±0.2	

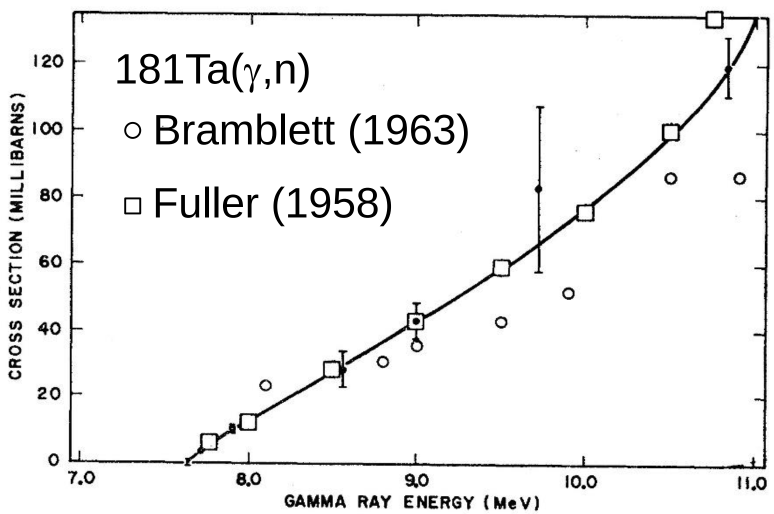

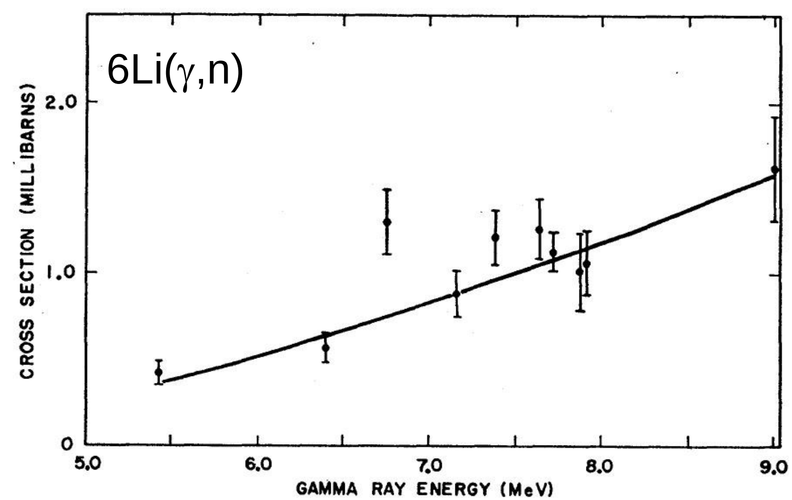

Green and Donahue, PR 135, B701 (1964)

II. Bremsstrahlung Radiation

- Electromagnetic radiation produced by the deceleration of a charged particle by a nucleus. Usually, electron accelerator is used.
- The electron loses kinetic energy according to the low of energy conservation.
- Strong intensity with continuous energy spectrum

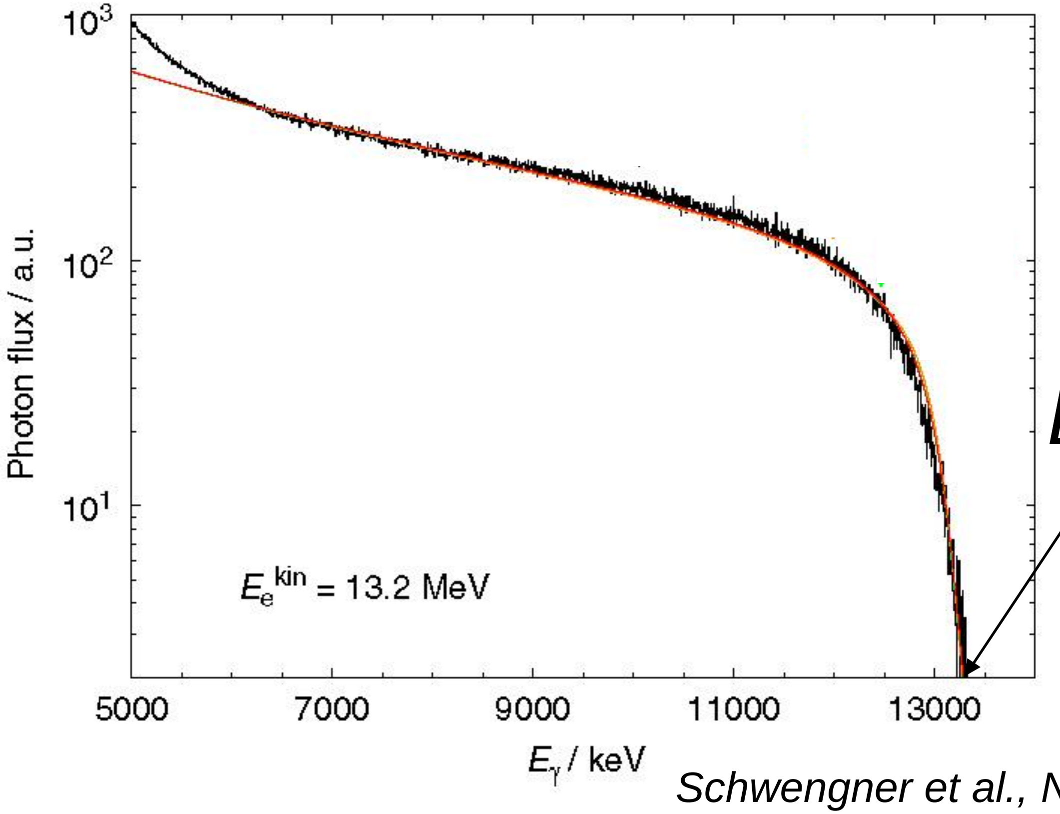

$$E_\gamma^{max} = E_e$$

Schwengner et al., NIM A555, 211 (2005)

Production of Bremsstrahlung Radiation

Bremsstrahlung facility at ELBE, Dresden, Germany

Superconducting electron linac

E_e<20 MeV

I<1 mA

At bremsstrahlung facilities, radiation shielding and collimator are important to minimize the production of neutrons and the scattering of photons in the measurement room.

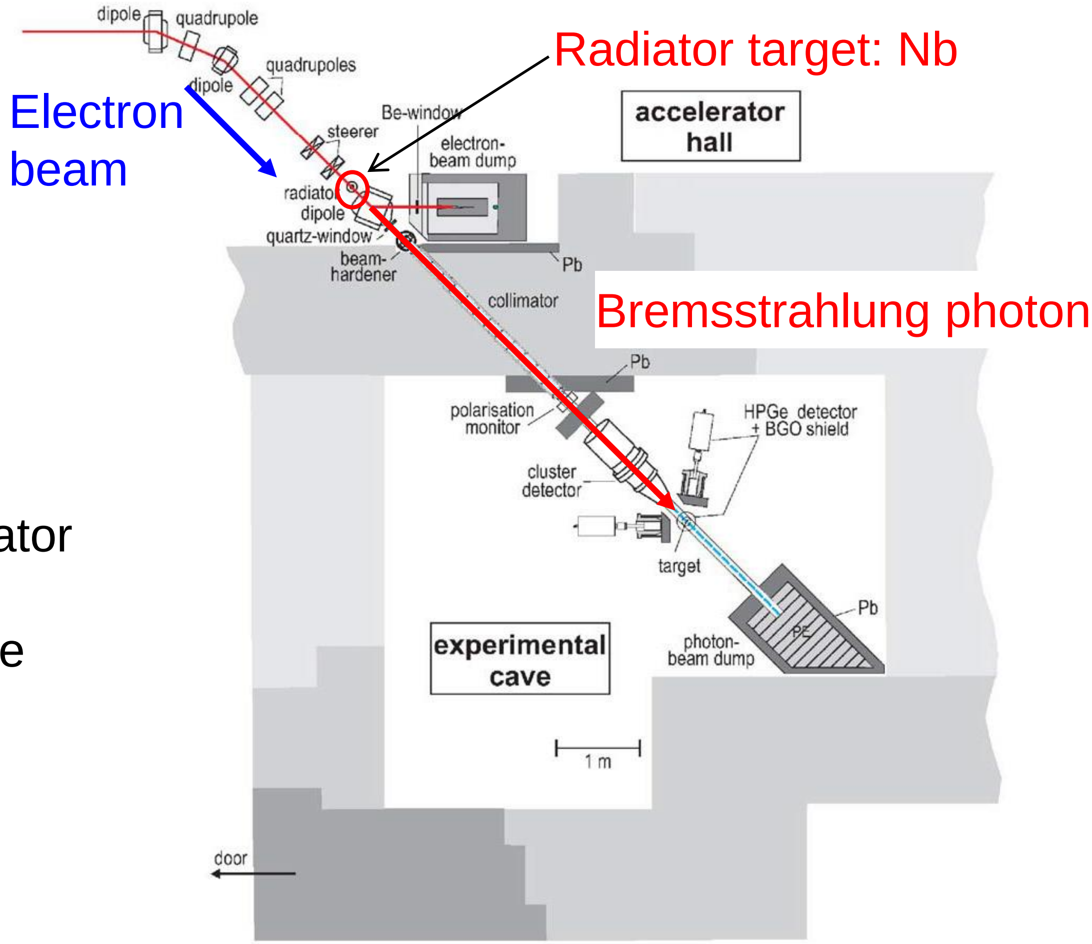

Schwengner et al., NIM A555, 211 (2005)

Photonuclear Reaction Yield

Bremsstrahlung radiation has a contentious energy spectrum.
$\rightarrow$ Photonuclear reaction yield is a folding of the cross section and the bremsstrahlung photon spectrum over the photon energy.

$$Y(E_0) = NR \int_{S_n}^{E_0} \sigma(E_\gamma) K(E_0, E_\gamma) \frac{dE_\gamma}{E_\gamma}$$

S_n: threshold energy, E_0: electron beam energy, E_γ: photon energy,
σ: photonuclear cross section, $K(E_0, E_\gamma)$: bremsstrahlung intensity spectrum

Cross section σ can be obtained by unfolding the yield curves measured in small increments of the electron energy.

The unfolding process requires;
1) accurate knowledge of the bremsstrahlung spectra for all electron energies,
2) stability in the accelerator parameters and large counting statistics,

because it includes the subtraction of the cross section yields measured at different electron energies.

Photonuclear Reaction Data

Majority of the photonuclear data measured with bremsstrahlung photons have been obtained at the Moscow State University, Russia and the University of Melbourne, Australia, etc.

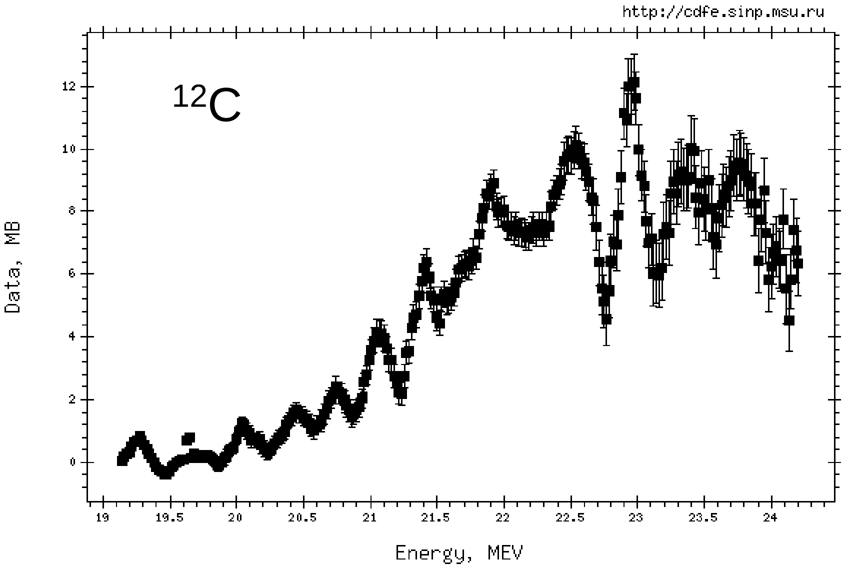

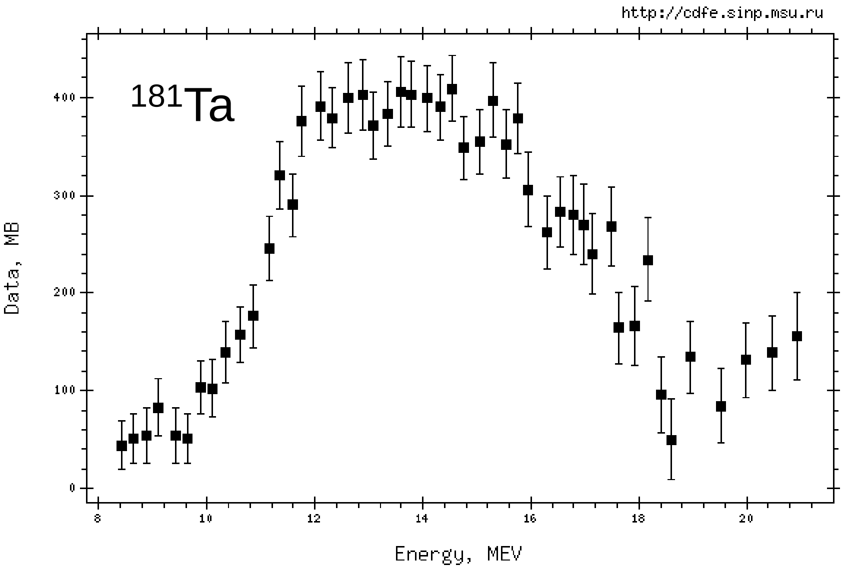

III. Positron Annihilation in Flight

- Quasi monoenergetic photon beam with variable energy
- Photonuclear cross section can be obtained directly.

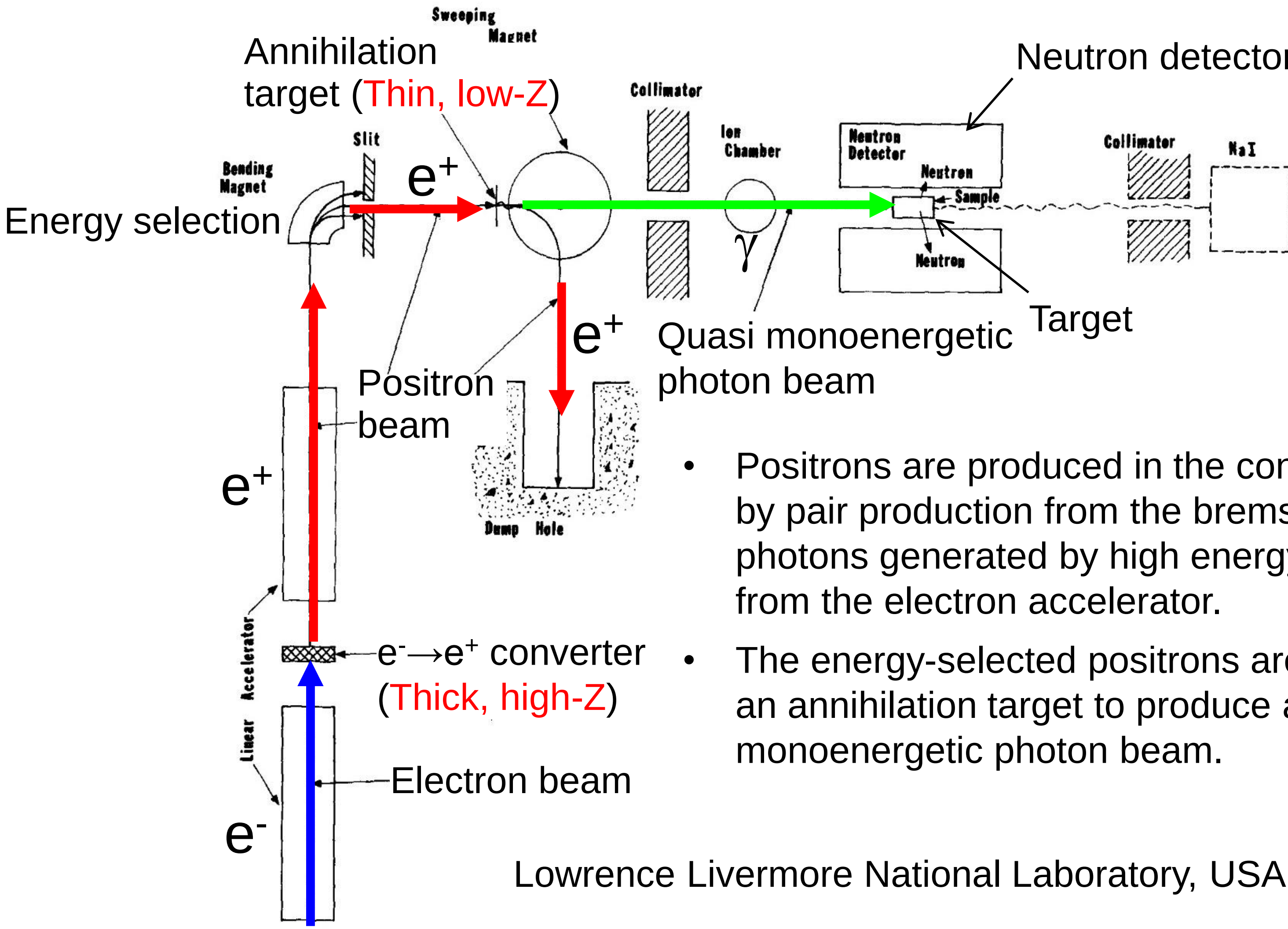

- Positrons are produced in the converter target by pair production from the bremsstrahlung photons generated by high energy electrons from the electron accelerator.
- The energy-selected positrons are used to hit an annihilation target to produce a quasi monoenergetic photon beam.

Lowrence Livermore National Laboratory, USA

Photon Facility at Saclay

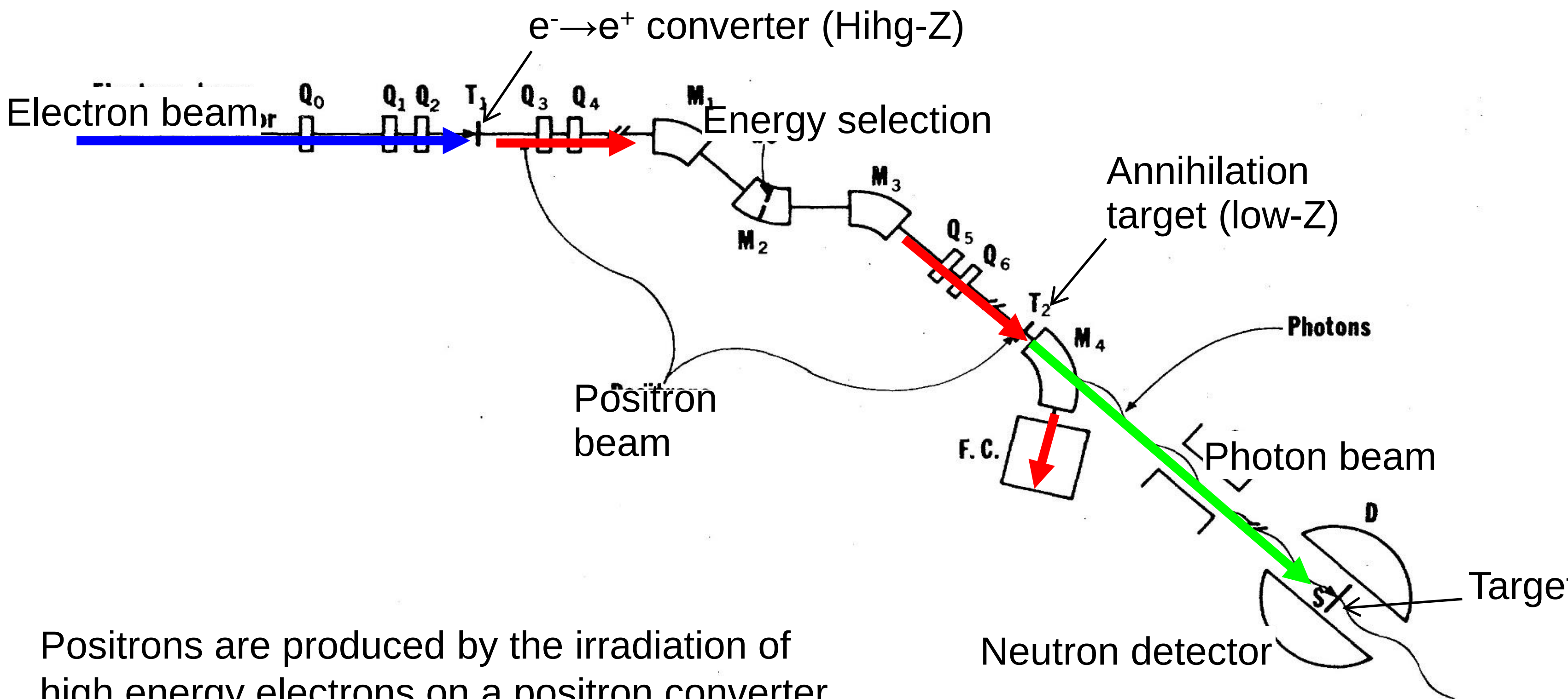

- Positrons are produced by the irradiation of high energy electrons on a positron converter target.
- The positron energy is selected by three dipole magnets.
- The energy selected positrons are used to bombard an annihilation target to produce a quasi monoenergetic photon beam.

Saclay, France

Photon Spectrum

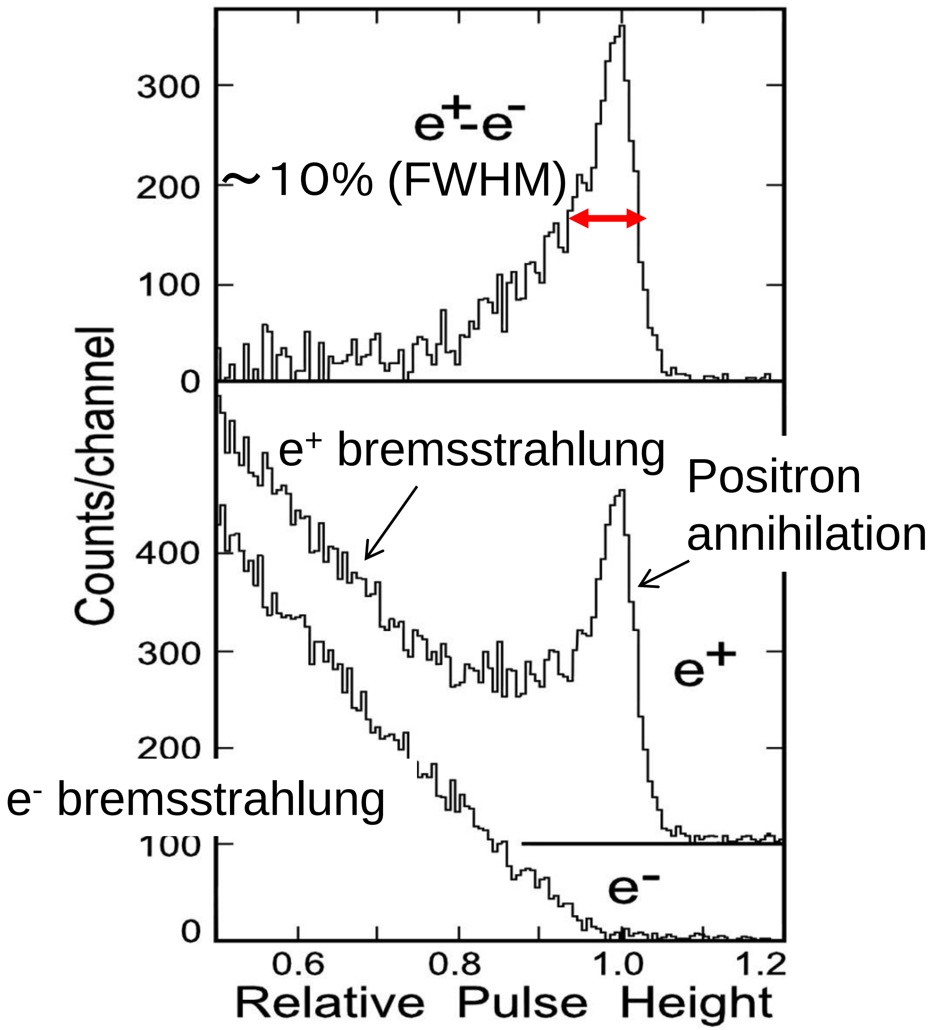

- Positron annihilation spectrum has two component: quasi mono-energetic and contentious energy.
- Measured cross section includes the contribution from the positron annihilation and e+ bremsstrahlung.
- The contribution from the e+ bremsstrahlung can be removed subtraction of the cross section obtained by the e^- bremsstrahlung photon.
- Energy spectrum of the positron annihilation component is obtained by subtraction of e- bremsstrahlung spectrum from the positron annihilation + e+ bremsstrahlung spectrum.

Photoneutron Data

A lot of the photoneutron data have been obtained by using quasi monoenergetic photon beam from positron annihilation in flight at LLNL, USA and Saclay, France during 1960s-1980s.

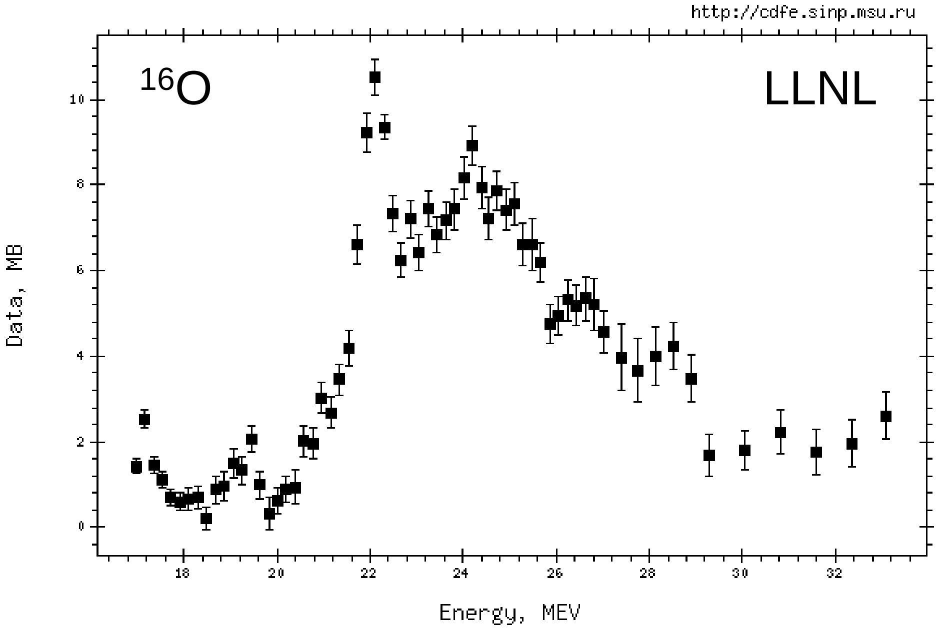

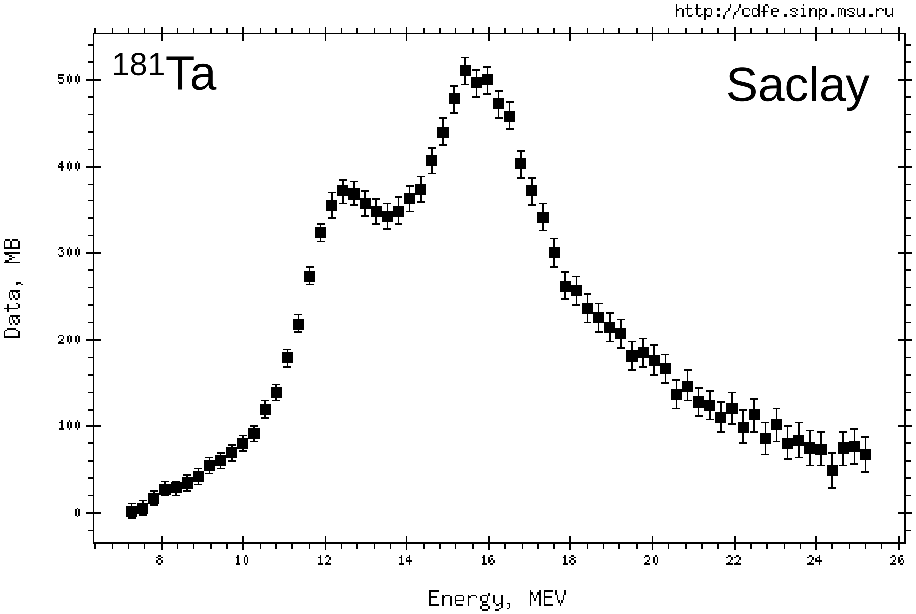

IV. Bremsstrahlung Tagged Photon

University of Illinois, USA

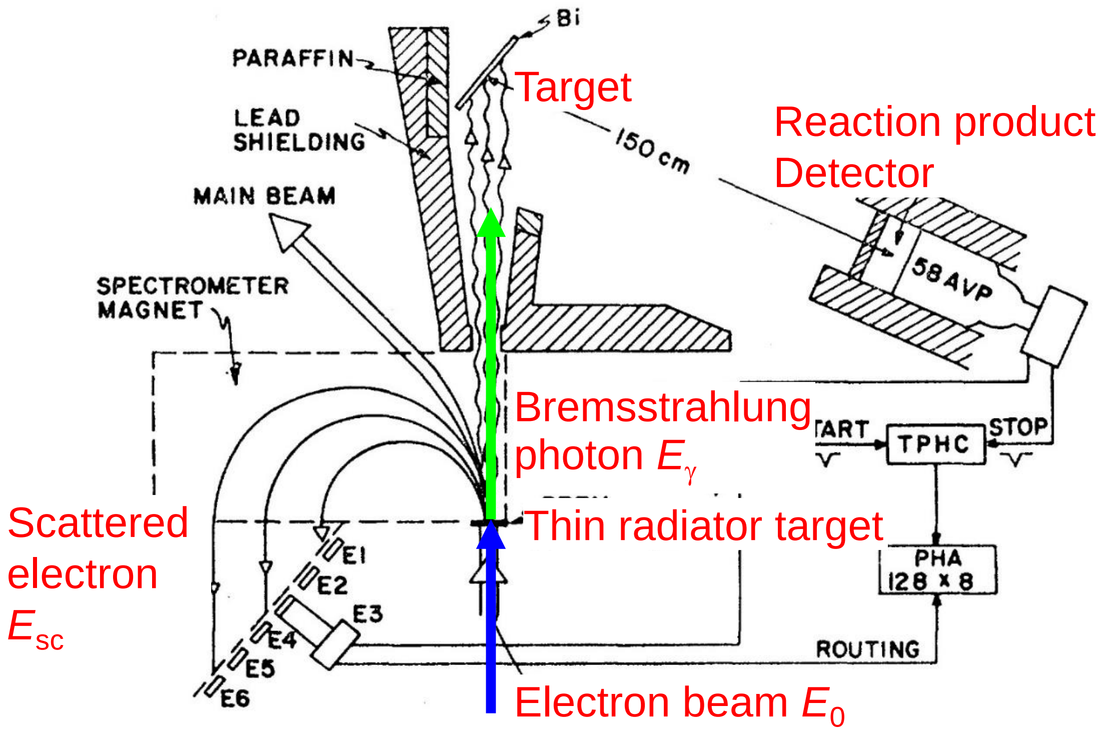

- Bremsstrahlung photons are produced in thin radiator by an electron beam.
- Electrons passing through the radiator are deflected by spectrometer magnet,
- and measured with detectors placed on the focal plane of the spectrometer.
- Energy resolution of photons depends on the spectrometer optics and the spatial distribution of the electron detector.

Photon energy: $E_\gamma = E_0 - E_{sc}$

Time coincidence between the scattered electron signal and a signal from the nuclear reaction product detector identifies that the reaction was produced by a photon with energy of E_γ.

Photonuclear Reaction Data

Photoneutron cross section

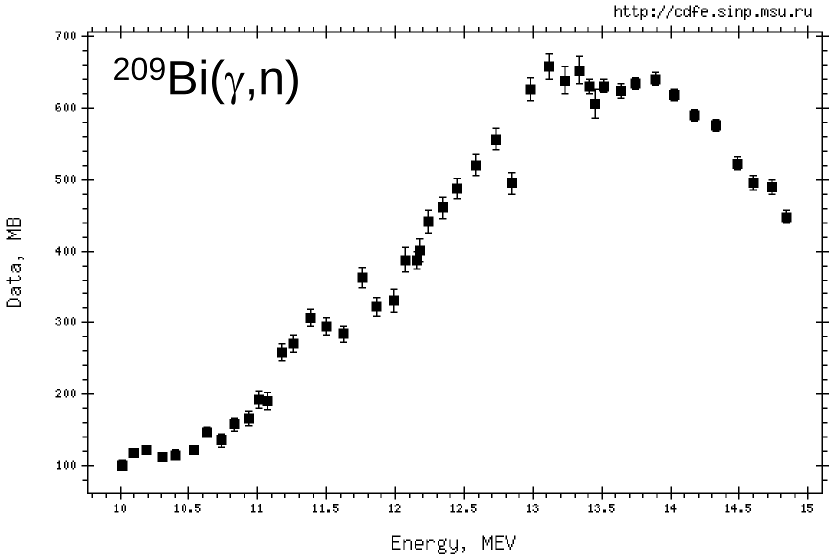

Neutron time-of-flight spectrum

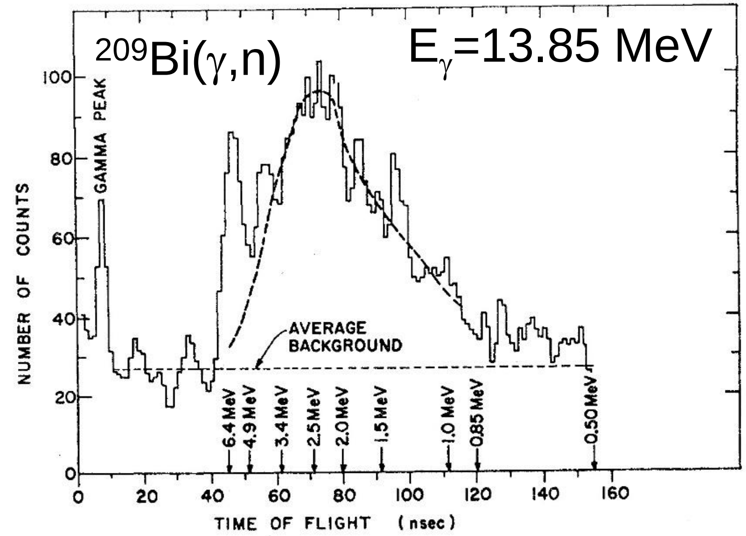

Both the incident photon energy and the emitted neuron energy can be measured simultaneously by this method.

1.3. Properties of Giant Dipole Resonance

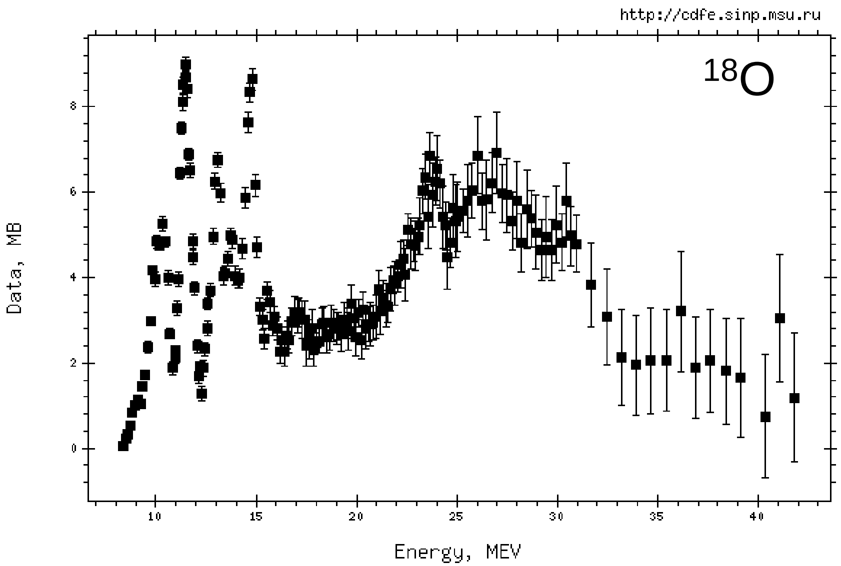

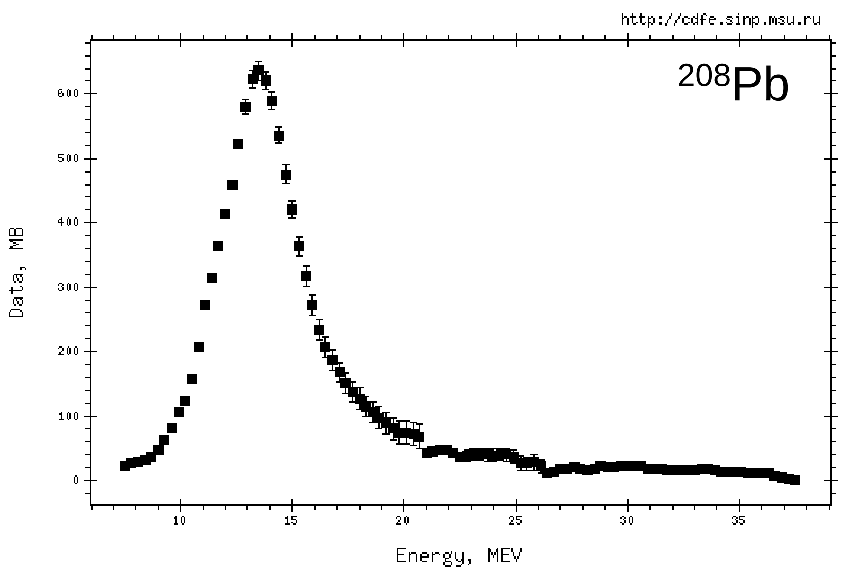

- Giant dipole resonances are systematically observed at 20-25 MeV for light nuclei and around 15 MeV for heavy nuclei.
- Collective vibration in which the bulk of protons move against the bulk of neutrons produces the electric dipole field of photons.

Goldhaber and Teller (1948)

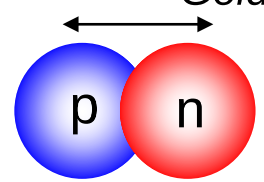

- Strongly fragmented over a wide energy range for light nuclei, due to low level density
- One or two broad peak for heavy nuclei, reflecting the gross feature of a nucleus

GDR in Deformed Nuclei

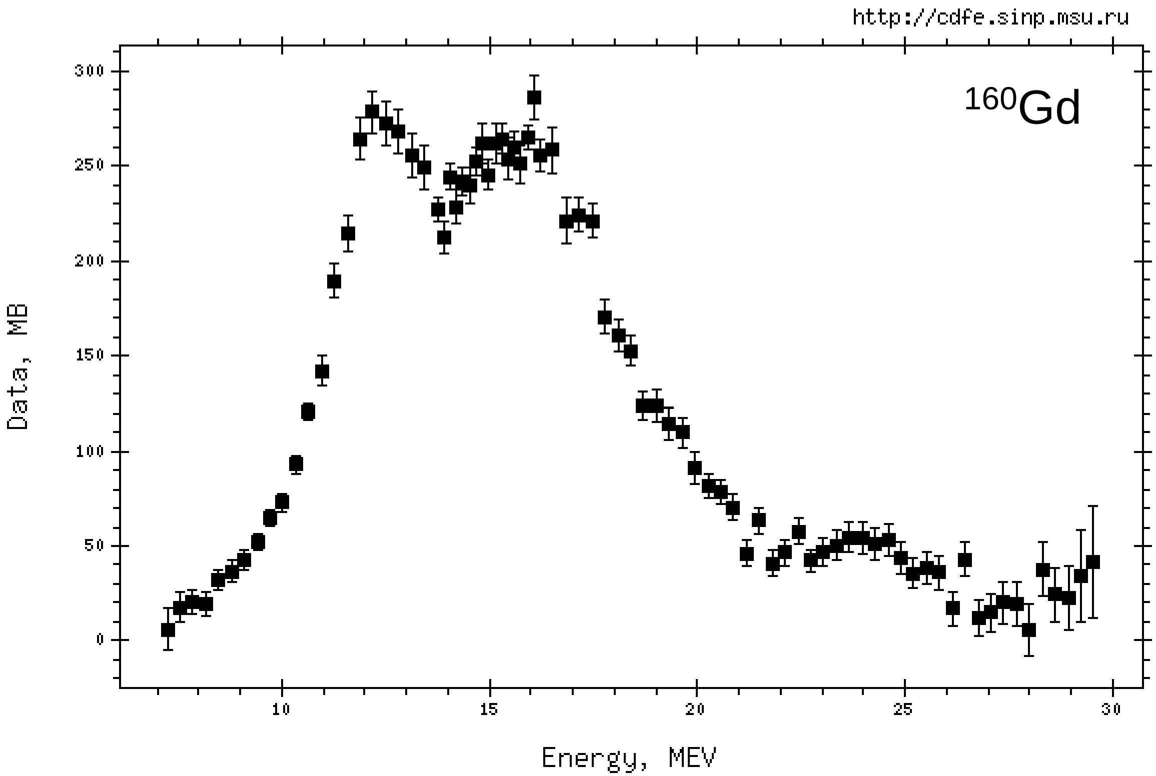

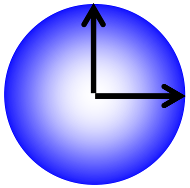

Spherical nuclei

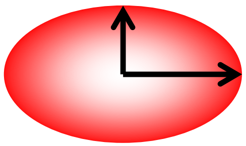

Deformed nuclei

- Strength distribution is split into two components for deformed nuclei.
- The lower and higher resonances correspond to an oscillation of neutrons versus protons along the long axis and the short axis, respectively.

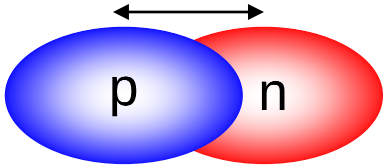

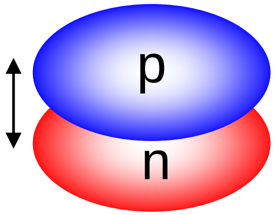

Lorentzian Parameters

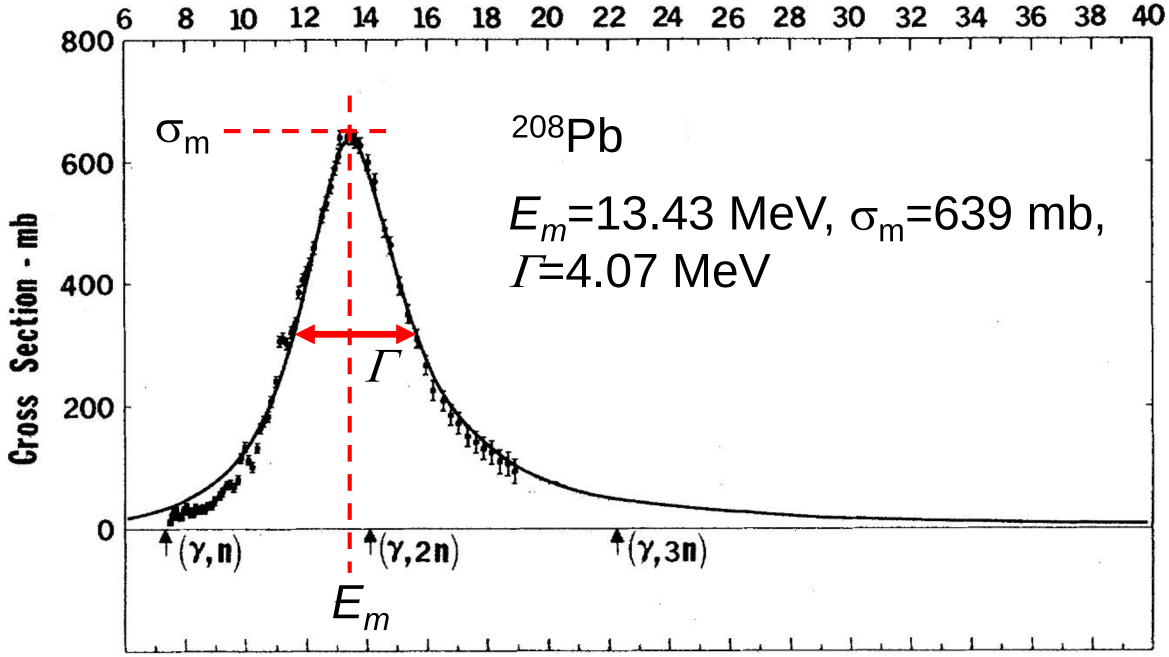

Lorentz function $$\sigma(E) = \frac{\sigma_m}{1 + [(E^2 - E_m{}^2)^2/E^2\Gamma^2]},$$

E_m: Peak energy, σ_m: Peak cross section, Γ: Resonance width in FWHM

GDR parameters are tabulated in literatures such as "Atlas of photoneutron cross sections" by Dietrich and Berman (1998).

Mass Dependence of GDR Energy

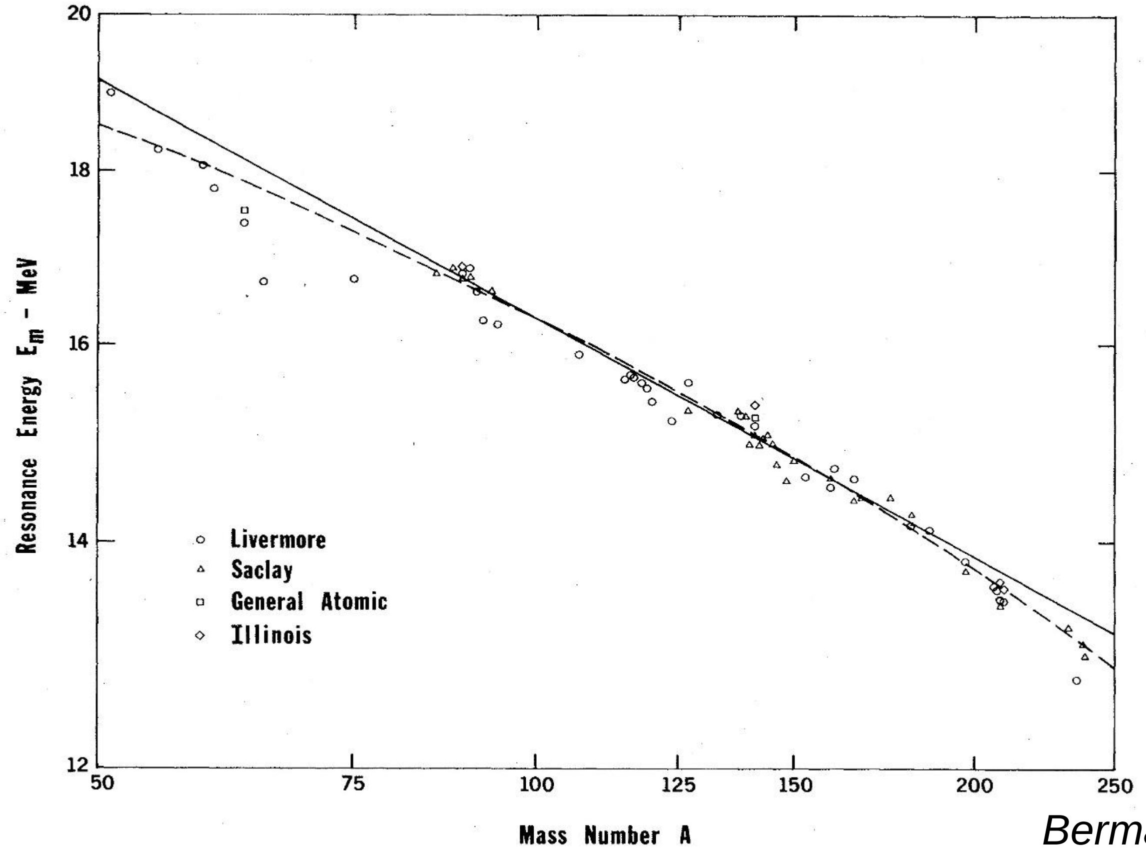

FIG. 45. The giant-resonance energy derived from the Lorentz-curve fits plotted versus mass number on a log–log scale. The solid line is the best two-parameter fit to the data of the form $E_m = c_1 A^{-1/c_2}$, from which $c_1 = 47.9$ MeV and $c_2 = 4.27$; the dashed line is the best three-parameter fit of the form $E_m = c_5 A^{1/3}(1 - e^{-A/A_0}) + c_6 A^{-1/6} e^{-A/A_0}$, from which $c_5 = 77.9$ MeV, $c_6 = 34.5$ MeV, and $A_0 = 238$.

Berman and Fultz, RMP 47, 713 (1975)

$$E_m = 31.2A^{-1/3} + 20.6A^{-1/6}\ \text{MeV}$$

Restoring force for displacement of the neutron and proton fluids is proportional to the nuclear radius ($A^{1/3}$) as well as the nuclear surface area ($A^{1/6}$).

Thomas-Reiche-Kuhn (TRK) E1 Sum Rule

Integrated photoabsorption cross section of electric dipole resonance

TRK sum rule $\int_0^\infty \sigma(E)\,dE = \frac{2\pi^2 e^2 \hbar}{Mc}\frac{NZ}{A} = 60\left(\frac{NZ}{A}\right)$ MeV·mb

Integrated total photoneutron cross section relative to the TRK sum rule

- TRK sum rule is not exhausted for nuclei with A<80; Cross section of charged particle emission such as (γ,p) has to be considered.
- The total photoneutron cross section exhausts the TRK sum rule for nuclei with A>100; Total photoneutron cross section is close to the TRK sum rule.

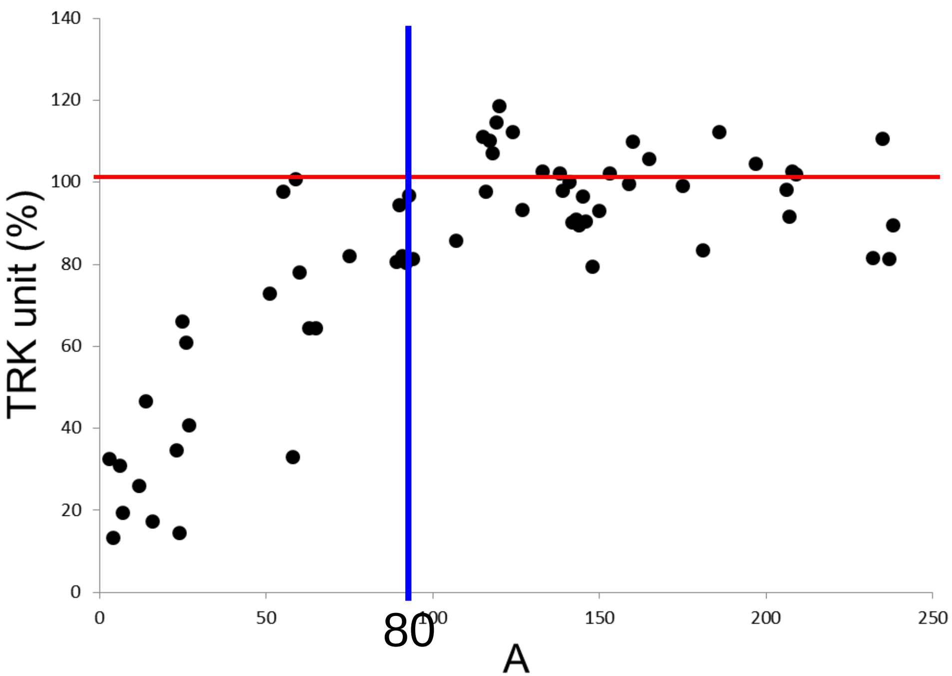

For heavier nuclei, contribution from meson exchange force should be included.

TRK sum rule $\rightarrow 60\left(\frac{NZ}{A}\right)(1+k)$, k =0.1-0.2

1.4. Compiled Photonuclear Reaction Data

Bibliographic data

- 10-th edition of the IAEA Bibliographical Series, V.I. Antonescu, Technical Report No. 10 (1964), references for both the theoretical and experimental works taken from the literatures in 1948-1963.
- Photonuclear Data Index 1955-1972, Photonuclear Data Index 1972-1982, E.G.Fuller, Report of the US National Bureau of Standards, experimental data tabulated for all nuclei that have been measured.
- Photonuclear Data Index 1976-1995, V.V. Varlamov, the Center for Photonuclear Experiments Data (CDFE) of the Institute of Nuclear Physics of the Moscow State University, includes a table of experimental photonuclear data from the results published in 1976-1995.
- Bibliographic Index to Photonuclear Reaction Data (1955-1992), T. Asami, Japan Atomic Energy Research Institute

Nuclear reaction database, EXFOR, Experimental Nuclear Reaction Data, which includes the data for reactions induced by neutrons, charged particles, and photons; maintained by international Network of Nuclear Data Centers, IAEA

https://www-nds.iaea.org/exfor/exfor.htm

Overviews of Photonuclear Reaction Data

- Atlas of photoneutron cross-sections obtained with monoenergetic photons, S.S. Dietrich and B.L. Berman, Atomic Data and Nuclear Data Tables 38, 199 (1988). Photonuclear data, GDR cross sections, Lorentzian parameters
- Photonuclear reaction cross-sections, Handbook on nuclear activation data, B. Forkman and R. Petersson, Technical Report Series No. 273 (1987), IAEA, data obtained by using bremsstrahlung and quasimonoenergetic photons
- Plots of the experimental and evaluated photoneutron cross-sections, A.I. Blokhin and S.M. Nasyrova, Technical Report 337 (1991), IAEA, using EXFOR
- Atlas of giant dipole resonance parameters and graphs of photonuclear reaction cross-sections, A.V. Varlamov, et al., Technical Report 394 (1999), IAEA, measured by using bremsstrahlung, positron annihilation in flight, tagged photon
- Handbook on photonuclear data for applications, Cross-sections and spectra, IAEA-TECDOC-1178 (2000)

Evaluated Photonuclear Data Libraries

Libraries	Published Year	Number of Nuclide
LA-150	1999	12
IAEA PDL	2000	164
KAERI rev 2	2003	143
JENDL/PD-2004	2004	68
ENDF/B-VII.1	2011	163（132 from KAERI）
TENDL-2014	2014	2629

Evaluation needs;

- Measured photonuclear reaction data
- Nuclear models describing photoabsorption, preequilibrium, compound, photofission
- Nuclear modeling code

JENDL Photonuclear Data Library

After JENDL/PD-2004

- Photonuclear data were newly measured.
- Several updates such as photonuclear reaction models, discrete level data, etc carried out.

The JAEA nuclear data evaluation group started to update the JENDL photonuclear data library to increase the reliability of evaluation as well as the number of nuclides included in the library.

JENDL/PD-2015

- Standard version; 181 nuclides (CCONE)
- Expanded version; 2674 nuclides (mostly Alice-F)

N.Iwamoto, JAEA

Calculation Code; CCONE

N.Iwamoto, JAEA

Nuclear reaction calculation code

Compound : Statistical model

- n,p,d,t,He3,α,γ emission
- Optical model (n,p,d,t,He3,α)
- Discrete level
  - RIPL-3 (2012)
- Gilbert-Cameron type level density
  - Constant temperature
  - Mengoni-Nakajima Fermi gas model
- Gamma strength function
  - E1 transition (MLO)
  - M1,E2 transitions (SLO)
- Quasideutron model

Preequilibrium : Two-component exciton model

+ gamma emission

Gamma energy=1~140MeV

Evaluation with CCONE (74 nuclides)

^{64,66,67,68,70}Zn, ^{70,72,73,74,76}Ge, ^{84,86,87,88}Sr, ^{90,91,92,94,96}Zr, ^{93}Nb, ^{92,94,96,98,100}Mo, ^{99}Tc, ^{105,106,107,108}Pd, ^{107,109}Ag, ^{112,114,116,117,118,119,120,122,124}Sn, ^{121,123}Sb, ^{124,126,128,130}Te, ^{127,129}I, ^{133}Cs, ^{141}Pr, ^{144,148,150,152,154}Sm, ^{152,154,156,158,160}Gd, ^{159}Tb, ^{165}Ho,^{181}Ta, ^{182,184,186}W, ^{197}Au, ^{206,207,208}Pb, ^{235,238}U, ^{237}Np

➔ Absorption cross section, production cross section, fission cross section, particle-gamma emission DDX

Evaluation for Zr-90

N.Iwamoto, JAEA

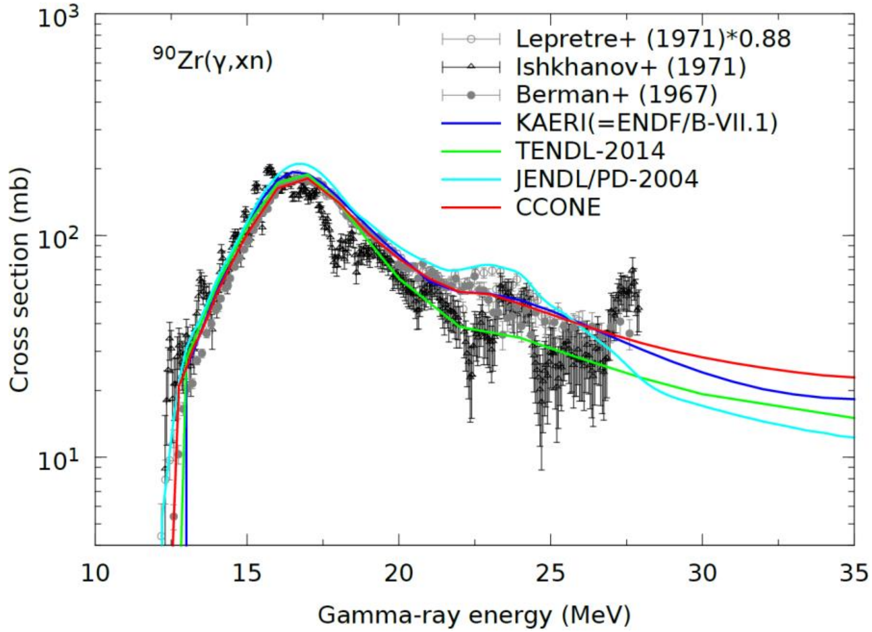

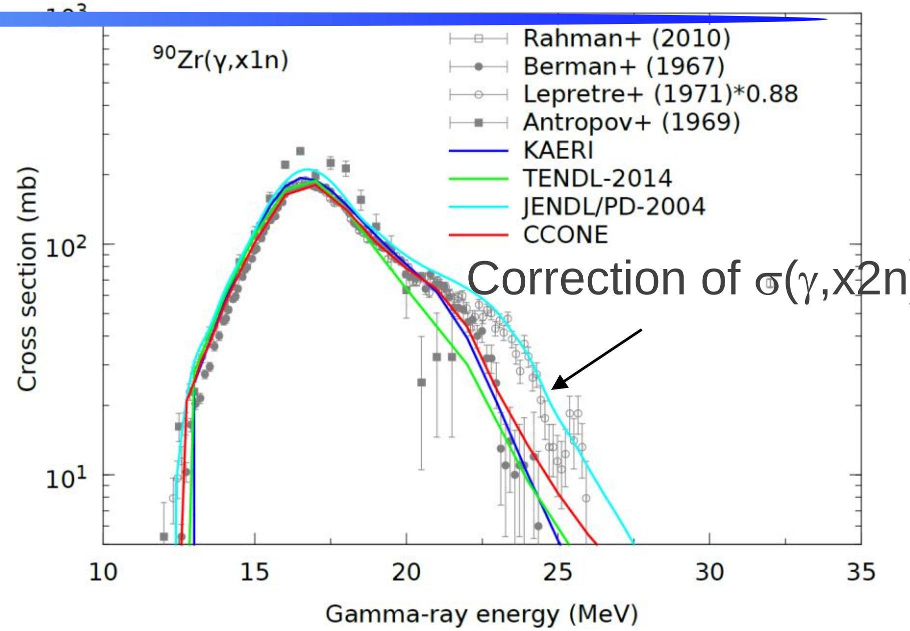

Berman, et al., PRC36,1286 (1987)

Saclay data *0.88

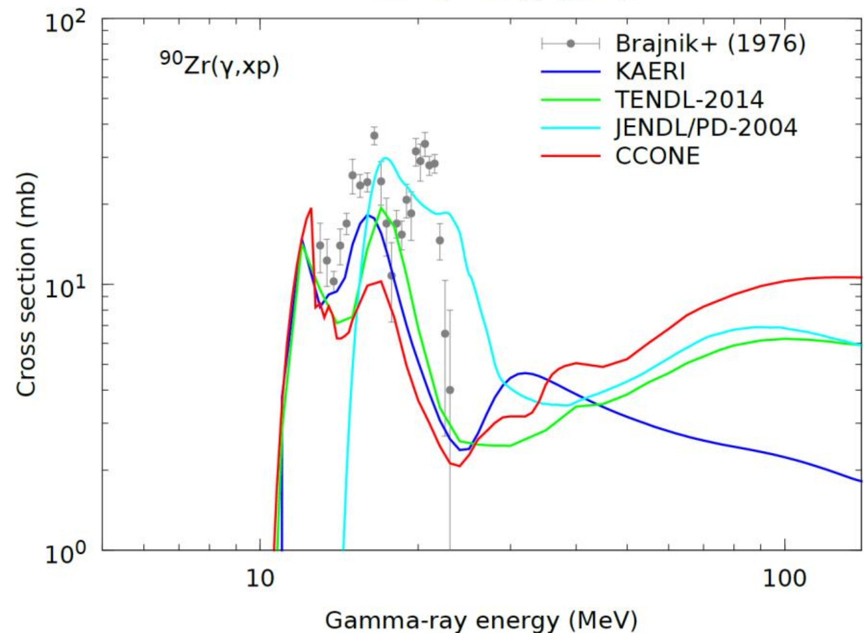

Evaluation for I-127

N.Iwamoto, JAEA

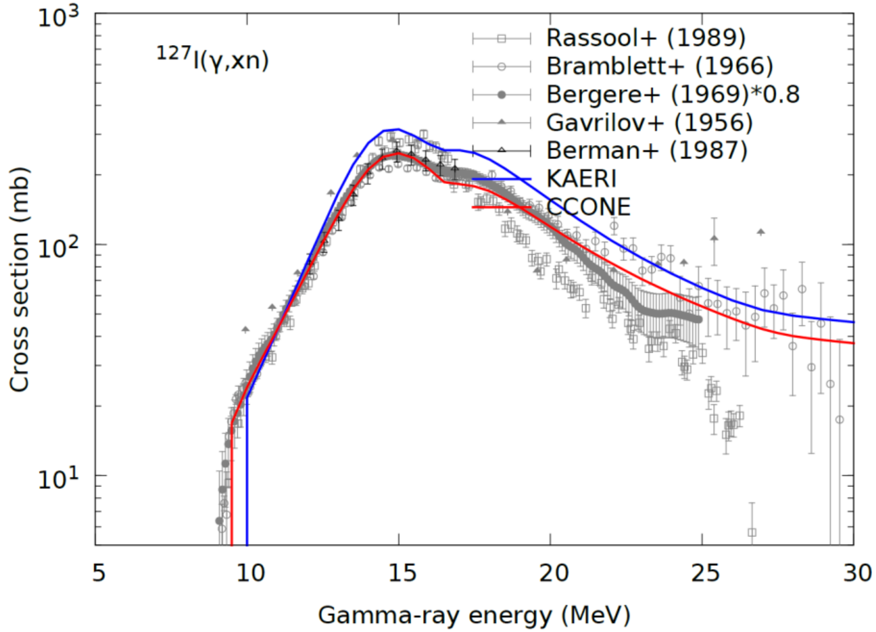

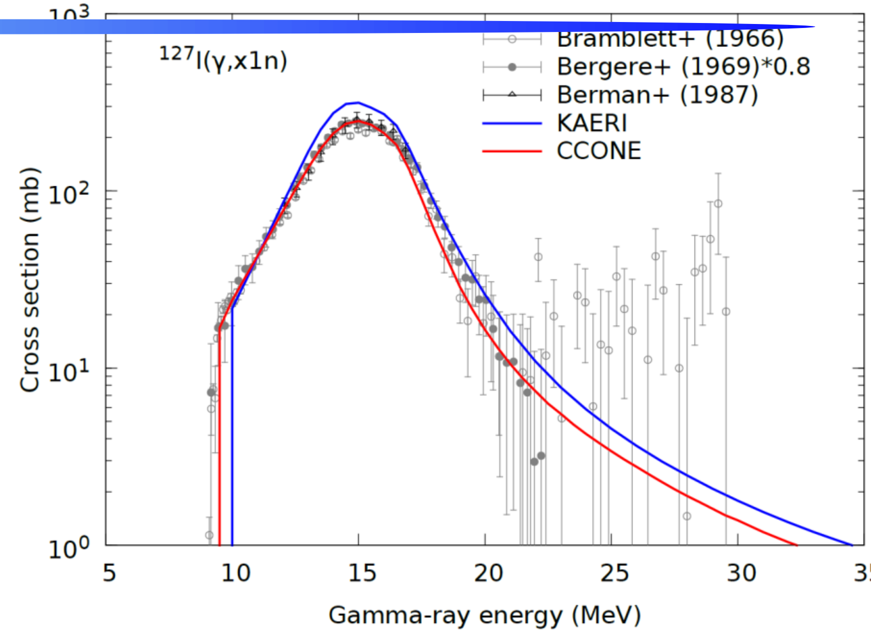

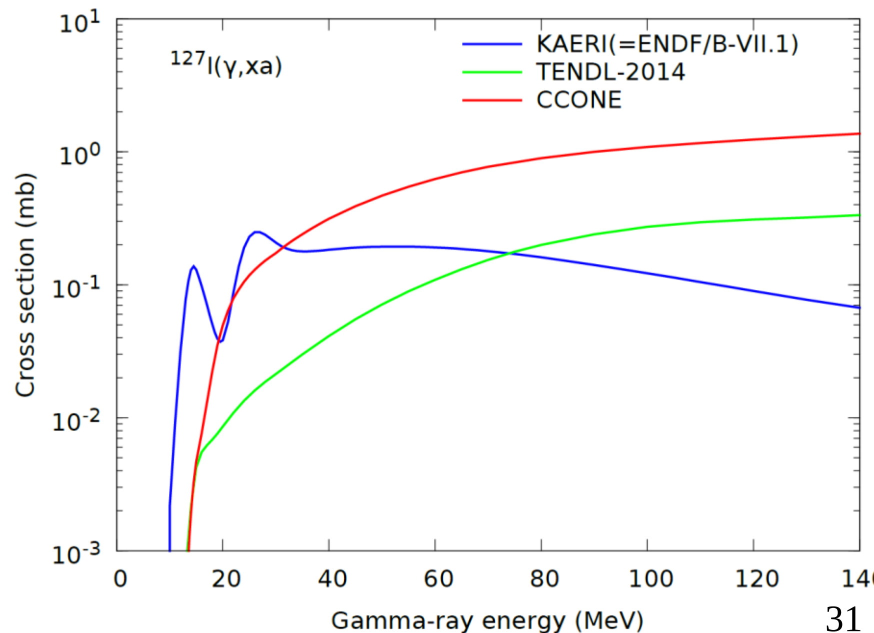

Berman, et al., PRC36,1286 (1987)

Saclay data *0.80

Evaluation for Sm-152

N.Iwamoto, JAEA

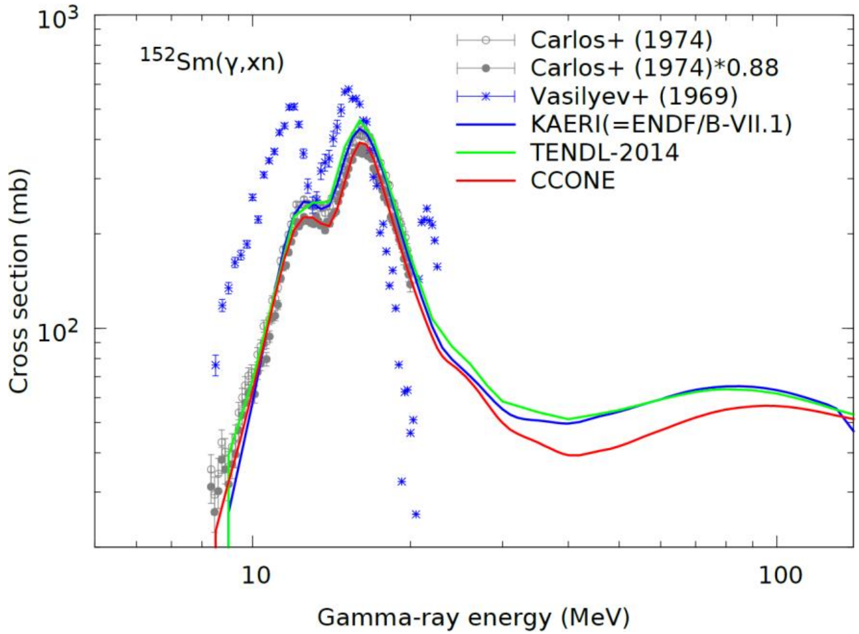

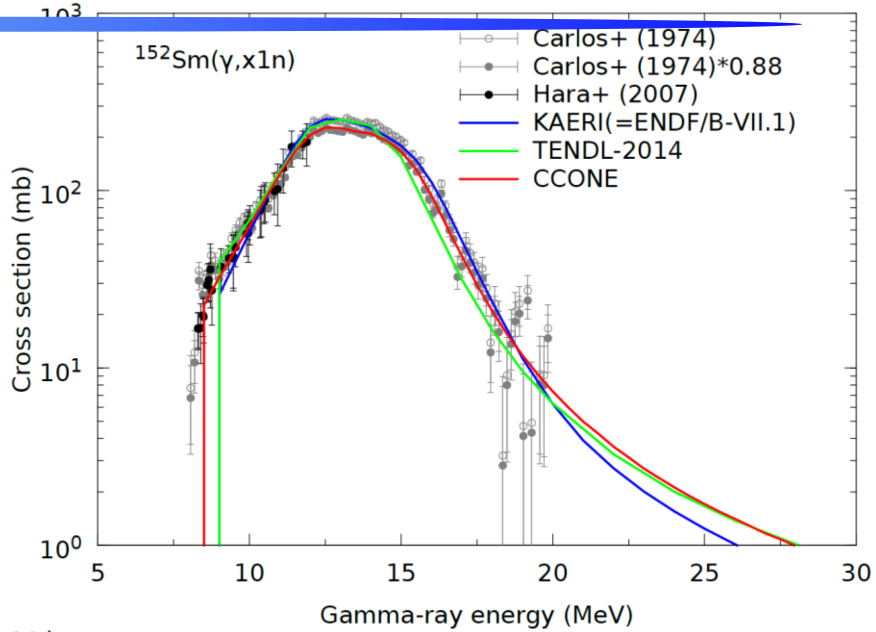

Berman, et al., PRC36,1286 (1987)

Saclay data *0.88

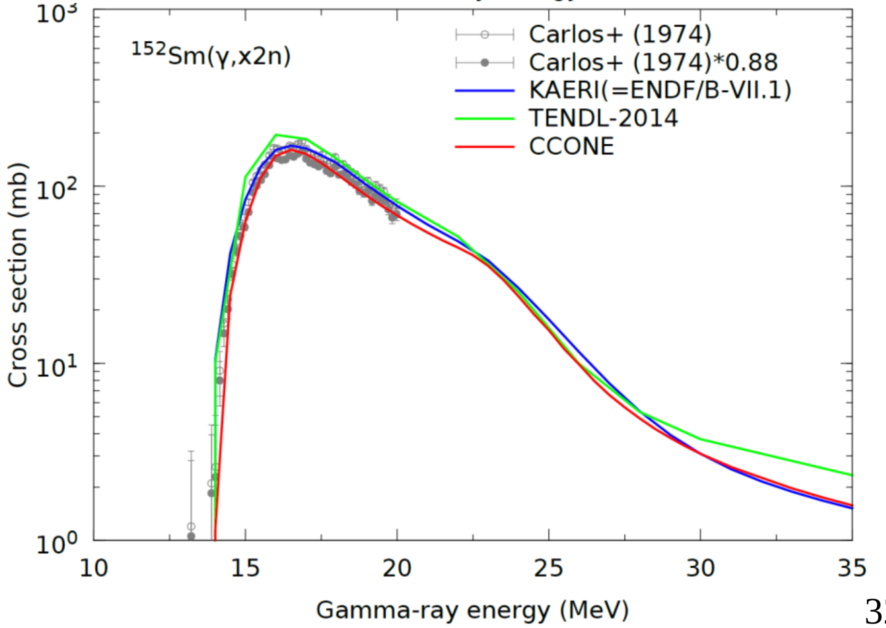

Evaluation for U-238

N.Iwamoto, JAEA

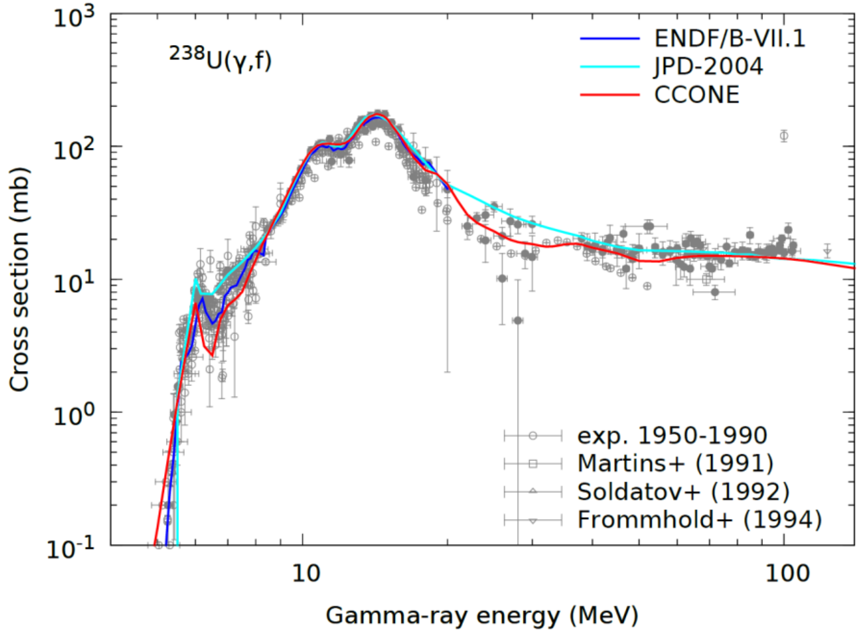

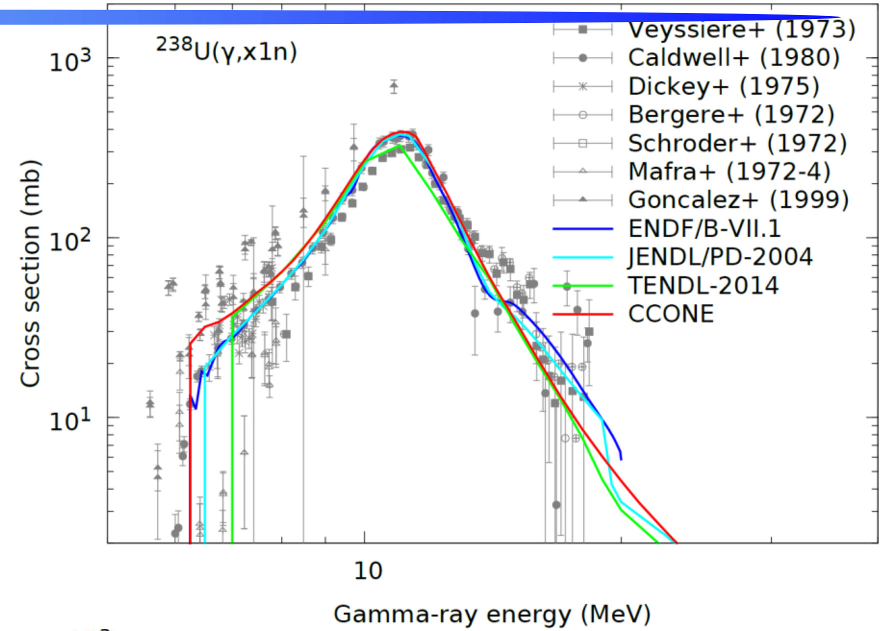

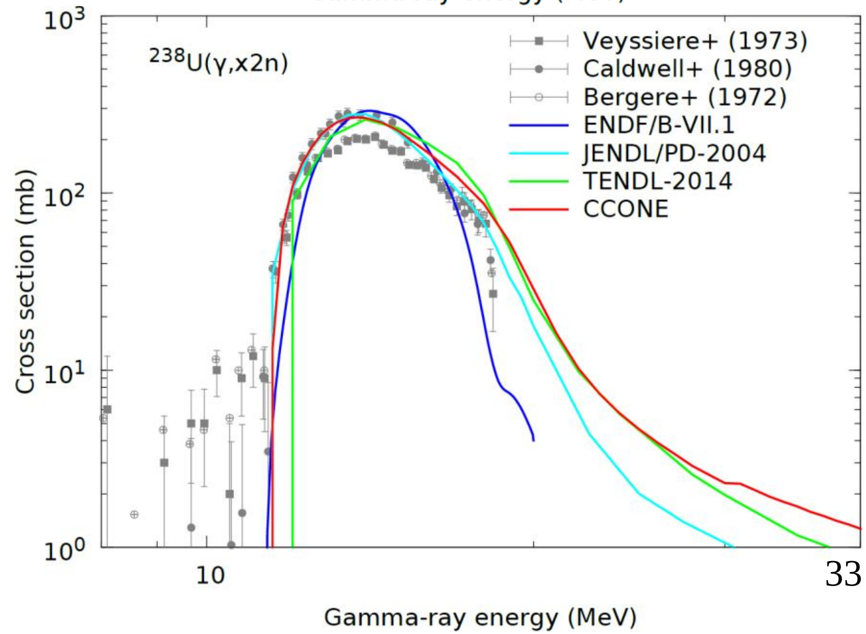

Discrepancy between the LLNL and Saclay Data

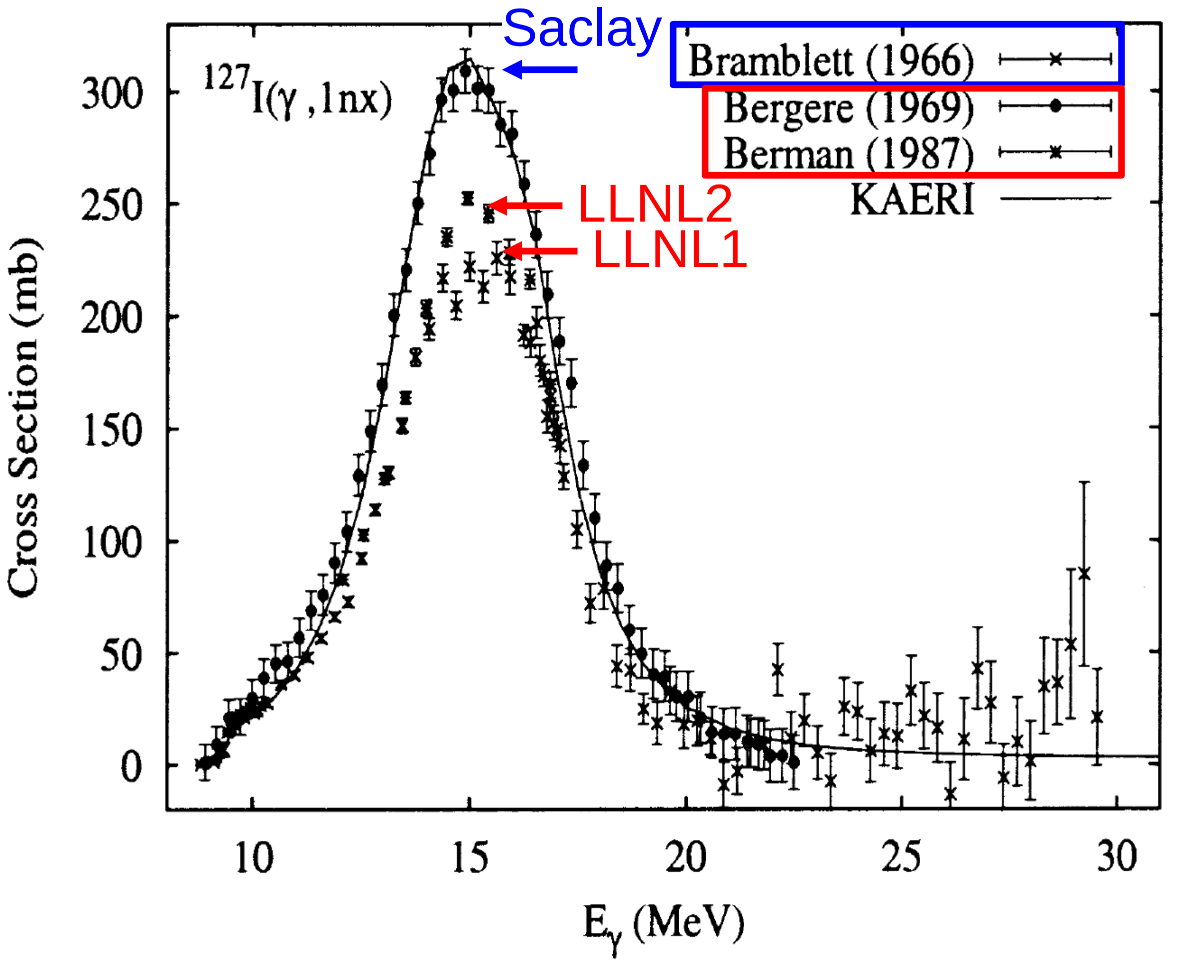

For I-127, LLNL data is 20% lower than Saclay data.

Photon flux, neutron detection efficiency, neutron-multiplicity counting, etc.

Berman et al., Phys. Rev. C36,1286(1987)

2.1. Laser Compton Scattering (LCS) γ Rays

Laser (Inverse) Compton scattering

- Quasi-monoenergetic photon beams are generated by Compton scattering between laser light and high energy electrons.
- When the photons collide with high energy electrons, the photons gain the energy from the electron kinetic energy.
- Scattered photons are linearly or circularly polarized.
- Photon energy can be tuned by changing the electron energy or the laser wave length

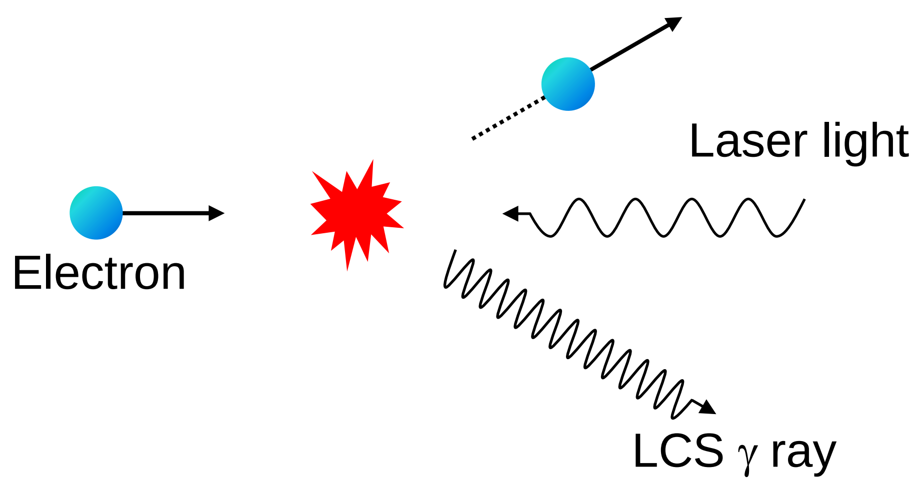

Energy of LCS Photons

$$E_\gamma = \frac{E_l\left(1-\beta\cos\theta_L\right)}{1-\beta\cos\theta + \frac{E_l\left\{1-\cos\left(\theta_L-\theta\right)\right\}}{E_e}}$$

E_l: Energy of laser photon
E_e: Kinetic energy of electron
β: Electron velocity /c
θ_L: Incident angle of laser photon
θ: Scattered angle of LCS photon

Head-on collision (θ_L=180°)

$$E_\gamma \approx \frac{4\gamma^2 E_l}{1+\left(\gamma\theta\right)^2 + 4\gamma E_l / mc^2}$$

$$\gamma = \frac{E_e}{mc^2}$$

Maximum energy at θ=0°

$$E_\gamma^{\max} \approx 4\gamma^2 E_l$$

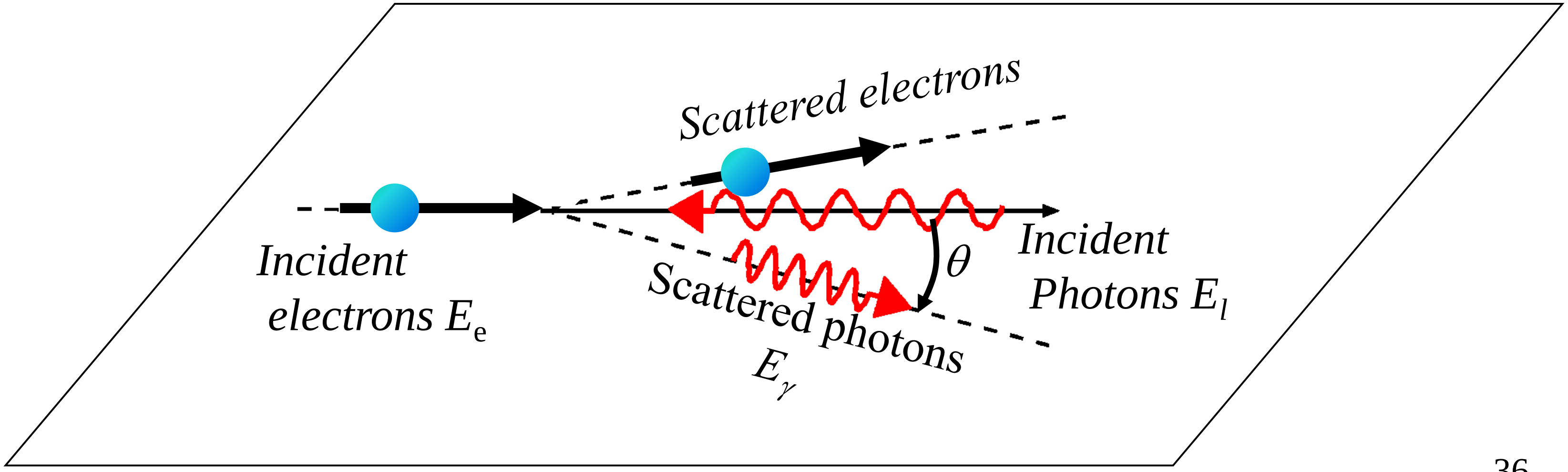

Strength Distribution of LCS Photons

The strength distribution of LCS photons can be calculated by Klein-Nishina formula.

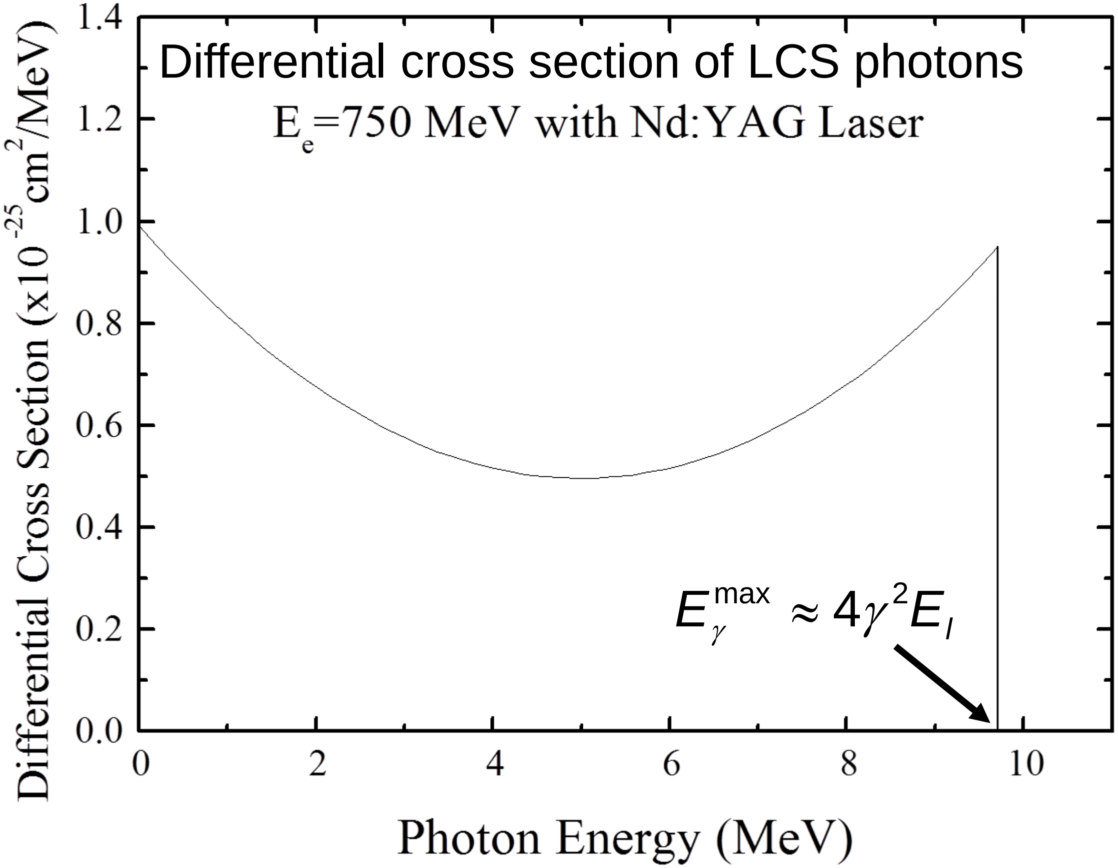

The strength has a maximum at the maximum photon energy and has a nearly symmetric shape.

Directivity of the LCS Photon Beam

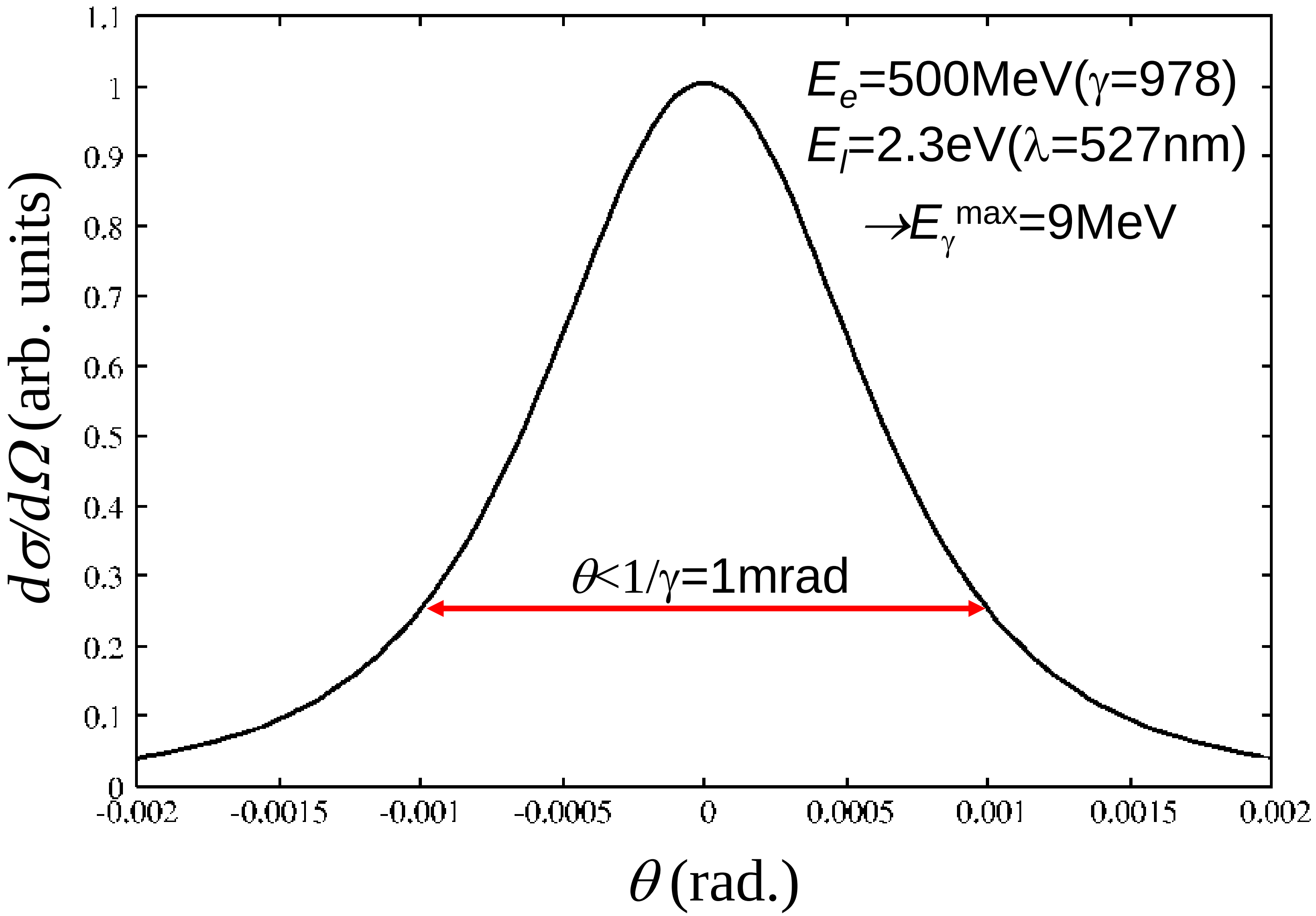

Most of the strength is concentrated into the forward direction within the scattering angle of 1 mrad which is the inverse of the γ.

Energy-Angle Correlation

$$E_\gamma \approx \frac{4\gamma^2 E_l}{1+(\gamma\theta)^2 + 4\gamma E_l/mc^2}$$

E_e=500MeV(γ=978)
E_l=2.3eV(λ=527nm)

⇨ E_γ^{max}=9MeV

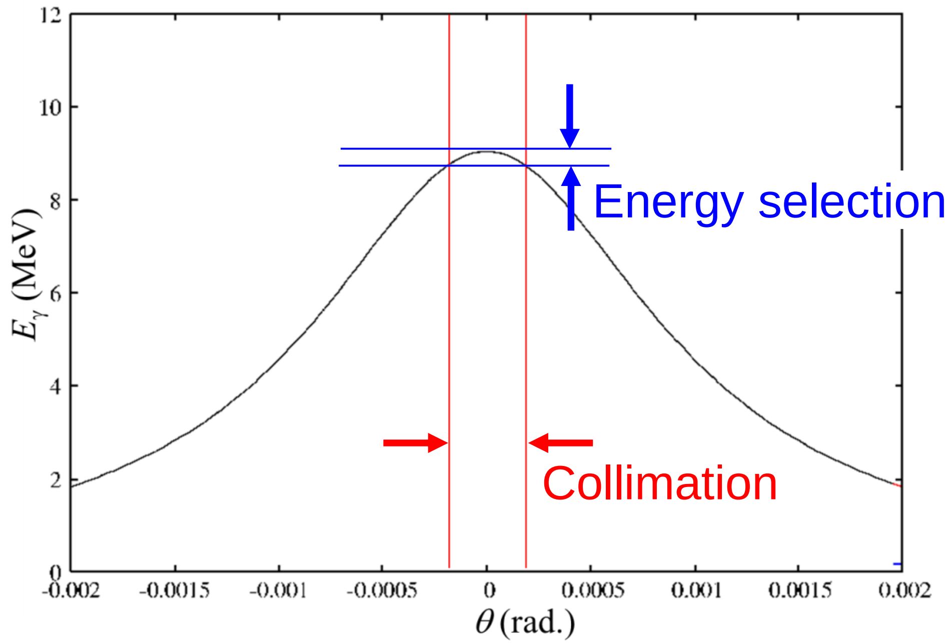

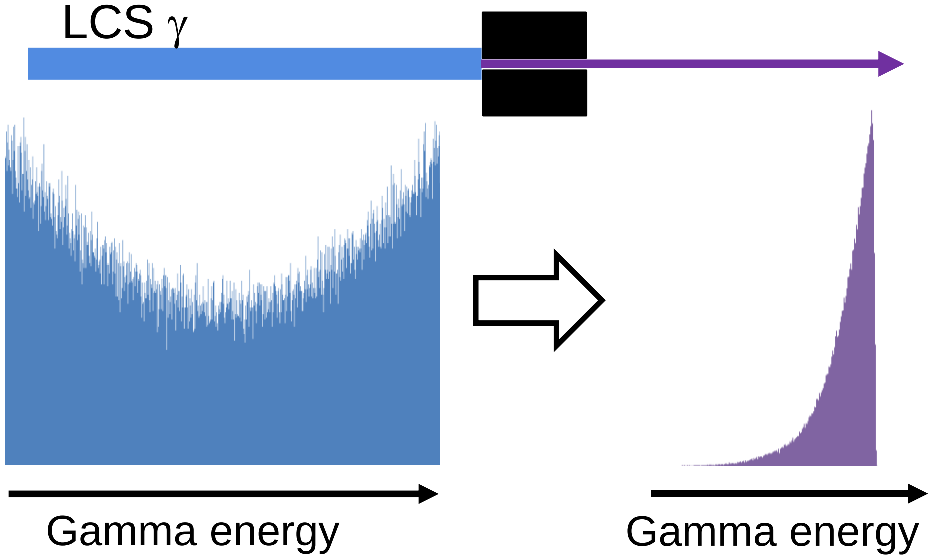

Collimator with 2mmϕ diameter hole placed 6m from collision point
Ω=0.16mrad ⇨ $\Delta E/E$=〜4%

The energy width also depends on the electron beam emittance related to the beam size and divergence at the collision point.

LCS γ Beam Line at AIST, Tsukuba

National Institute of Advanced Industrial Science and Technology (AIST)

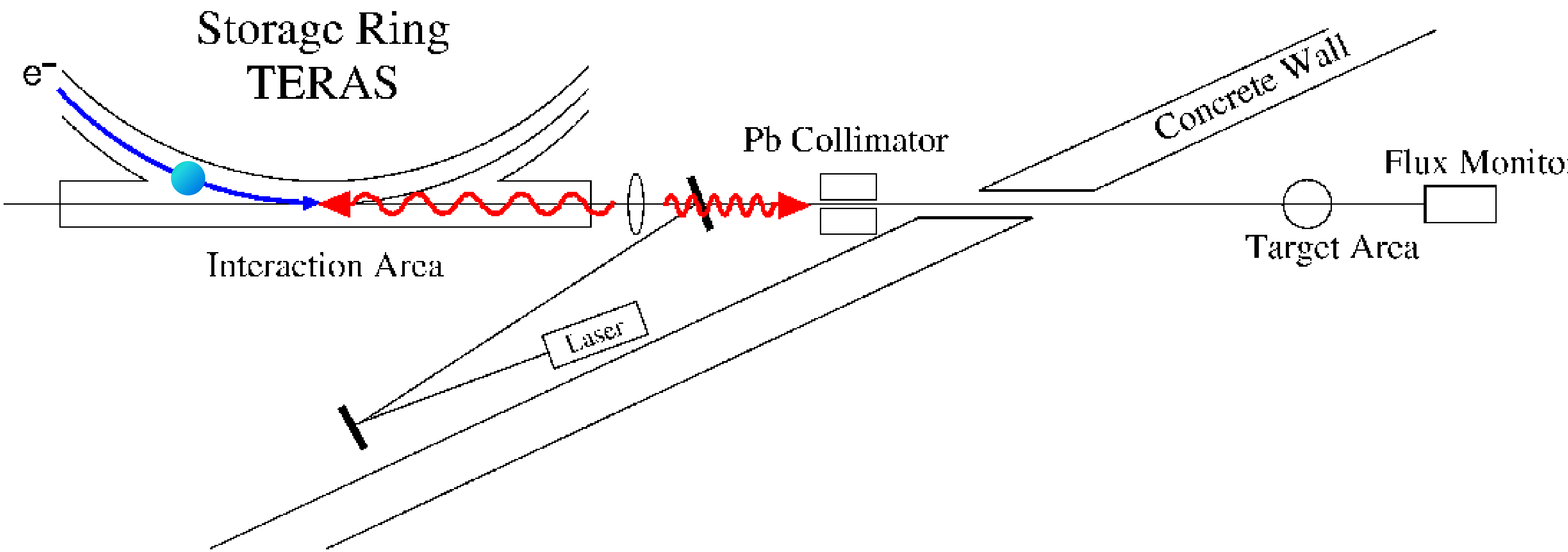

Electron beam: $300<E_e<800$ MeV

Nd:YLF laser: λ=1053nm（primary）

527nm（second）

Laser power: ~ 40W

⇨

LCS γ energy: $1<E_\gamma<40$ MeV

Intensity: ~ 10^6 /s

$\Delta E_\gamma/E_\gamma$: ~ 5-10%

Energy Distribution of the LCS Photon beam

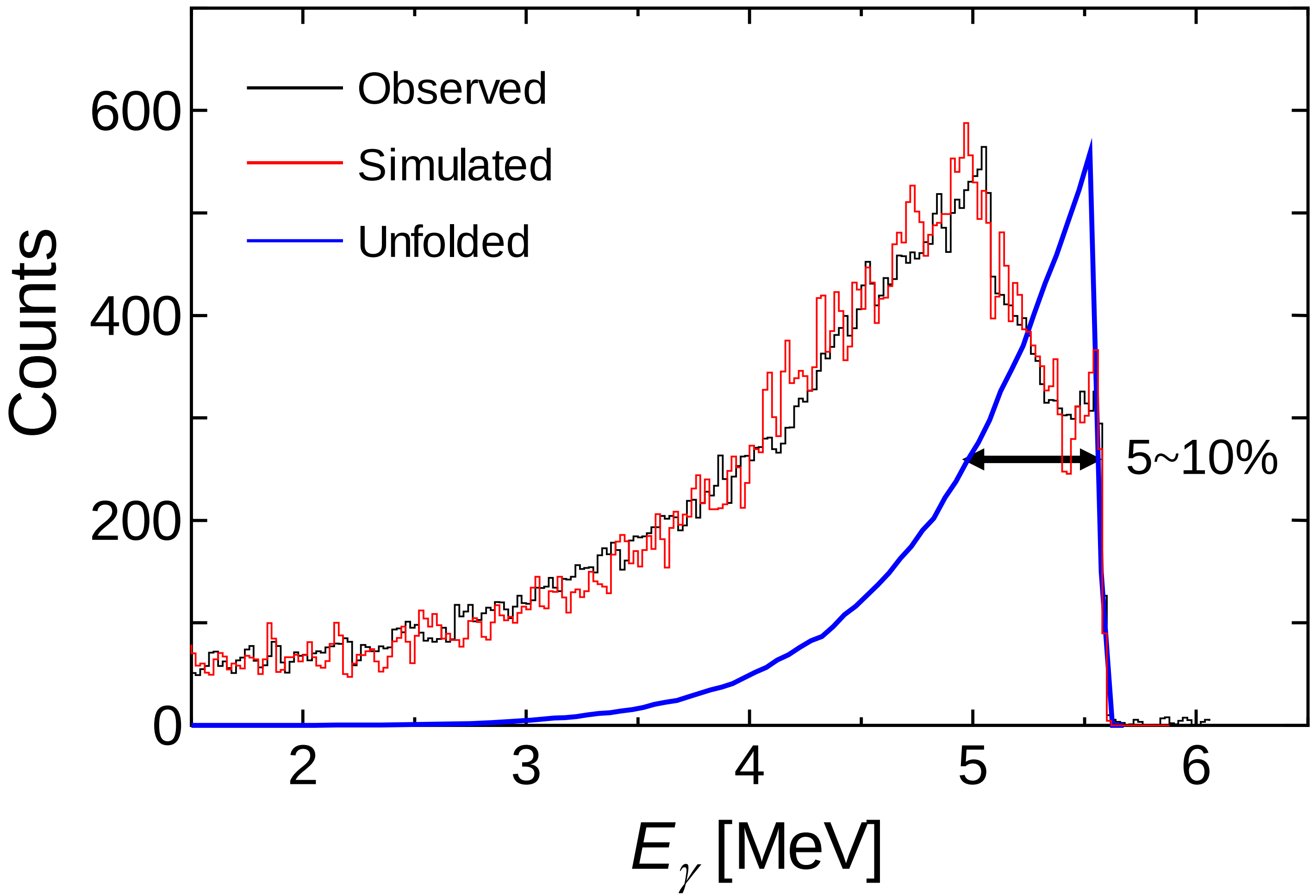

2.2. Nuclear Astrophysics

~100 elements

~300 stable nuclei

Most of heavy nuclei (Z>26) were produced by two types of neutron capture reactions; slow (s) and rapid (r) processes.

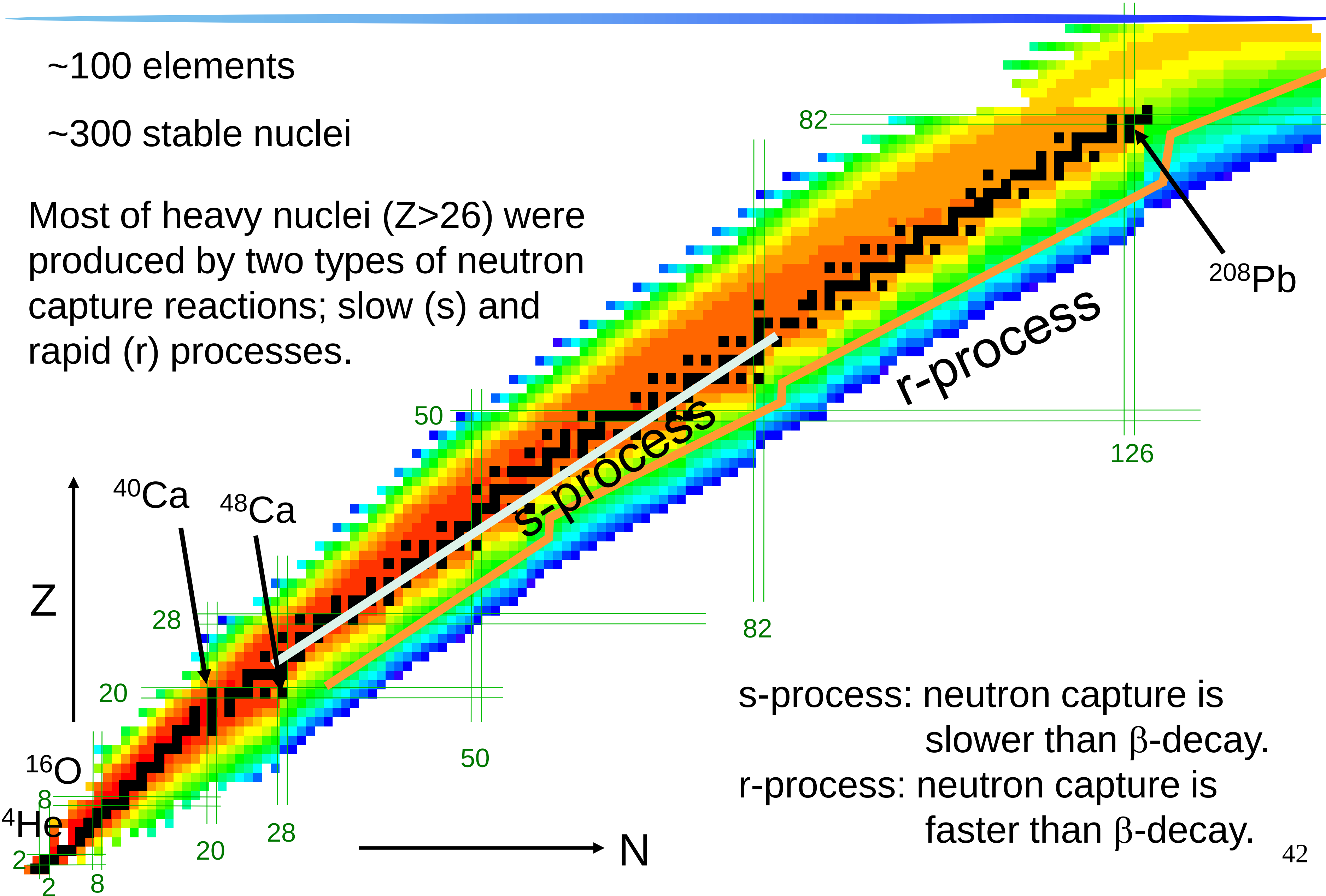

s-process: neutron capture is slower than β-decay.
r-process: neutron capture is faster than β-decay.

Relative Abundance of Heavy Elements

- Several peaks around neutron numbers N of 50, 82, and 126.
- The abundance peaks for the s-process nuclei appear at N=50, 82, and 126.
- The r-process peaks are seen at N≈46, 76, and 116. In the r-process, these nuclei are produced by β-decays after the production of neutron-rich unstable nuclei with the neutron magic number.

Small neutron capture cross section for the magic number nuclei
→ large abundance

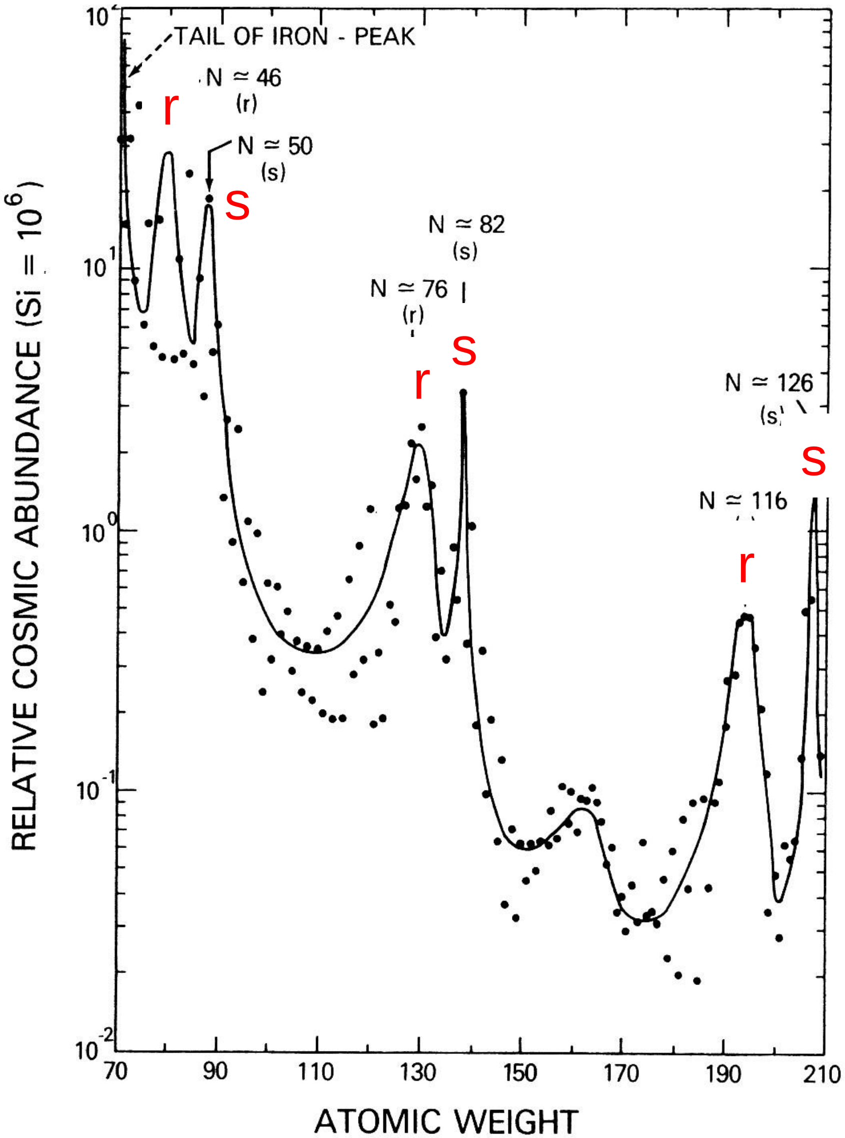

Fowler, Rev. Mod. Phys. 56, 194 (1984).

P-Nuclei

•35 proton-rich heavy nuclei which cannot be synthesized in the neutron capture processes. → p-nuclei

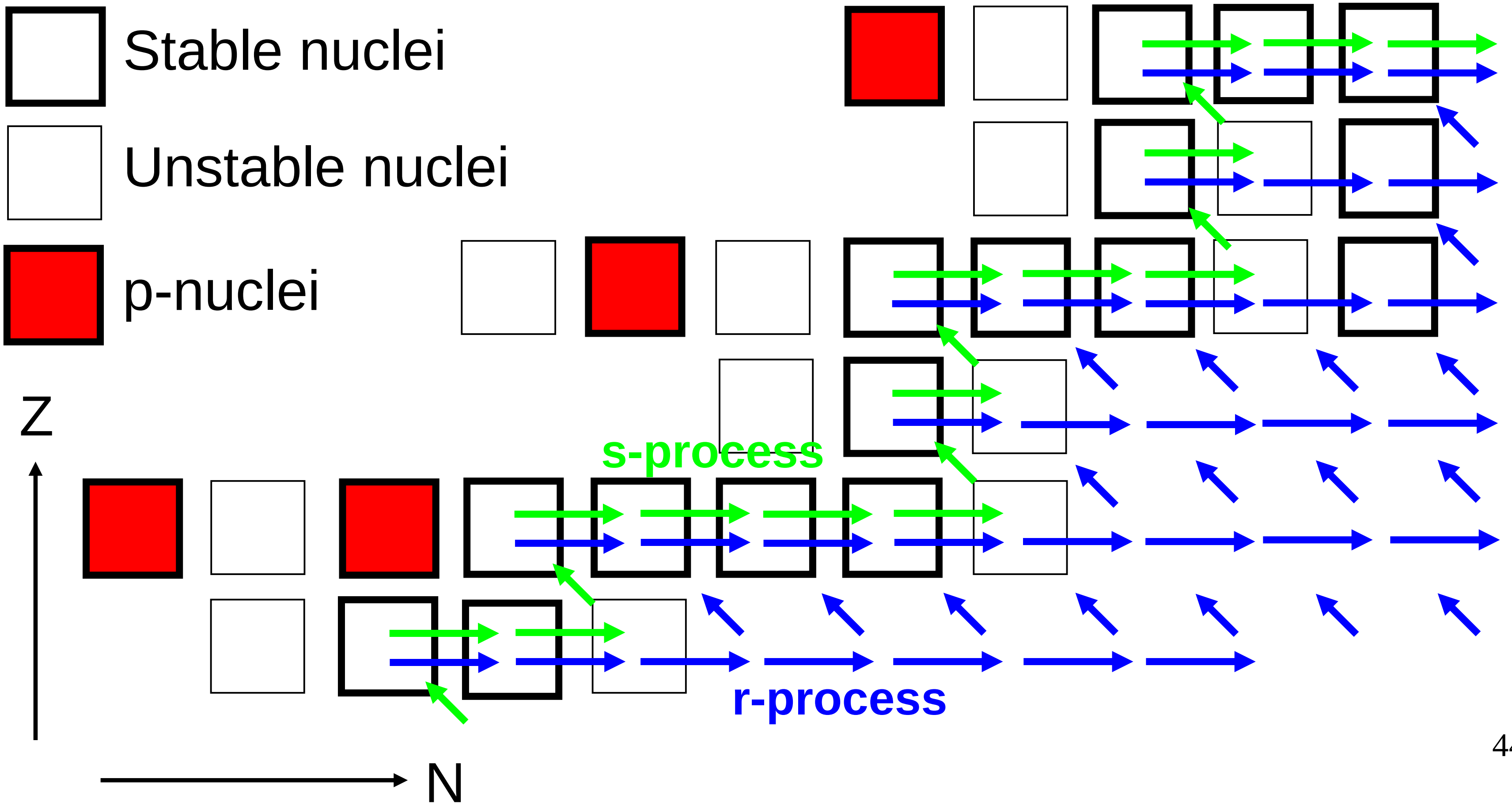

P-Nuclei

- 35 proton-rich heavy nuclei which cannot be synthesized in the neutron capture processes. → p-nuclei
- The abundance relative to the s-process nuclei is 0.01 to 0.1%

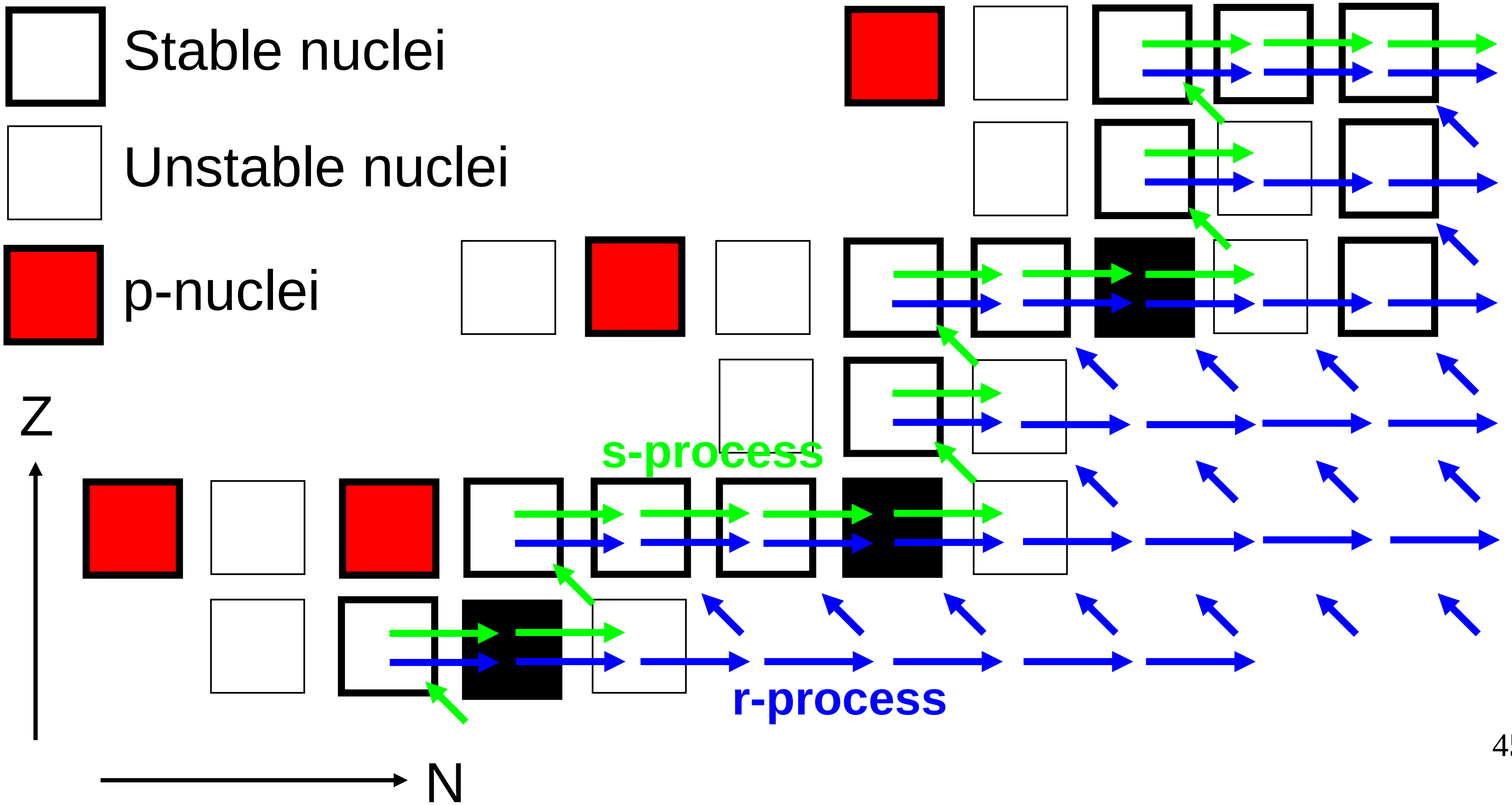

Origin of P-Nuclei

Most of heavier p-nuclei are thought to be produced by a series of photo-disintegration reactions such as (γ,n), (γ,p), and (γ,α).

γ-process

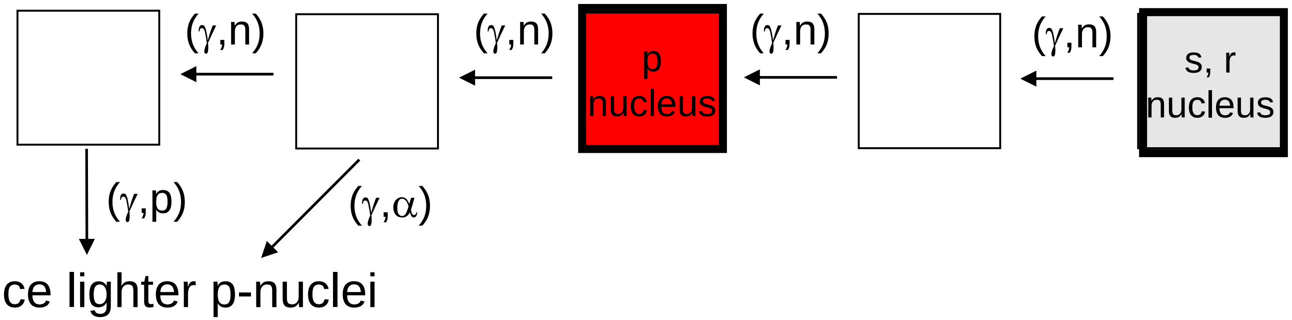

Typical conditions of γ-process

Temperature: 2-3$\times 10^9$K

Density: 10^6 g/cm^3

Time scale: a few seconds

Production site

Oxygen and neon-rich layer of massive stars during supernova explosion

P-Process Frontiers; ν-Process

Woosley (1990) has proposed neutrino(ν)-process as the origin of some p-nuclei.

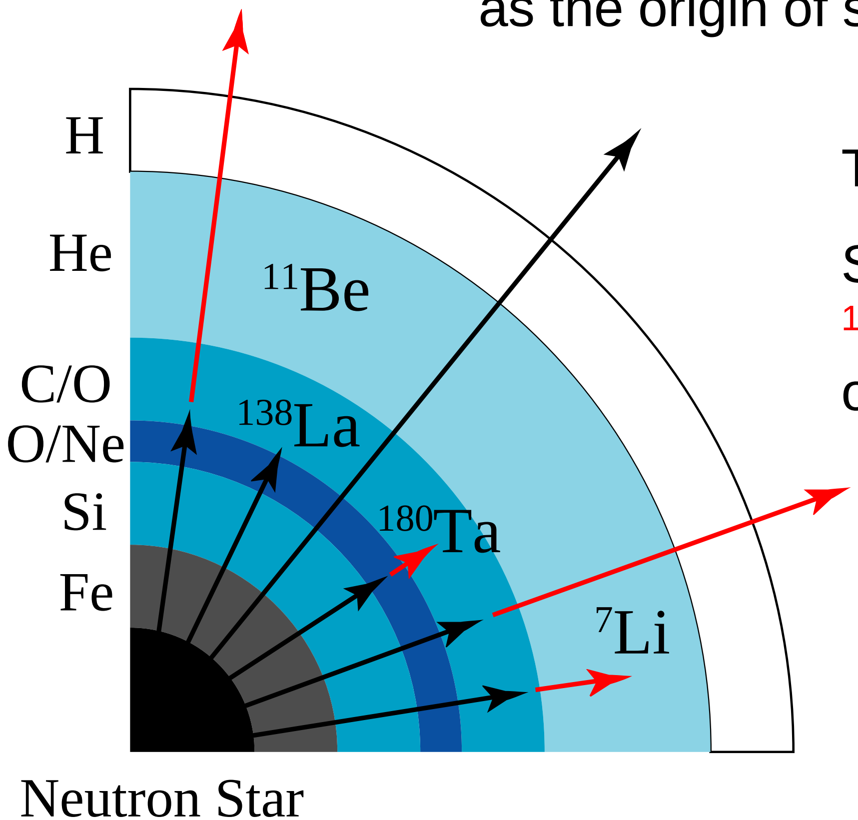

T. Yoshida, PRL (2005)

Synthesis of light elements ^{7}Li and ^{11}Be constrains the energy spectrum of the neutrino.

T. Yoshida, PRL (2006)

ν-process can constrains the mixing parameter for neutrino oscillation.

Core collapse supernova explosions, neutrino wind

The rarest p-nuclei of ^{138}La and ^{180}Ta are thought to be produced in the oxygen and neon-rich layer by neutrino reactions during supernova explosion.

Statistical Quantities in Hauser-Feshbach Model

Abundance calculations of p-nuclei
  ~1000 stable/unstable nuclei
  ~10000 nuclear reactions

It is impossible to measure all reaction rates experimentally.

⇩

Reaction rates are calculated by using the Hauser-Feshbach statistical model

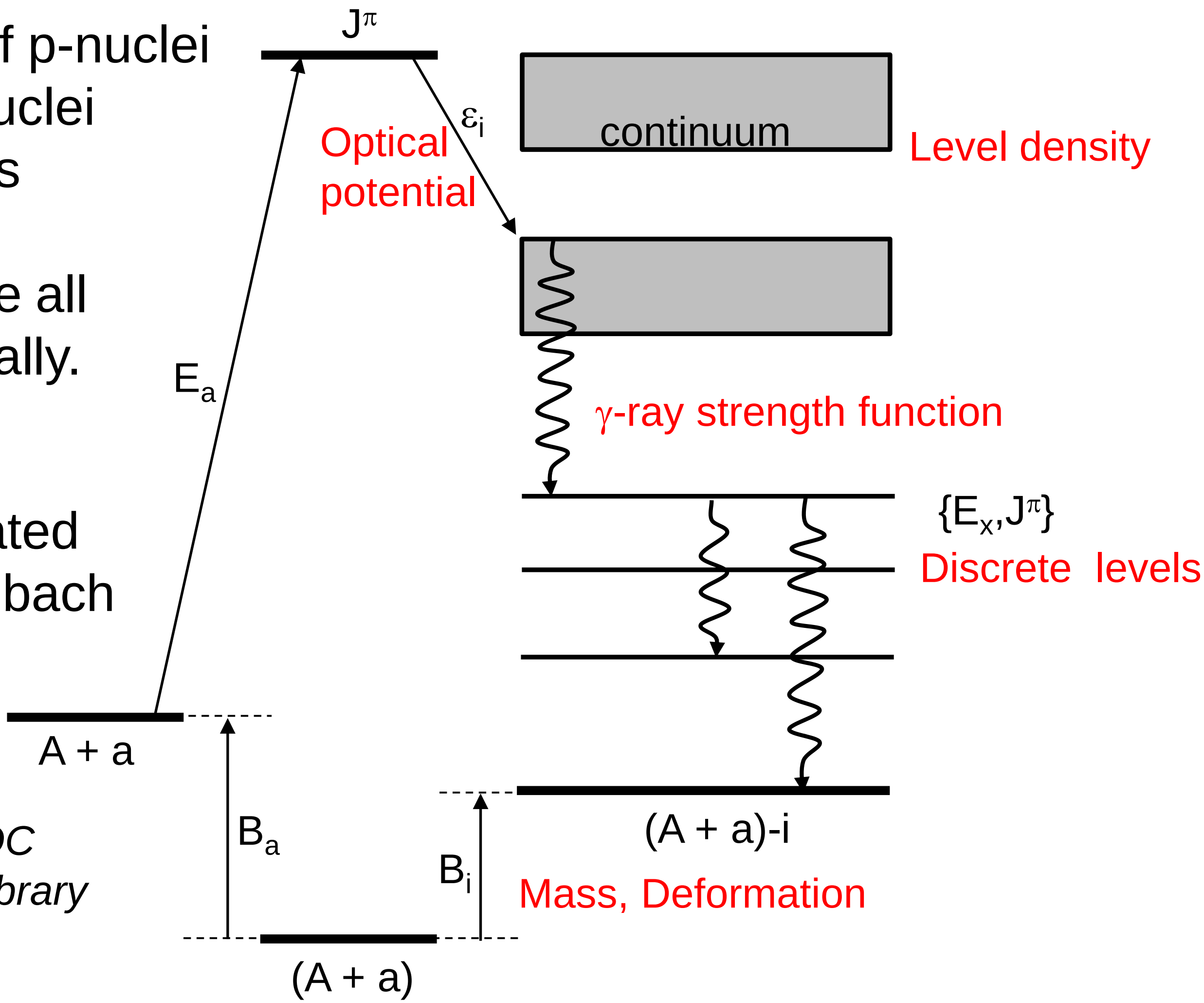

RIPL Handbook/IAEA-TECDOC
Reference Input Parameter Library
http://www-nds.iaea.org/ripl/

Experimental data of photonuclear reactions are used for the restriction of the model parameters such as γ-ray strength function and level density.

Stellar Reaction Rates for P-Nuclei

- A large number of photoneutron cross section data at the GDR region are available.
- However, astrophysically important energy for the production of p-nuclei is not identical to the GDR region.

$$\lambda(T) = \int_0^\infty c \underbrace{n_\gamma(E,T)}_{\text{photon number}} \underbrace{\sigma_\gamma(E)}_{(\gamma,n)\ \text{cross section}} dE$$

P.Mohr et al., Phys.Lett.B488(2000)127

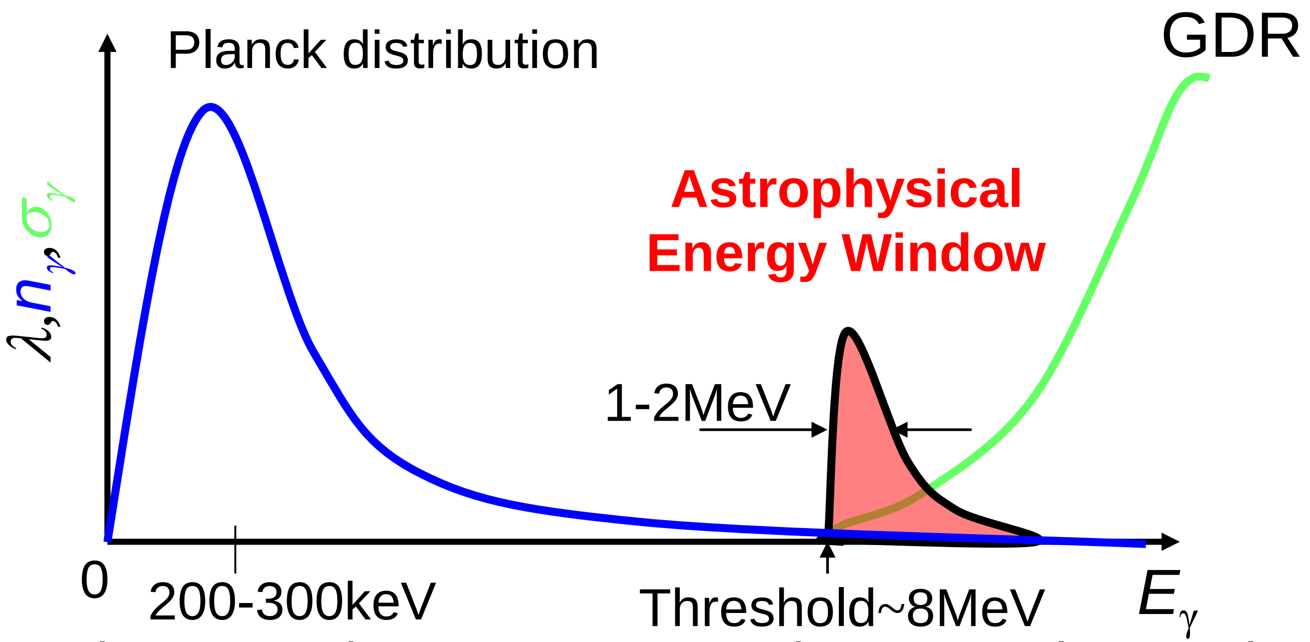

Cross sections near the neutron separation energy have to be measured.

Photoneutron Measurements at AIST

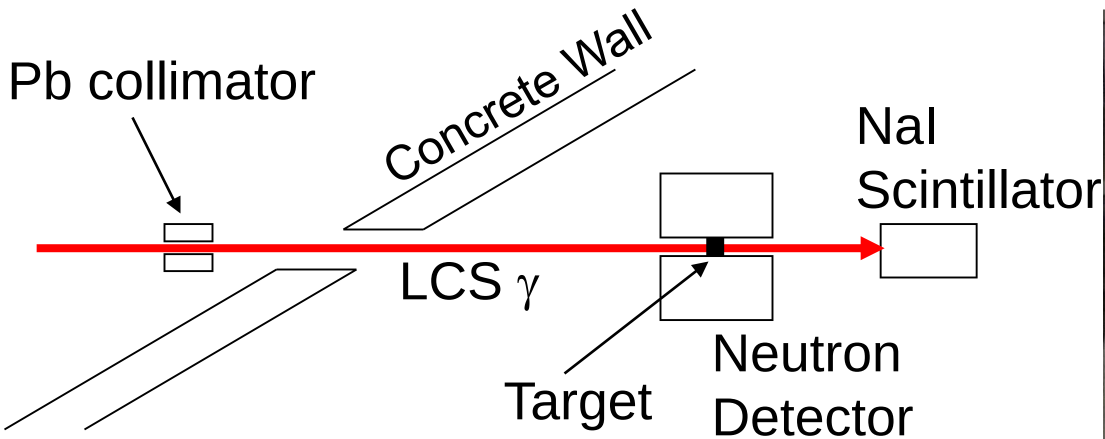

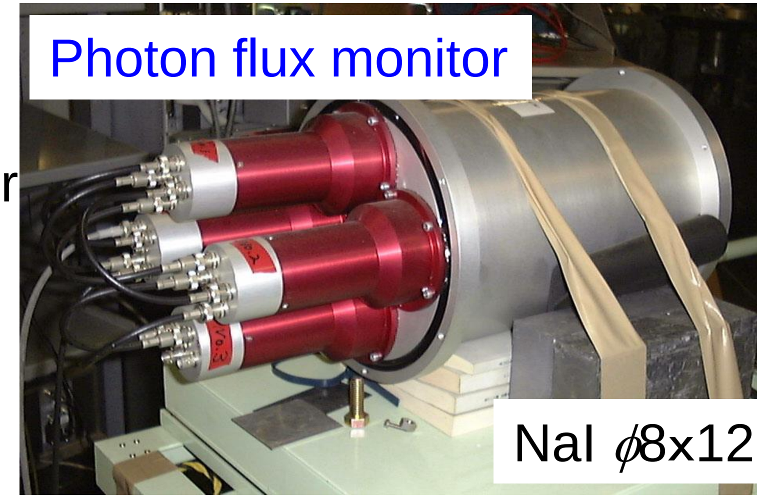

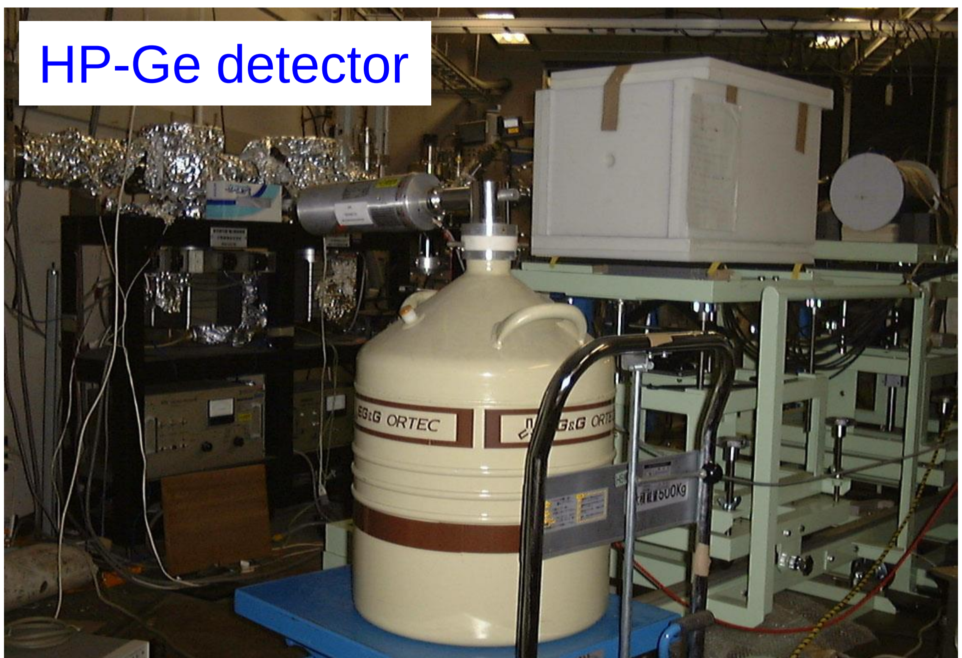

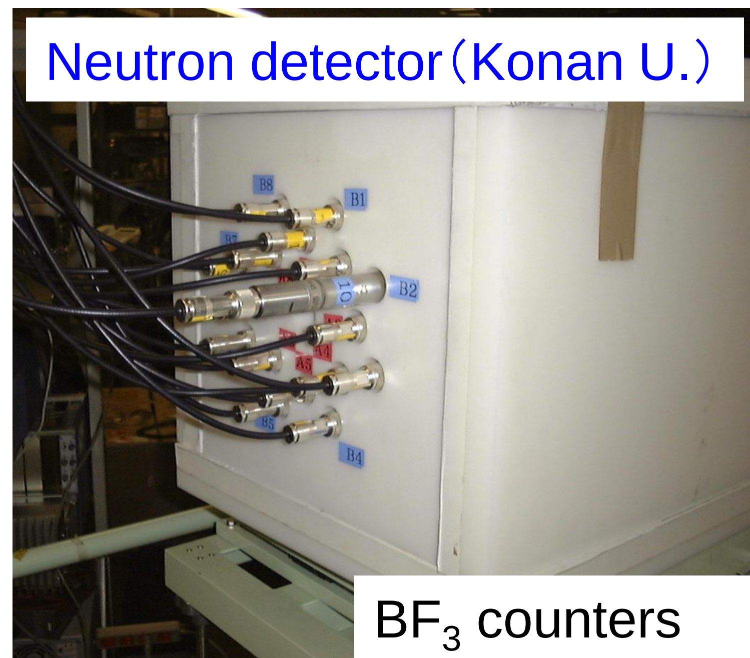

Photoneutron Cross Section for ^{181}Ta

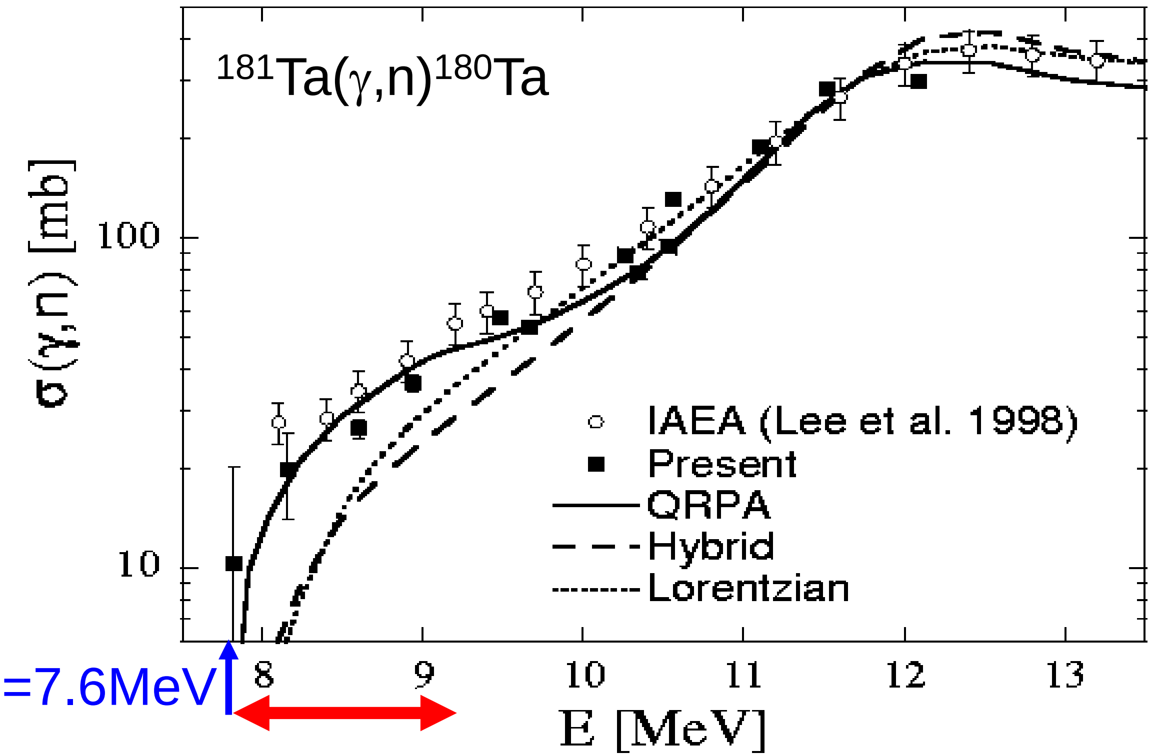

S_n=7.6MeV

Astrophysical Energy Window

^{180}Ta: Rarest isotope

Abundance: 0.012%

H. Utsunomiya et al., Phys. Rev. C67, 015807 (2003)

(γ,n) Cross Sections of ^{186}W and ^{187}Re

^{186}W(γ,n)^{185}W

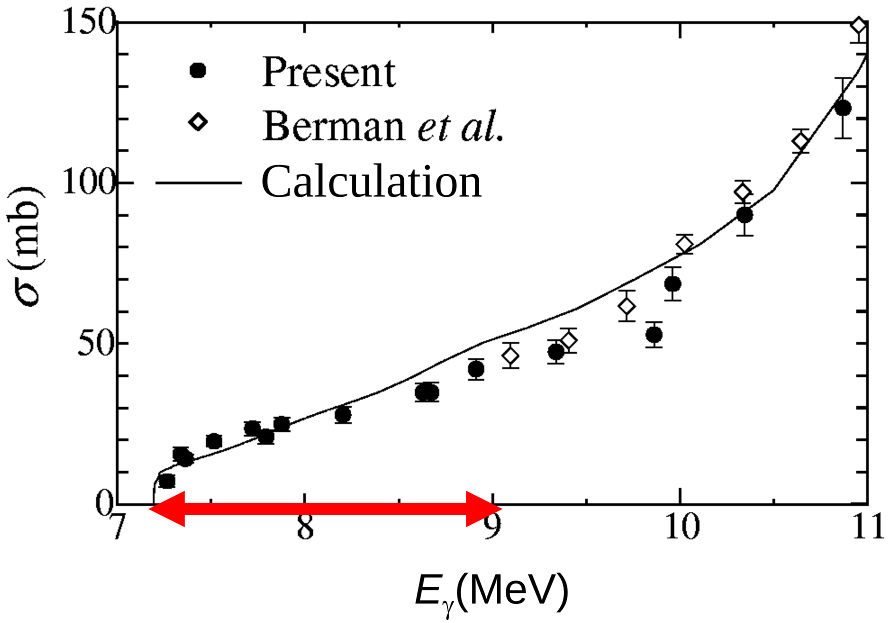

^{187}Re(γ,n)^{186}Re

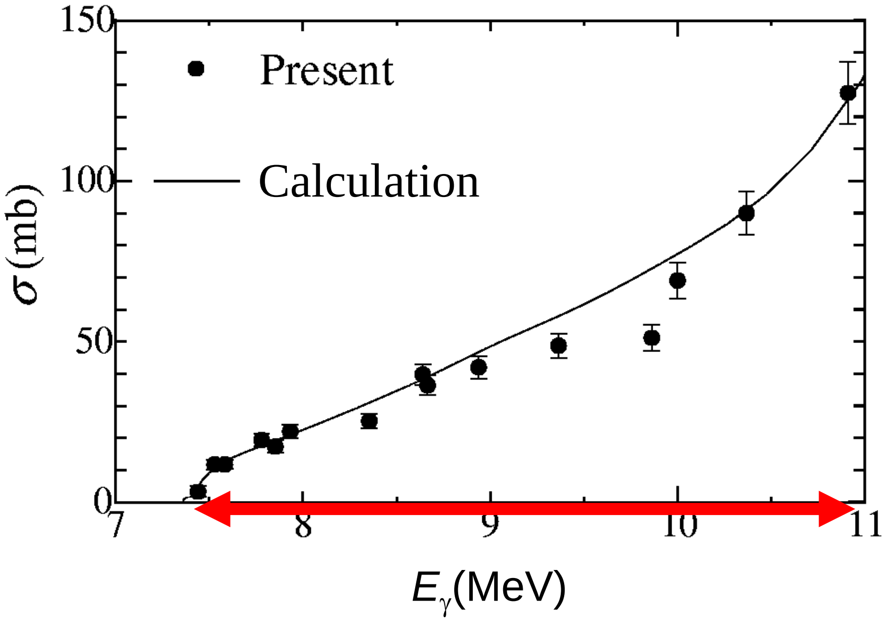

T.Shizuma et al., PRC72(2005)025808

First photoneutron cross section data near the neutron separation energy

Pygmy Dipole Resonance

Extra electric dipole resonance found in neutron-rich nuclei

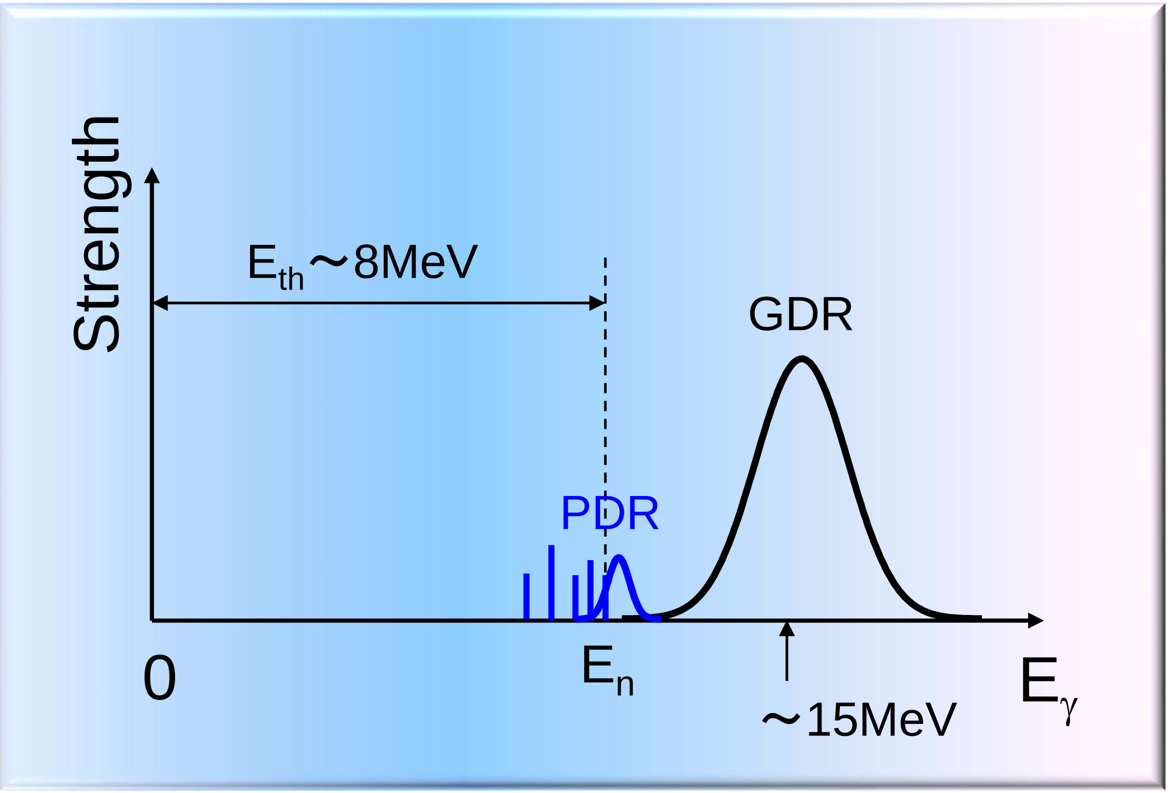

GDR: Electric giant dipole resonance

PDR: Electric pygmy dipole resonance

Pygmy Dipole Resonance

E1 strength for ^{208}Pb from (γ,γ')

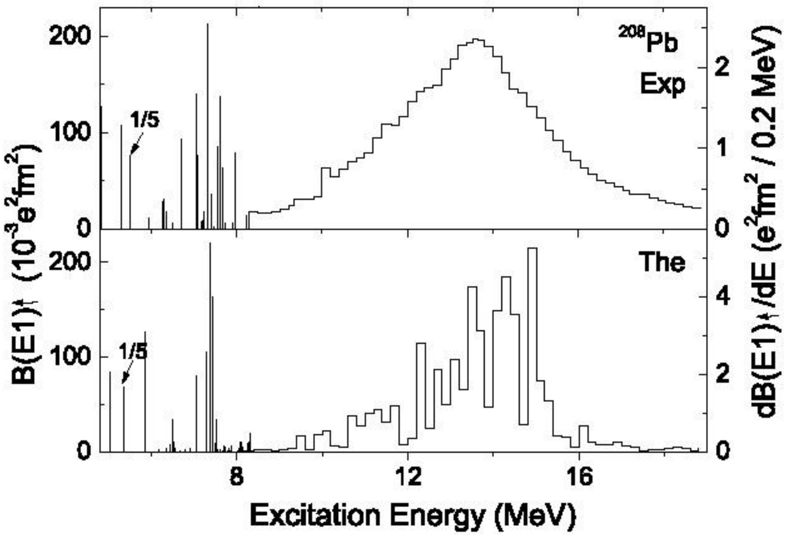

N.Ryezayeva et al., PRL89(2002)272502

Deferential cross section for ^{132}Sn from (p,p')

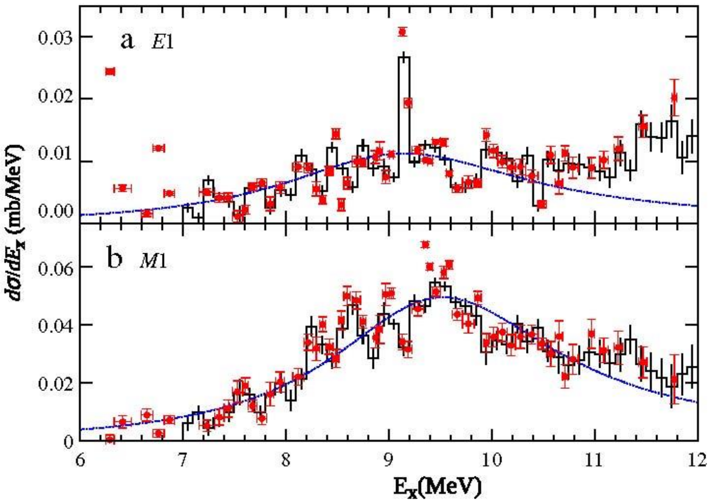

3.2% of TRK sum rule

C.Iwamoto et al., PRL108(2012)262501

GDR

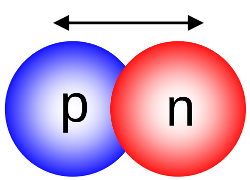

PDR

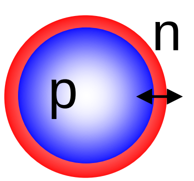

Protons and neutrons move in phase in the nuclear interior, but at surface neutron oscillate against the proton and neutron core, producing electric dipole strength.

Neutron Skin Thickness in ^{208}Pb

Thickness of the neutron skin can be estimated by dipole polarizabilty α_D

$$\alpha_D = \frac{\hbar c}{2\pi^2 e^2}\int \frac{\sigma_{\mathrm{abs}}}{\omega^2} d\omega,$$

$$\alpha_D = 20.1(6)\mathrm{fm}^3/e^2$$

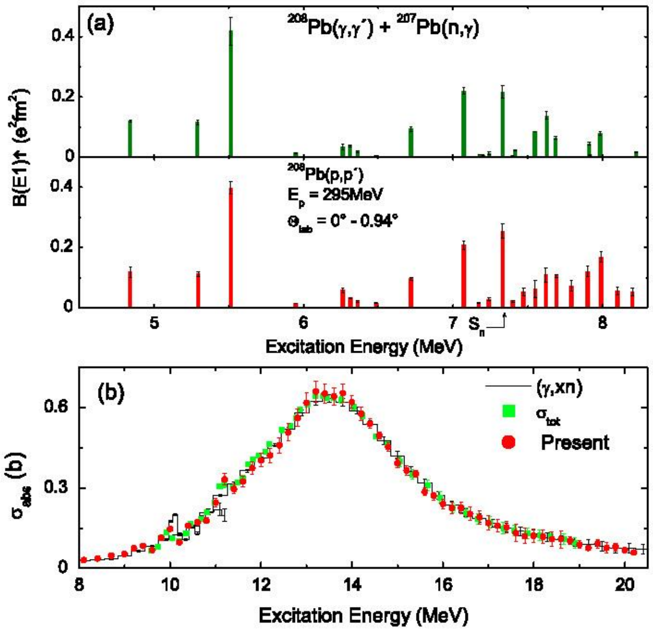

FIG. 3 (color online). (a) $B(E1)$ strengths in ^{208}Pb in the region $E_x \simeq 4.8$–8.2 MeV as deduced from the present work in comparison with (γ, γ') and (n, γ) experiments [26,29–31]. (b) Photoabsorption cross sections in the GDR region from the present work compared to (γ, xn) [32] and total photoabsorption [33] measurements.

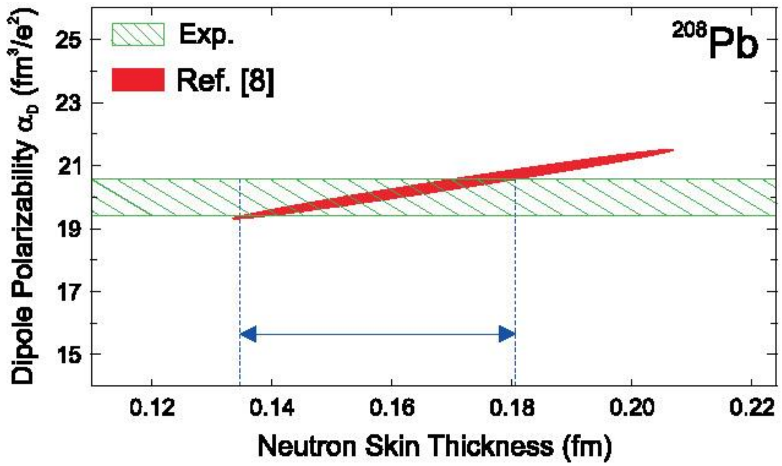

FIG. 5 (color online). Extraction of the neutron skin in ^{208}Pb based on the correlation between r_{skin} and the dipole polarizability α_D established in Ref. [8].

$$r_{skin} = 0.156^{+0.025}_{-0.021}\,\mathrm{fm}$$

A.Tamii et al., PRL107(2011)062502

2.3. Nuclear Physics with NRF

Photonuclear data below neutron separation energy can be obtained by nuclear resonance fluorescence (NRF) measurements.

NRF takes place via only electro-magnetic interaction.

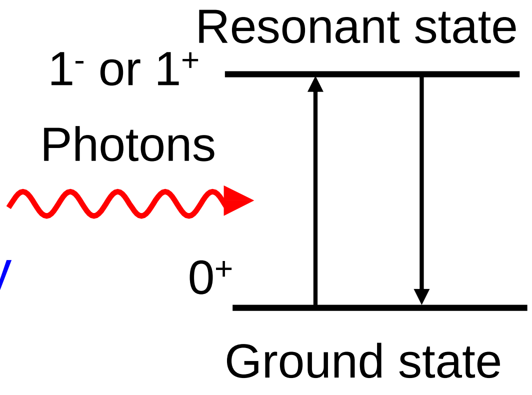

- Model independent extraction of transition probability

$$\Gamma_0 = 8\pi \sum_{\Pi L=1}^{\infty} \frac{(L+1)\left(E_\gamma / \mathrm{hc}\right)^{2L+1}}{L\left[(2L+1)!!\right]^2} \frac{2J_0+1}{2J+1} B\left(\Pi L, E_\gamma\right)\uparrow$$

- Selective excitation of 1^-, 1^+, and 2^+ states

Dipole (E1 & M1) and quadrupole (E2) responses

Using linearly polarized photon beams, the transition multipolarity (E1 or M1) can be determined.

Scattering Cross Section

Absorption cross section

Breit-Wigner formula

$$\sigma_{abs} = \frac{\pi}{2}\frac{2J+1}{2J_0+1}\left(\frac{\hbar c}{E_\gamma}\right)^2 \frac{\Gamma\Gamma_0}{(E-E_x)^2+(\Gamma/2)^2}$$

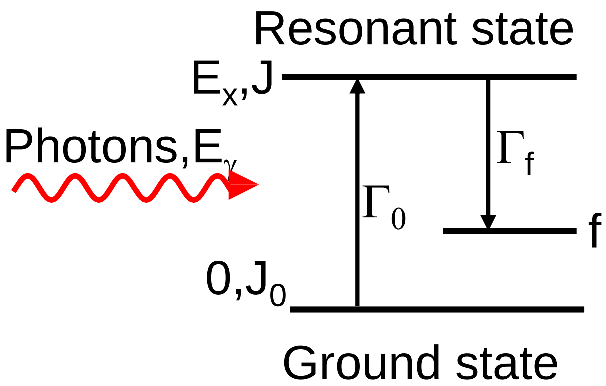

$$\Gamma=\Gamma_0+\Gamma_f$$

Integrated absorption cross section

$$\sigma_{abs}\Gamma = \int_0^\infty \sigma_{abs}\,dE = \frac{\pi}{2}\frac{2J+1}{2J_0+1}\left(\frac{\hbar c}{E_\gamma}\right)^2 \int_0^\infty \frac{\Gamma\Gamma_0}{(E-E_x)^2+(\Gamma/2)^2}\,dE$$

$$= \frac{2J+1}{2J_0+1}\left(\pi\frac{\hbar c}{E_\gamma}\right)^2 \Gamma_0$$

Scattering cross section to a state f

$$I_s = \frac{2J+1}{2J_0+1}\left(\pi\frac{\hbar c}{E_\gamma}\right)^2 \Gamma_0\frac{\Gamma_f}{\Gamma}$$

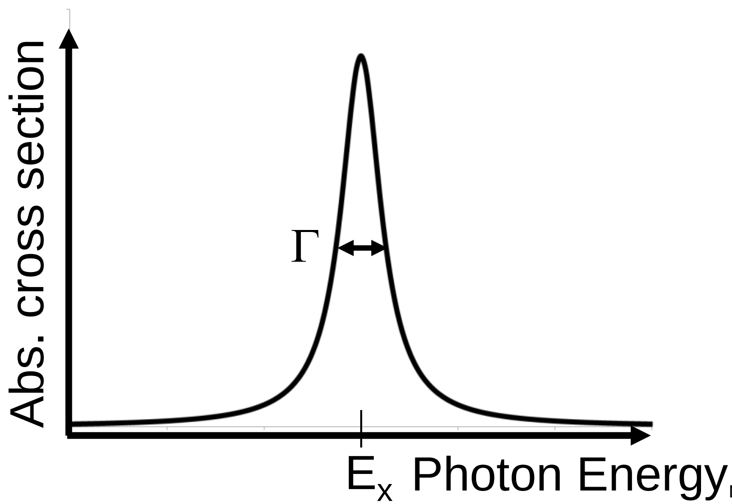

Special Case; $\Gamma=\Gamma_0=\Gamma_f$

Scattering cross section

$$I_s = \frac{2J+1}{2J_0+1}\left(\pi\frac{\hbar c}{E_\gamma}\right)^2 \Gamma_0$$

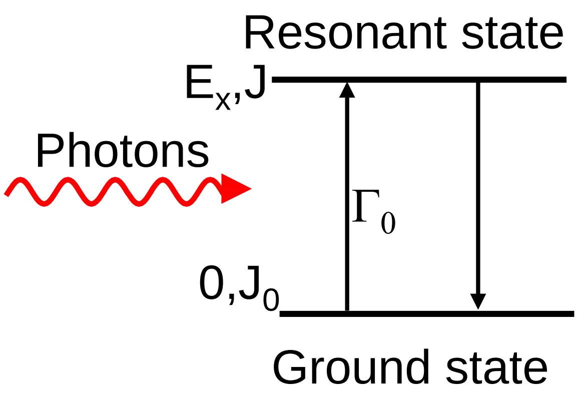

For 0→1→0 spin sequence in even-even nuclei,

$$I_s = 3\left(\pi\frac{\hbar c}{E_\gamma}\right)^2 \Gamma_0$$

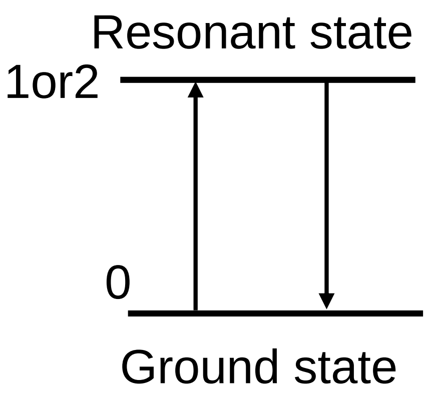

For 0→2→0 spin sequence,

$$I_s = 5\left(\pi\frac{\hbar c}{E_\gamma}\right)^2 \Gamma_0$$

Decay width to the ground state can be extracted from the scattering cross section which is obtained by the NRF measurement.

Reduced Transition Probability

- Comparison with nuclear theory can be made through reduced transition probabilities.
- Relation between Γ_0 and $B(\Pi L)$ is obtained by the single particle model;

$$\Gamma_0 = 8\pi \sum_{\Pi L=1}^{\infty} \frac{(L+1)(E_\gamma/\hbar c)^{2L+1}}{L[(2L+1)!!]^2} \frac{2J_0+1}{2J+1} B(\Pi L, E_\gamma)\uparrow$$

For even-even nuclei

$$B(E1)\uparrow = 2.866 \cdot 10^{-3} \frac{\Gamma_0}{E_\gamma^3} \left[e^2 fm^2\right]$$

$$B(M1)\uparrow = 0.2598 \cdot 10^{-3} \frac{\Gamma_0}{E_\gamma^3} \left[\mu_N^2\right]$$

$$B(E2)\uparrow = 6201 \frac{\Gamma_0}{E_\gamma^5} \left[e^2 fm^4\right]$$

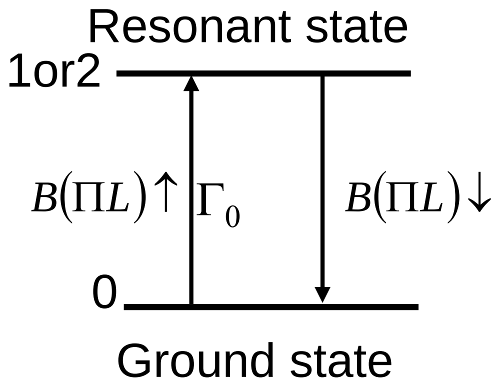

$$B(\Pi L)\uparrow = \frac{2J+1}{2J_0+1} \cdot B(\Pi L)\downarrow$$

Angular Correlation (Unpolaried)

$$W(\theta) = \sum_{\nu} A_{\nu}(1) A_{\nu}(2) P_{\nu}(\cos\theta)$$

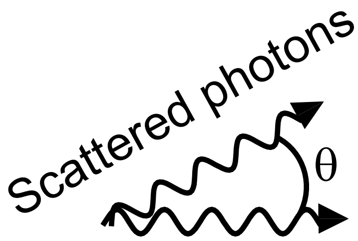

$P_{\nu}(\cos\theta)$:Legendre polynomials of the νth order

$A_{\nu}(1), A_{\nu}(2)$:Expansion coefficients

For dipole transitions in even-even nuclei

$$W(\theta)_{Dipole} = \frac{3}{4}\left(1 + \cos^2\theta\right) \quad \text{for } 0 \rightarrow 1 \rightarrow 0$$

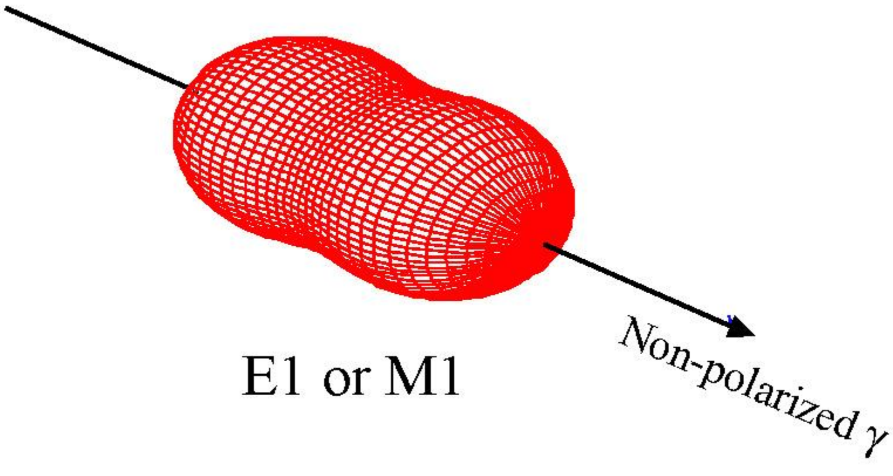

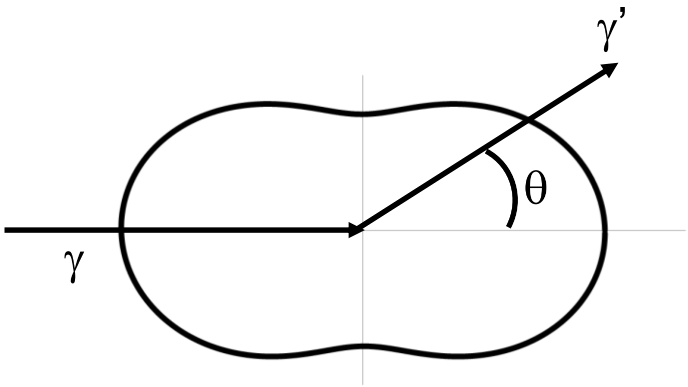

For Quadrupole Transitions (Unpolaried)

Even-even nuclei

$$W(\theta)_{Quadrupole} = \frac{5}{4}\left(1 - 3\cos^2\theta + 4\cos^4\theta\right) \quad \text{for } 0 \rightarrow 2 \rightarrow 0$$

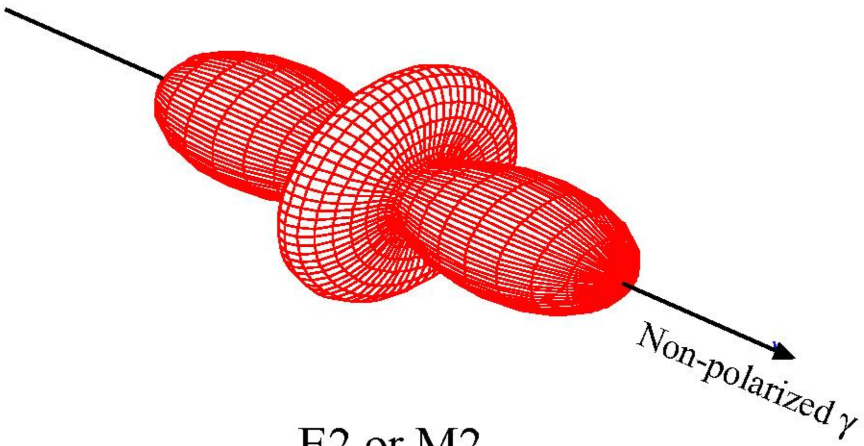

E2 or M2

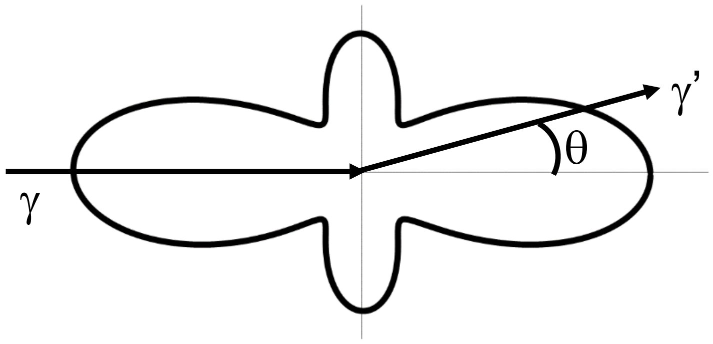

Angular Correlation (Linearly Polarized)

$$W(\theta,\phi) = W(\theta) + (\pm)L_{1'} \sum_{\nu} A'_{\nu}(1) A_{\nu}(2) P_{\nu}^{(2)}(\cos\theta)\cos(2\phi)$$

$W(\theta)$: Angular correlation for unpolarized photons

ϕ: Angle between the electric field vector of the incident photon beam and the scattering plane

$(\pm)L_{1'}$: +1 for electric and -1 for magnetic transitions $L_{1'}$

$P_{\nu}^{(2)}$: Unnormalized associated Legendre polynomials

For 0→1→0 spin sequence in even-even nuclei

$$W(\theta,\phi)_{dipole} = W(\theta)_{dipole} \pm \frac{3}{4}\left(1-\cos^2\theta\right)\cos 2\phi$$

plus sign for M1, minus sign for E1

Angular Correlation (Linearly Polarized)

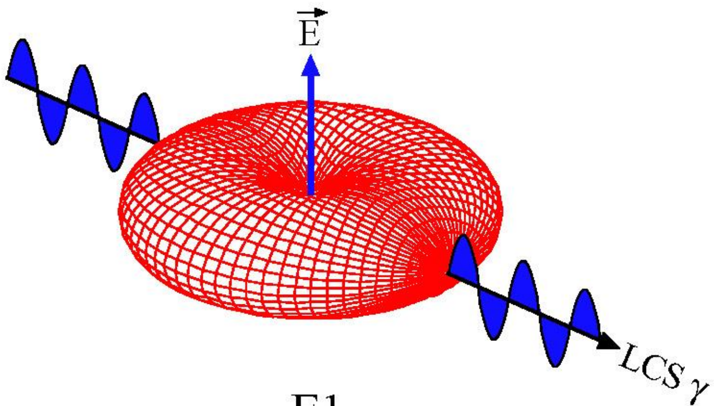

E1

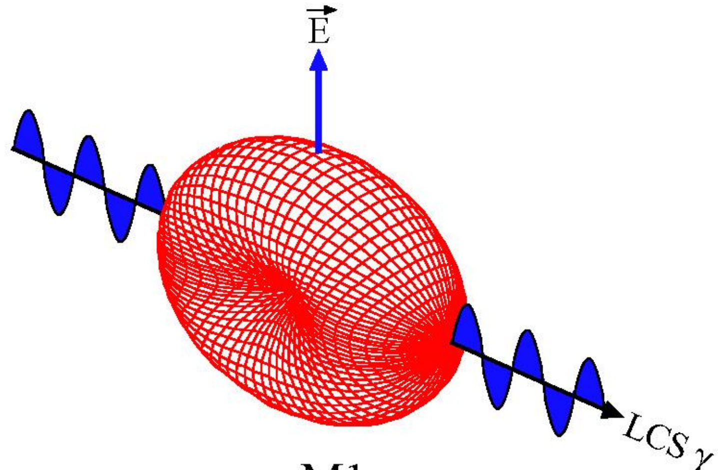

M1

At θ=90°

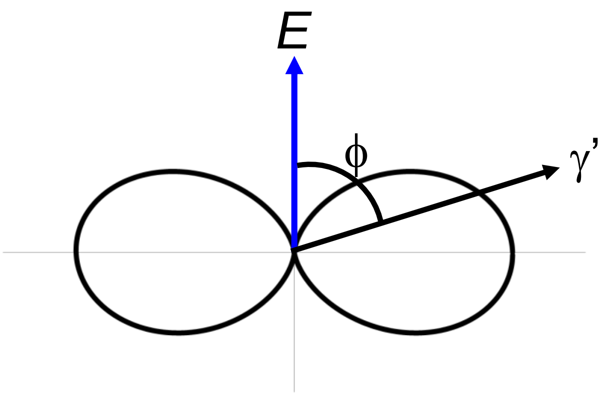

maximum at ϕ=90° or 270 °
minimum at ϕ=0 ° or 180 °

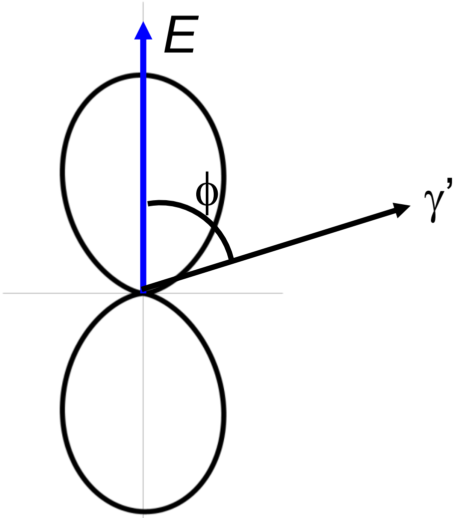

maximum at ϕ=0 ° or 180 °
minimum at ϕ=90° or 270 °

Angular Correlation (Linearly Polarized)

For 0→2→0 spin sequence in even-even nuclei

$$W(\theta,\phi)_{quadrupole} = W(\theta)_{quadrupole} \pm \frac{5}{4}\left(1-5\cos^2\theta+4\cos^4\theta\right)\cos 2\phi$$

plus sign for E2, minus sign for M2

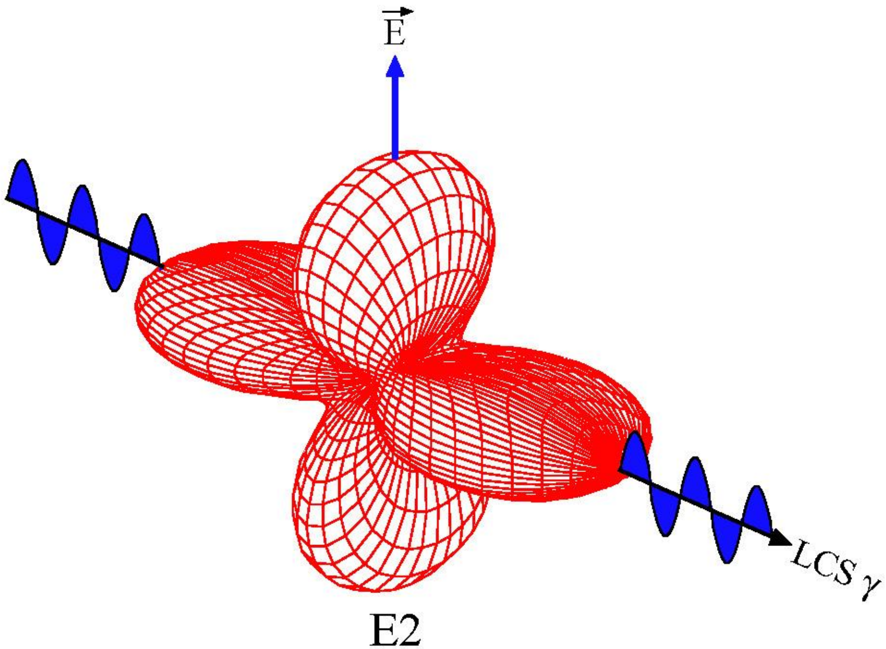

At θ=90°

maximum at ϕ=0° or 180°
minimum at ϕ=90° or 270°

Same as the magnetic dipole case

Principle of E1/M1 Determination

Sensitivity of the polarization effects to the angular correlation is maximum at the scattering angle θ of 90 degrees.

For 0→1→0 spin sequence in even-even nuclei

$$W(90^\circ,\phi)_{dipole} = \frac{3}{4} \pm \frac{3}{4}\cos 2\phi$$ plus sign for M1, minus sign for E1

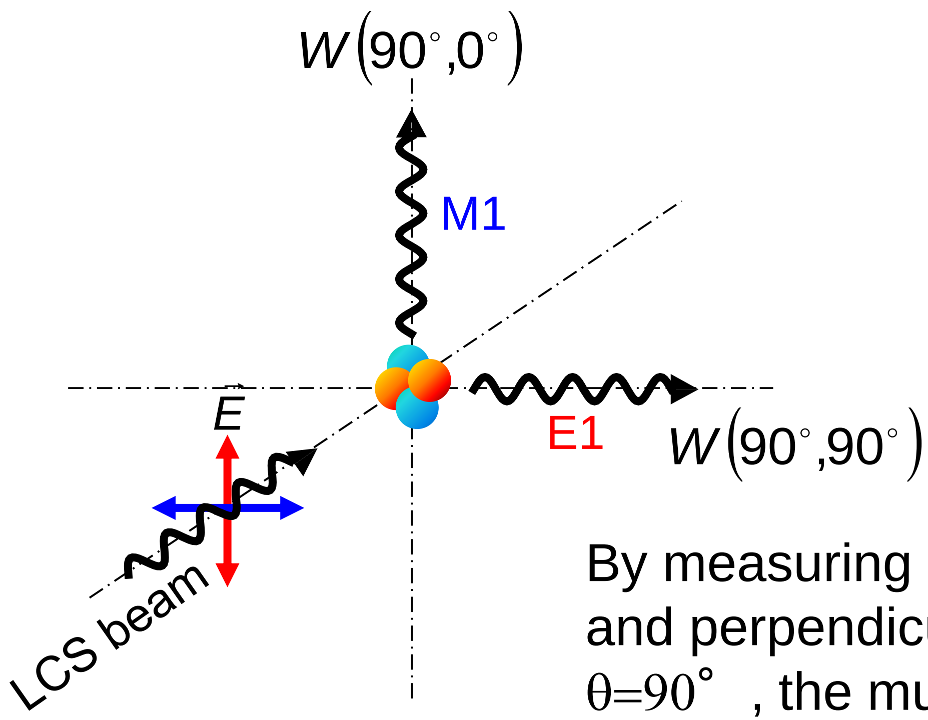

Intensity asymmetry

$$A = \frac{W(90^\circ,0^\circ) - W(90^\circ,90^\circ)}{W(90^\circ,0^\circ) + W(90^\circ,90^\circ)}$$

$$= \begin{matrix} +1 \text{ for } M1 \text{ transiton} \\ -1 \text{ for } E1 \text{ transition} \end{matrix}$$

By measuring NRF γ-rays scattered in parallel and perpendicularly to the polarization axis at $\theta=90^\circ$, the multipolarity of the transitions can be determined.

M1/E2 Assignment

Intensity asymmetry is similar for M1 and E2, but the angular correlation is different from each other.

$$W(\theta)_{Dipole} = \frac{3}{4}\left(1 + \cos^2\theta\right)$$

$$W(\theta)_{Quadrupole} = \frac{5}{4}\left(1 - 3\cos^2\theta + 4\cos^4\theta\right)$$

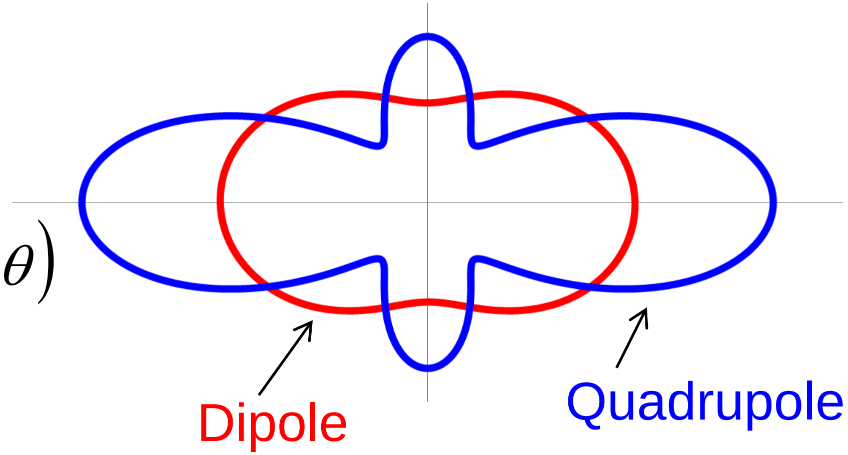

$$\frac{W(90^\circ)}{W(145^\circ)} = 0.6$$ for dipoles (0→1→0)

$$\frac{W(90^\circ)}{W(145^\circ)} = 1.3$$ for quadrupoles (0→2→0)

By measuring the intensity ratios between the scattering angle of 90 and 145 degrees, the determination of M1 and E2 can be made.

NRF Measurements at AIST

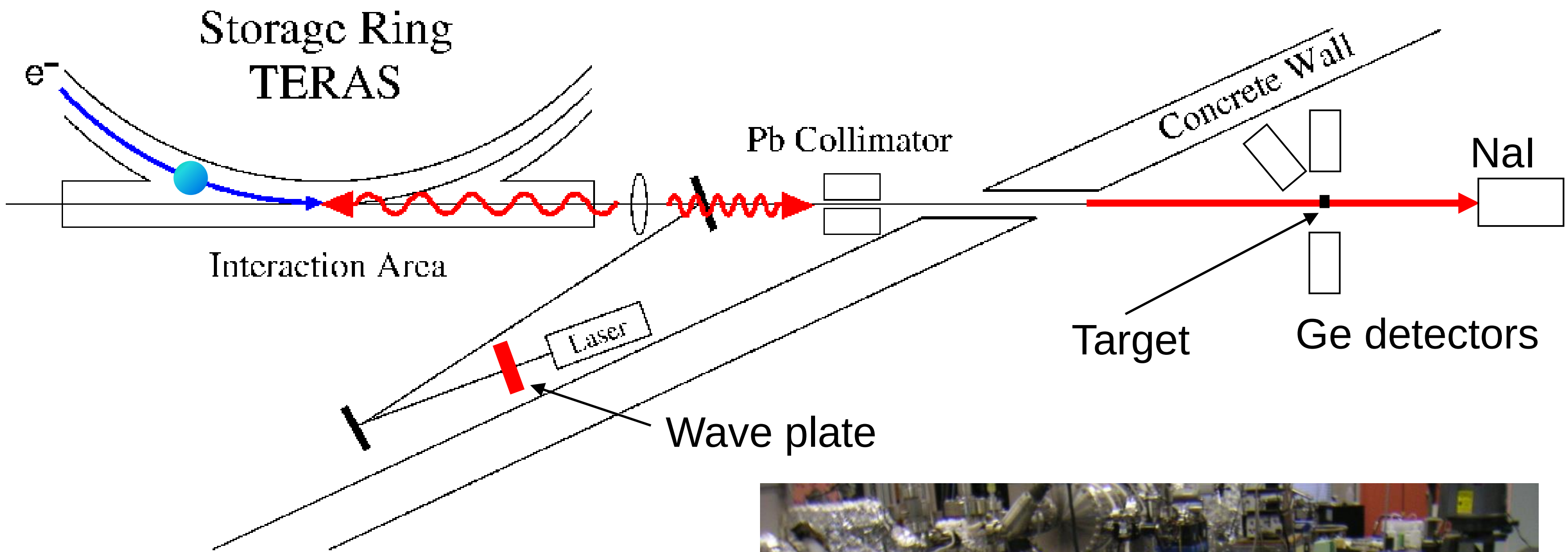

Vertical

Horizontal

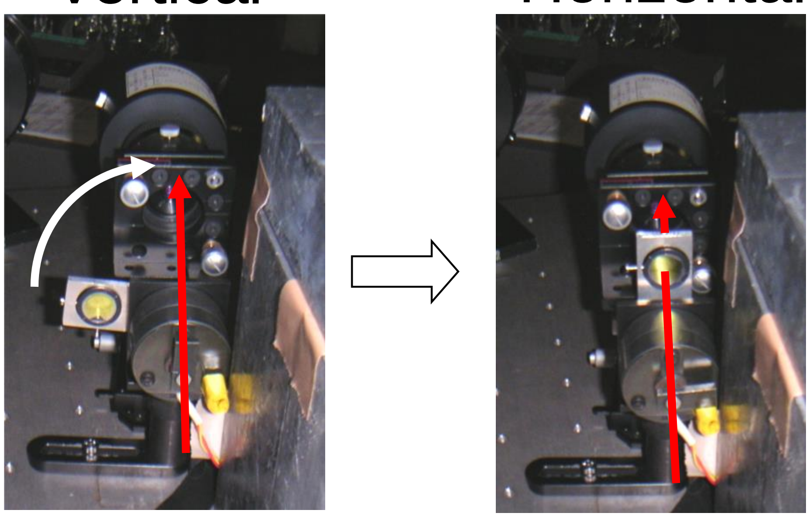

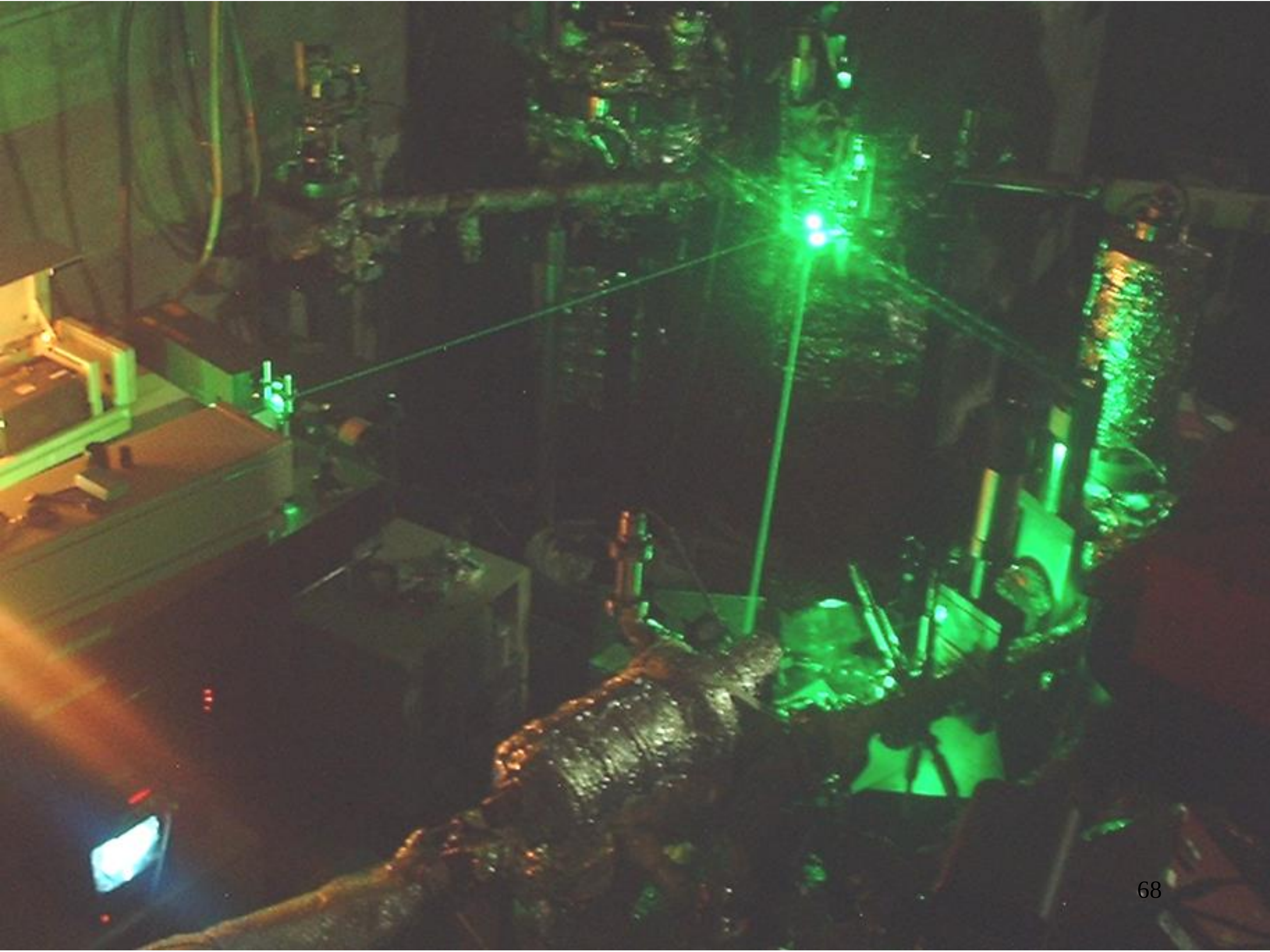

NRF Spectrum for Pb-208

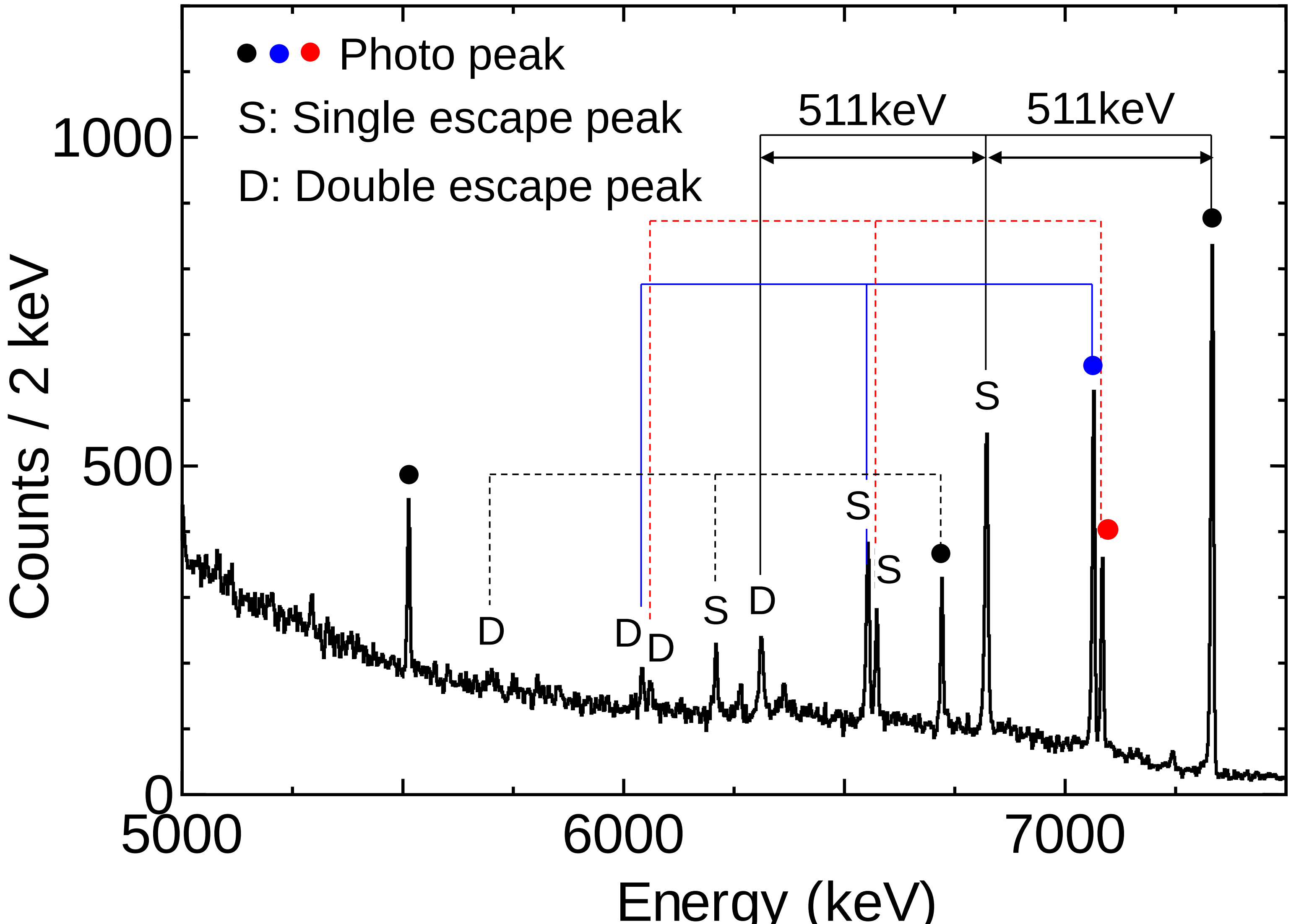

It is useful to measure scattered γ-rays by changing the energy of incident photon beam about 500 keV.

NRF Spectra in ^{208}Pb

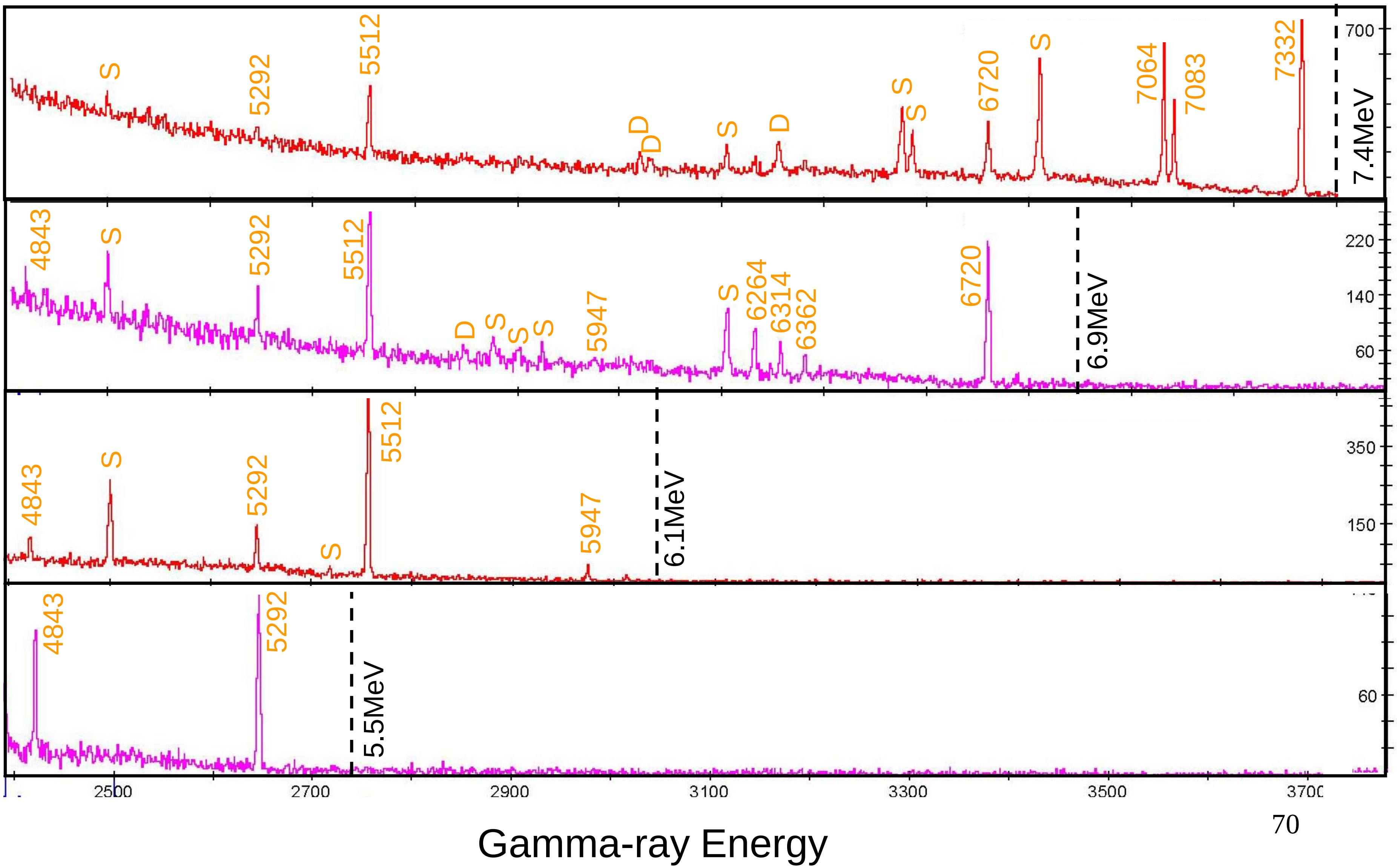

E1/M1 Determination

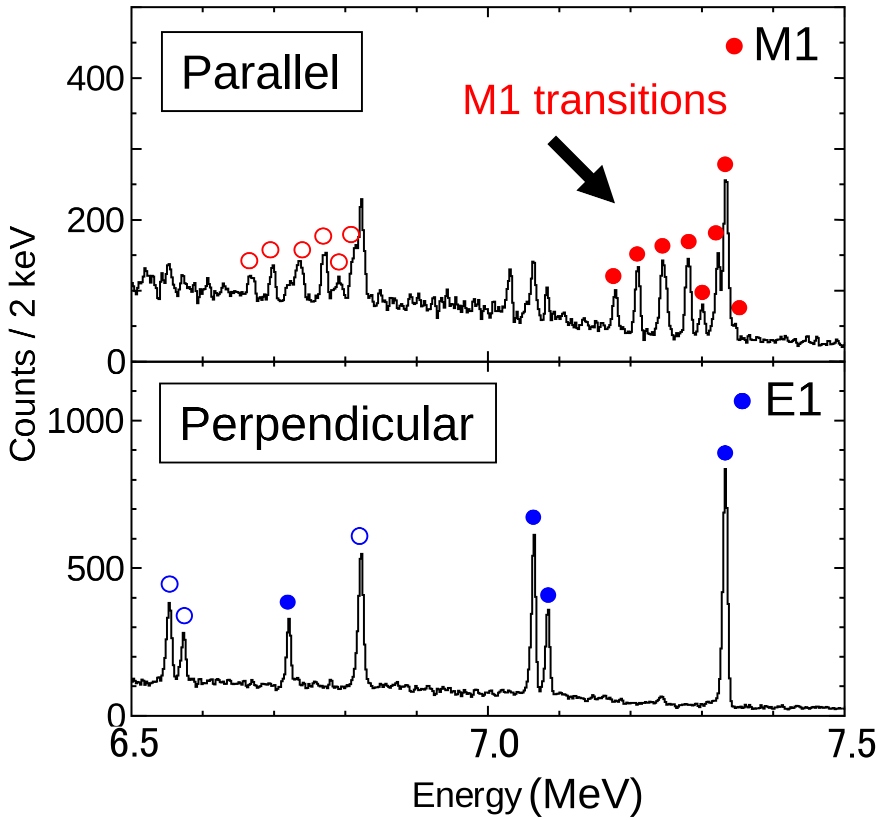

$$Asym. = \begin{cases} +0.85 \text{ for } M1, E2 \text{ transitons} \\ -0.85 \text{ for } E1 \text{ transitions} \end{cases}$$

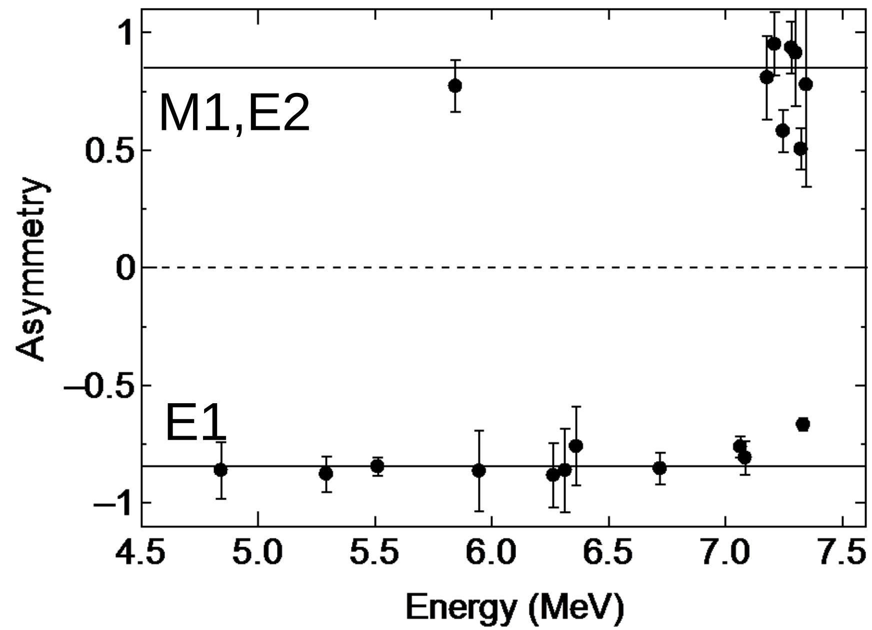

Measured asymmetry A' is less than unity because of the finite detector solid angle.

$$A' = PA = \begin{cases} +P \text{ for } M1, E2 \text{ transitons} \\ -P \text{ for } E1 \text{ transitions} \end{cases}$$

$$0 < P < 1$$

M1/E2 Assignment

Intensity asymmetry is similar for M1 and E2, but angular correlation is different.

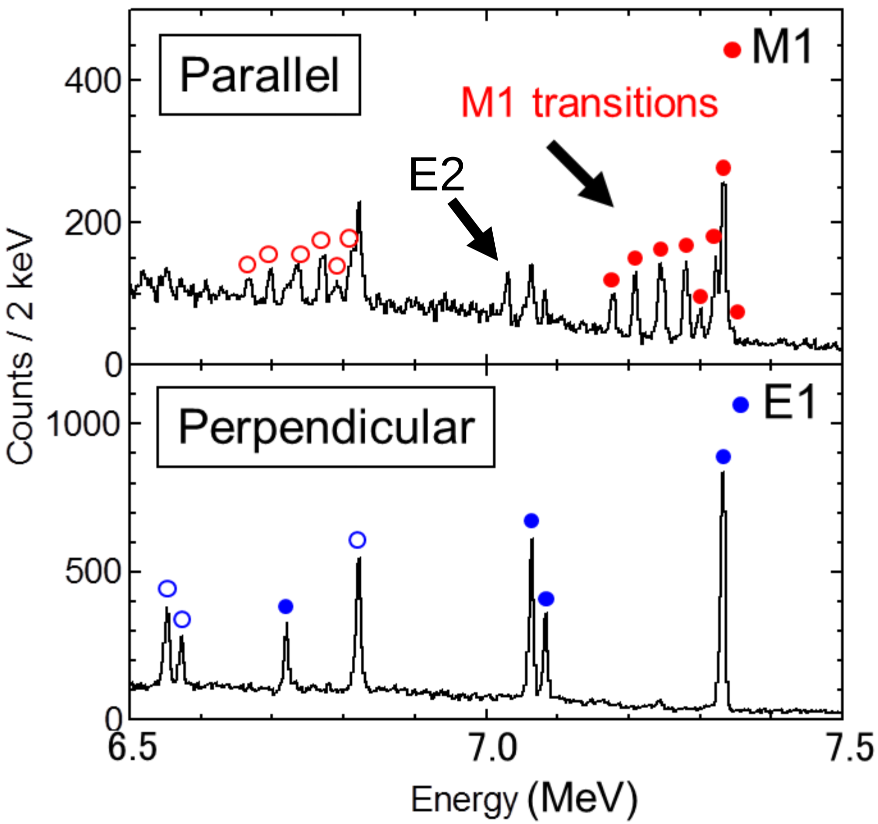

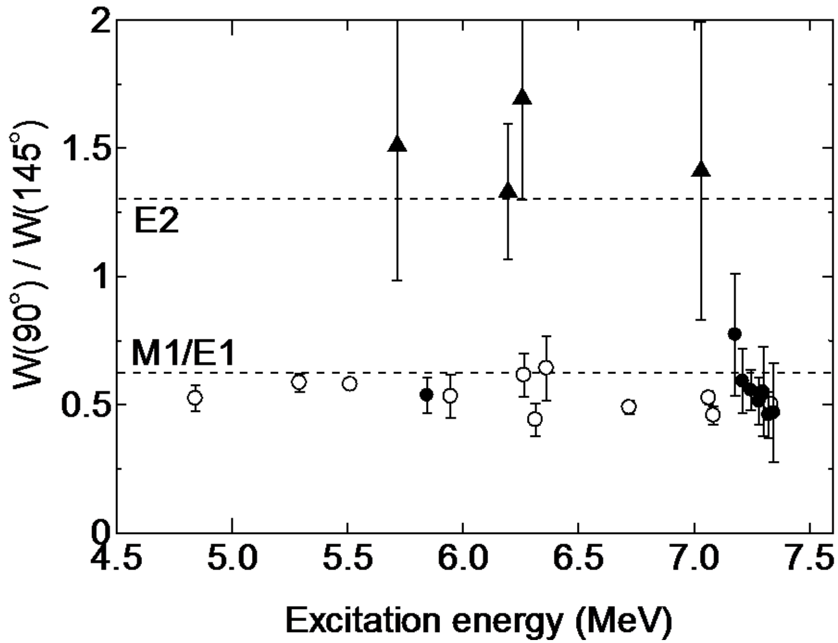

$$\frac{W(90^\circ)}{W(145^\circ)} = 0.6$$ for dipoles

$$\frac{W(90^\circ)}{W(145^\circ)} = 1.3$$ for quadrupoles

T. Shizuma et al., Phys. Rev. C 78 061303(R) (2008)

M1 Strength in ^{208}Pb

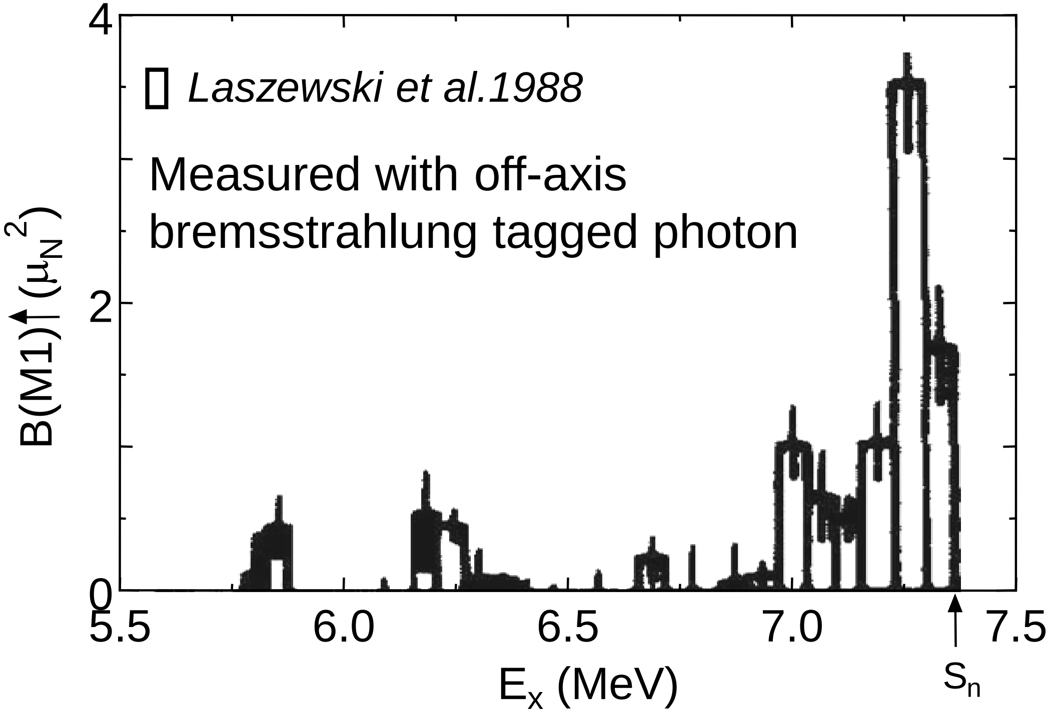

$B(M1)=8.8^{+1.0}_{-0.8}\,\mu_N^2$ (E_x=6.7-7.4MeV) *Laszewski et al., PRL61, 1710 (1988).*

Bremsstrahlung photon is partially linearly polarized at off-axis component.

M1 Strength in ^{208}Pb

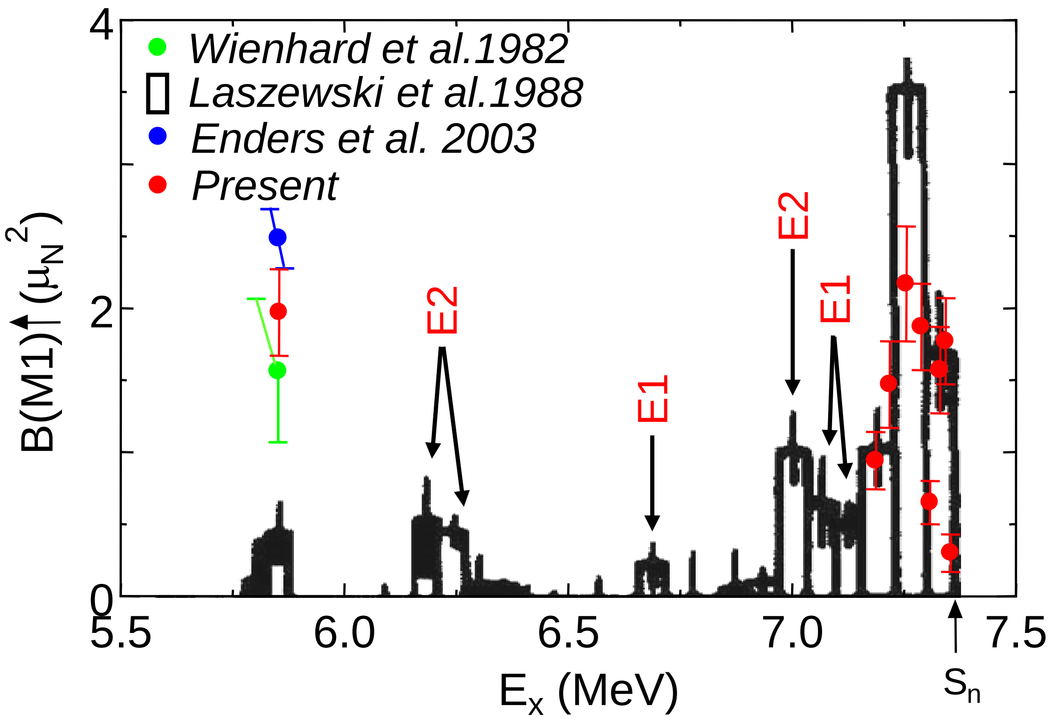

$B(M1)=8.8^{+1.0}_{-0.8}\ \mu_N^2\ (E_x=6.7\text{-}7.4\mathrm{MeV})$ *Laszewski et al., PRL61, 1710 (1988).*

→ $B(M1)=\sim 6\ \mu_N^2$ at $E_x=7.1\text{-}7.4\mathrm{MeV}$

$B(M1)=11.1\pm 0.5\ \mu_N^2\ (E_x=7.1\text{-}7.4\mathrm{MeV})$ this experiment

T.Shizuma et al., PRC 78 061303(R) (2008).

Magnetic Dipole Mode

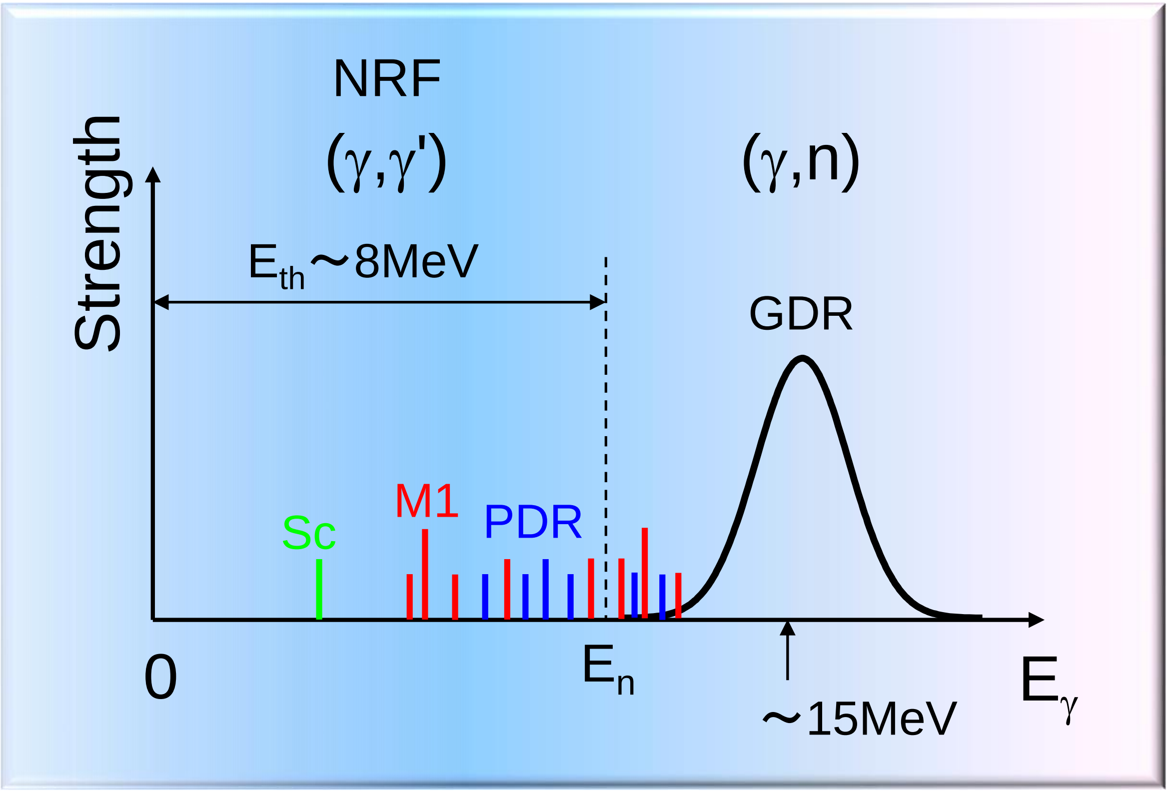

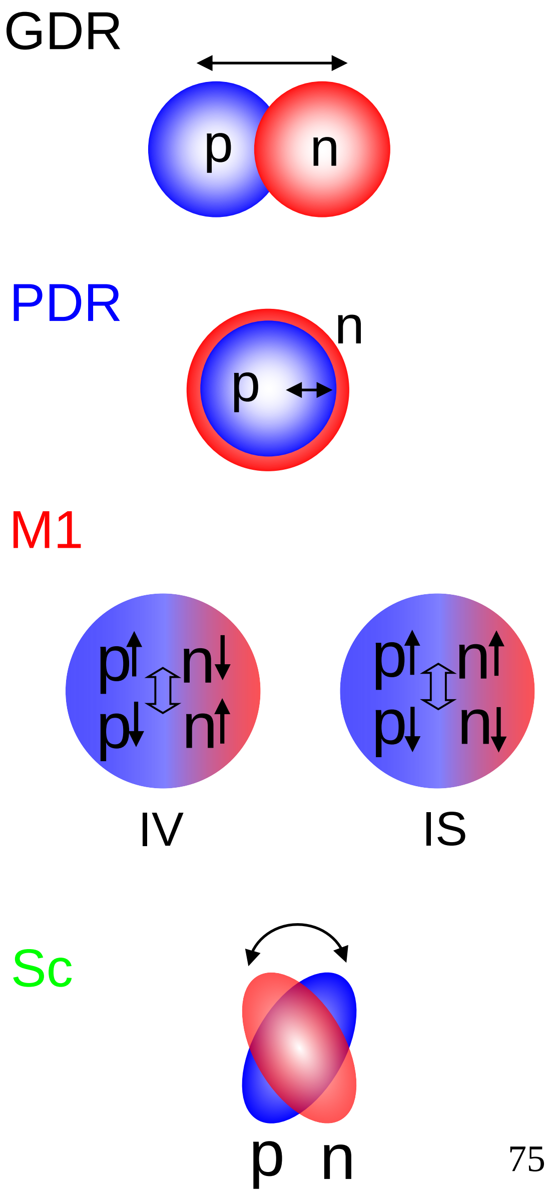

M1: Spin-flip magnetic dipole mode (M1, spin part)

intrinsic spin oscillation of protons and neutrons

Sc: Scissors mode (M1, orbital part)

orbital spin rotation in deformed nuclei

Spin-Flip M1 Mode

Particle-hole excitation across the major shell

Particle state : (ℓ+1/2)

Hole state : (ℓ-1/2)

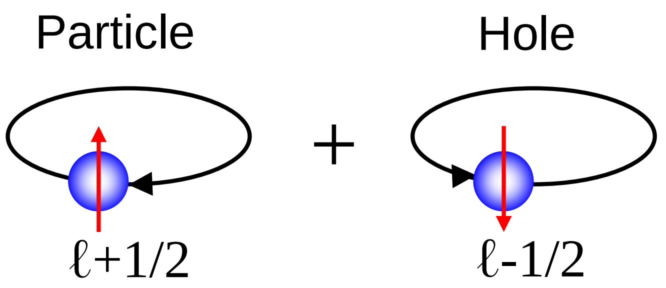

Shell-model transition of (ℓ+1/2)→(ℓ-1/2) which flips the intrinsic spin plays a role. ex. $f_{7/2} \rightarrow f_{5/2}$ transition in fp shell nuclei

⬇ Interaction between proton and neutron p-h states

Two types of intrinsic spin oscillation;

In phase : Isoscaler (IS)

Out-of-phase: Isovector (IV)

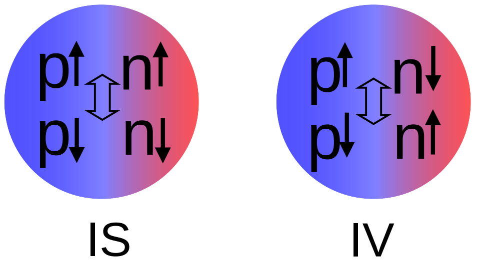

Magnetic Dipole Operator

$$T(M1) = \sum_{i=1} \left\{ g_l(i)\vec{l}_i + g_s(i)\vec{s}_i \right\} = T(M1)_{IS} + T(M1)_{IV}$$

g_l, g_s: orbital and spin g factors

l, s: orbital and intrinsic spins

$$g_l^p = 1, g_l^n = 0$$

$$g_s^p = 5.586, g_s^n = -3.826$$

$$\begin{aligned}
T(M1)_{IS} &= g_l^{IS}\vec{L} + g_s^{IS}\vec{S} \\
&= \frac{g_l^p + g_l^n}{2}\vec{L} + \frac{g_s^p + g_s^n}{2}\vec{S} \\
&= \frac{1}{2}\vec{J} + \frac{g_s^p + g_s^n - 1}{2}\vec{S} \\
&= \frac{1}{2}\vec{J} + 0.38\vec{S}
\end{aligned}$$

$$g_l^{IS} = \frac{g_l^p + g_l^n}{2}$$

$$g_s^{IS} = \frac{g_s^p + g_s^n}{2}$$

$$\vec{J} = \vec{L} + \vec{S}$$

Magnetic Dipole Operator

$$T(M1)_{IV} = g_l^{IV}\vec{L} + g_s^{IV}\vec{S}$$

$$= \sum_i t_z(i)\vec{l}_i + \left(g_s^p - g_s^n\right)\sum_i t_z(i)\vec{s}_i$$

Gamow-Teller

$$= \frac{1}{2}\left(\vec{L}_p - \vec{L}_n\right) + \frac{g_s^p - g_s^n}{2} T(M1)_{\Delta T_z = 0}$$

$$= \frac{1}{2}\left(\vec{L}_p - \vec{L}_n\right) + 4.71 T(M1)_{\Delta T_z = 0}$$

orbital part spin part

$$g_l^{IV} = \frac{g_l^p - g_l^n}{2} = \frac{1}{2}$$

$$g_s^{IV} = \frac{g_s^p - g_s^n}{2} = 4.71$$

$t_z = 1/2$ for protons

$t_z = -1/2$ for neutrons

The isovector component has larger contribution to the magnetic dipole strength than the isoscaler component, because of the large coefficient for the spin part compared to the isoscaler spin part.

$$T(M1)_{IS} = \frac{1}{2}\vec{J} + 0.38\vec{S}$$

spin part

Comparison of M1 Strength

orbital vs. spin

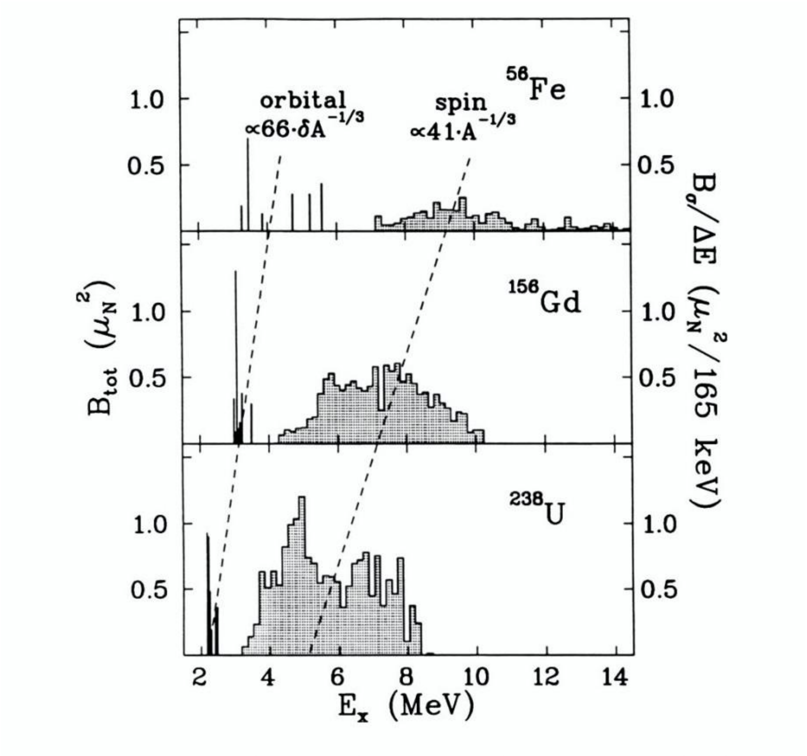

Spin strength has the large fraction for all nuclei.

A. Richter, Prog. Part. Nucl. Phys. 34, 261(1995).

isoscalar vs. isovector

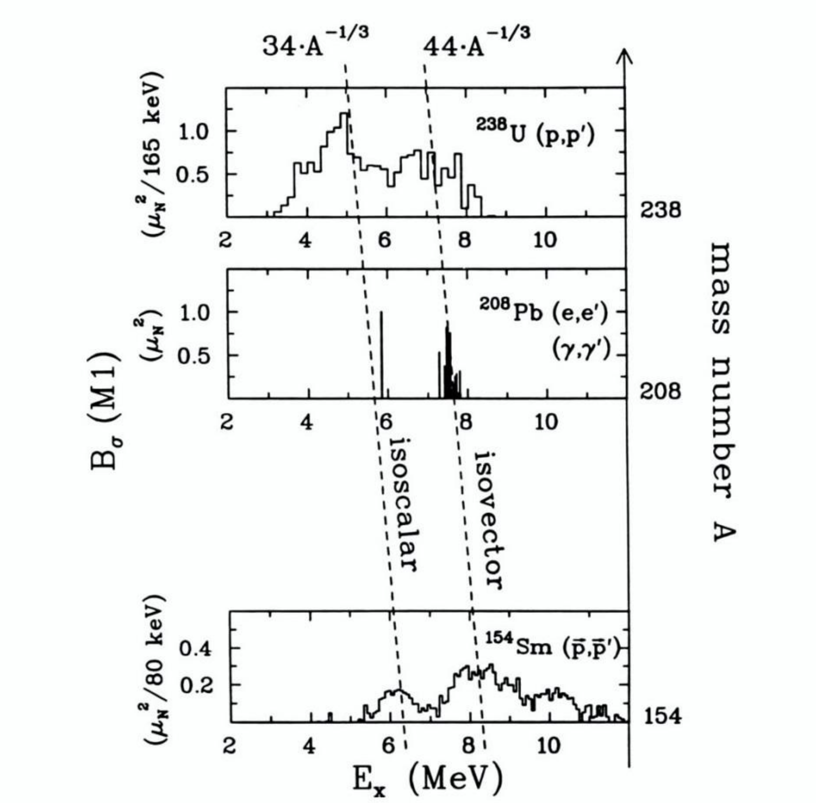

^{238}U, ^{154}Sm: High level density, deformed nuclei

^{208}Pb: Low level density, spherical

2.4. Application of NRF; Nondestructive Assay

Nuclear resonance fluorescence (NRF)

Isotope-specific identification

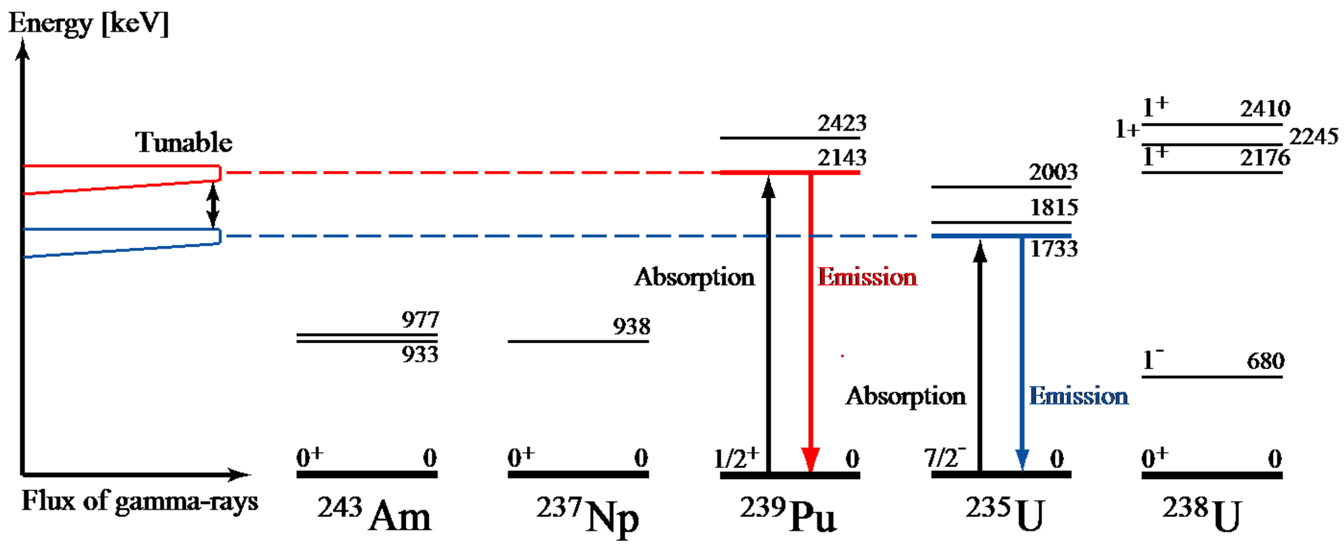

High energy γ rays (MeV) are used: High penetrability

⇨ Applicable for isotope-specific identification of materials shielded by heavy thick metals such as spent nuclear fuel

R.Hajima, et al., J. Nucl. Sci. Tech. 45, 441 (2008).

NRF-Based Detection Methods

Scattering method

NRF γ-rays from the sample are directly measured by using γ-ray detectors.

Transmission method

Transmitted γ-rays are used to irradiate a witness plate consisting of the isotope of interest. NRF γ-rays from the witness plate are measured by γ-ray detectors.

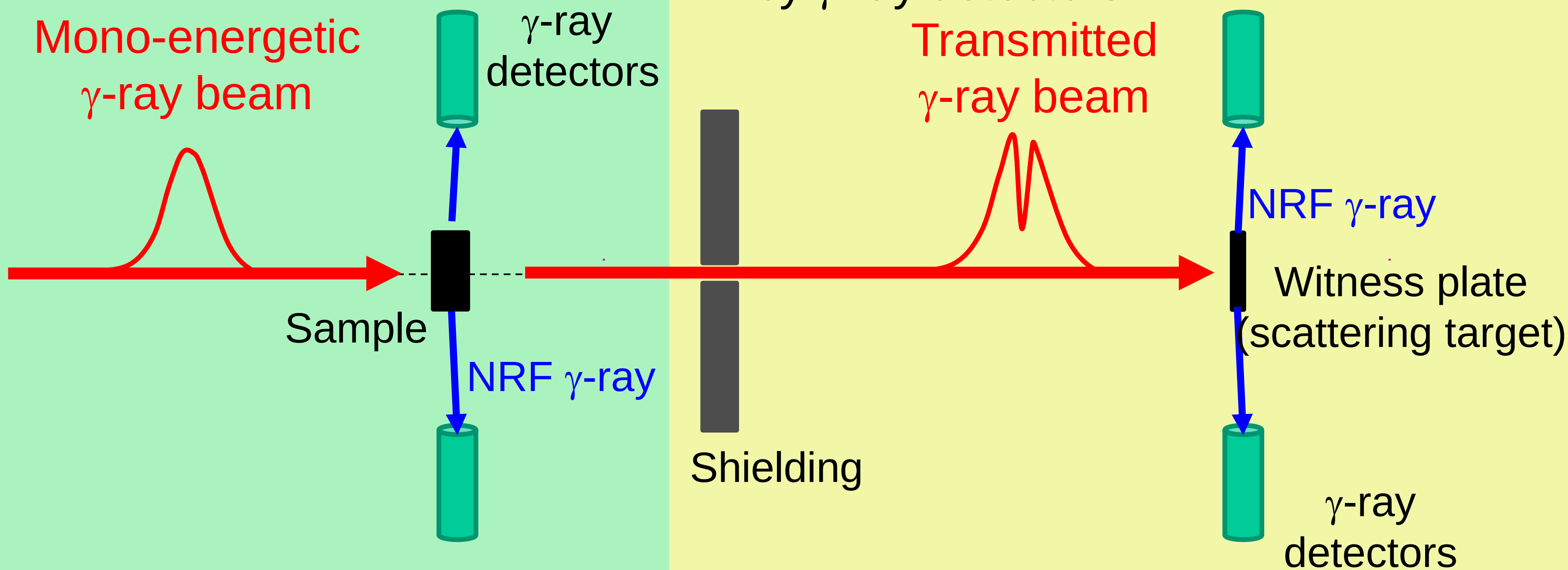

Demonstration of the NDA Method

Experiments at the High Intensity gamma-ray Source (HIgS) facility in Duke University, USA

- Mono-energetic LCS γ-ray beam produced from inverse Compton scattering using intra-cavity FEL photons
  - E_γ:1.8-60 MeV
  - $\Delta E/E$: a few %
  - I_γ: $\sim 10^{6-7}$ photons/s

Measured Beam Profile

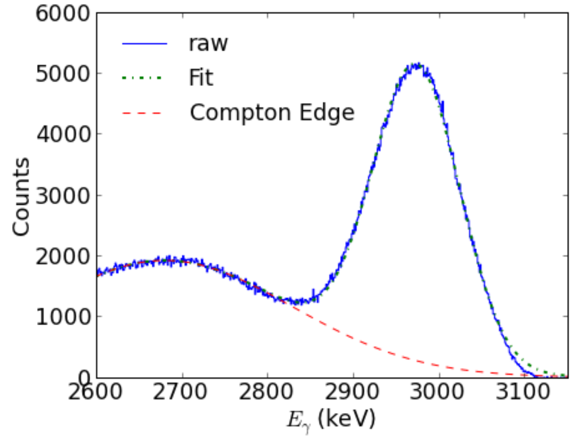

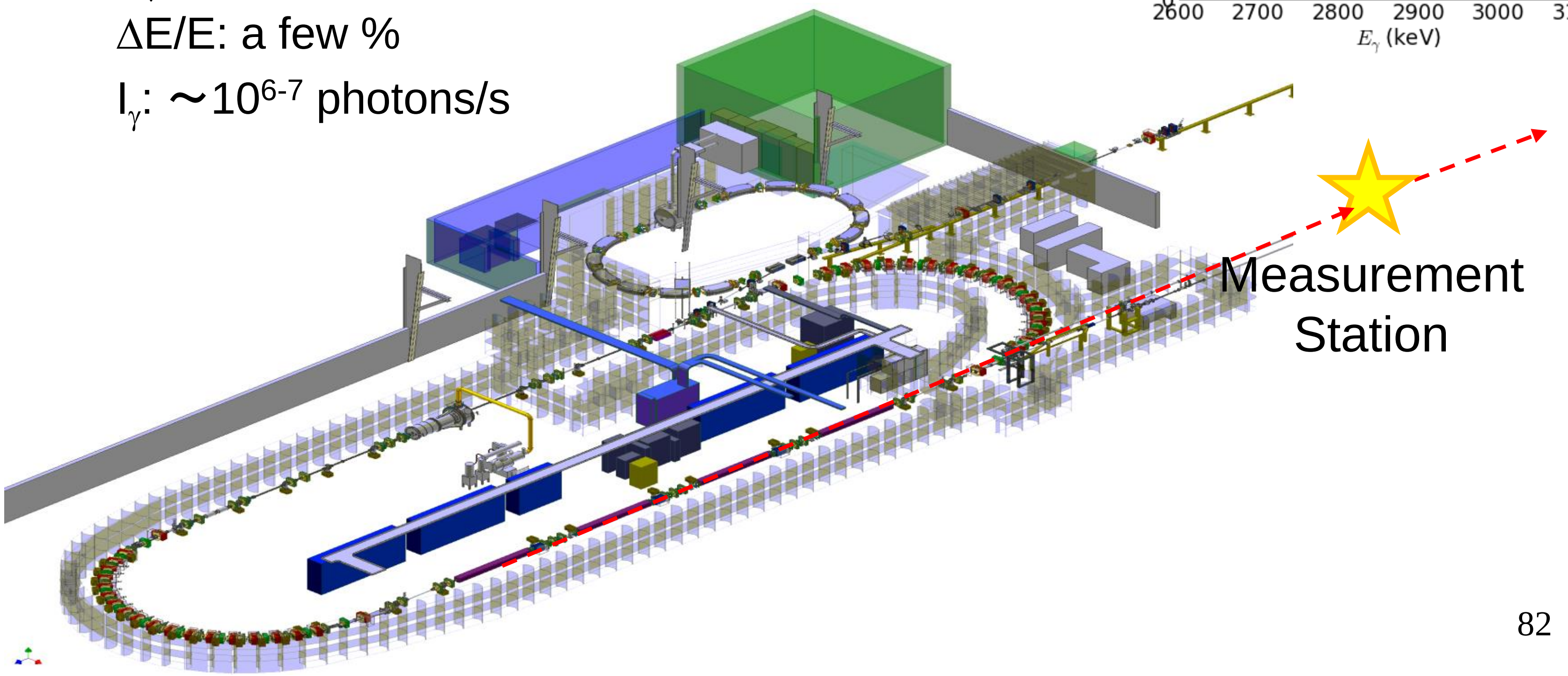

Experimental Setup for Scattering Method

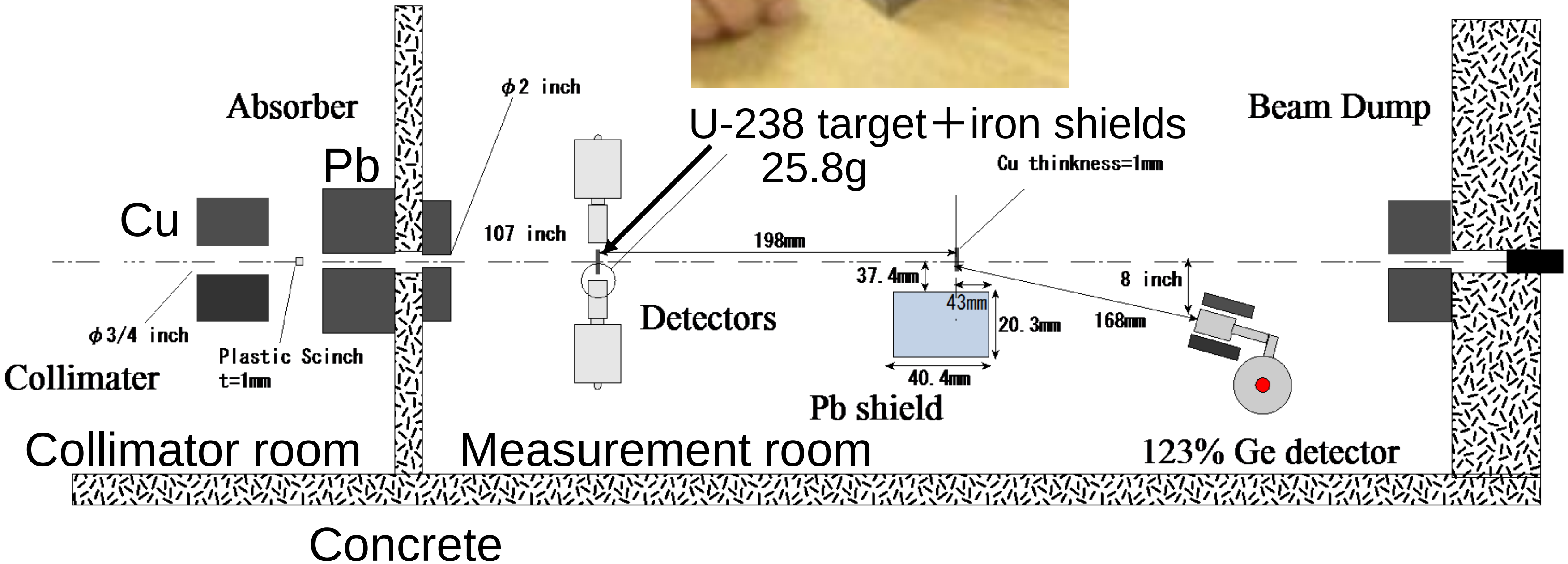

U-238 Target and Ge detectors

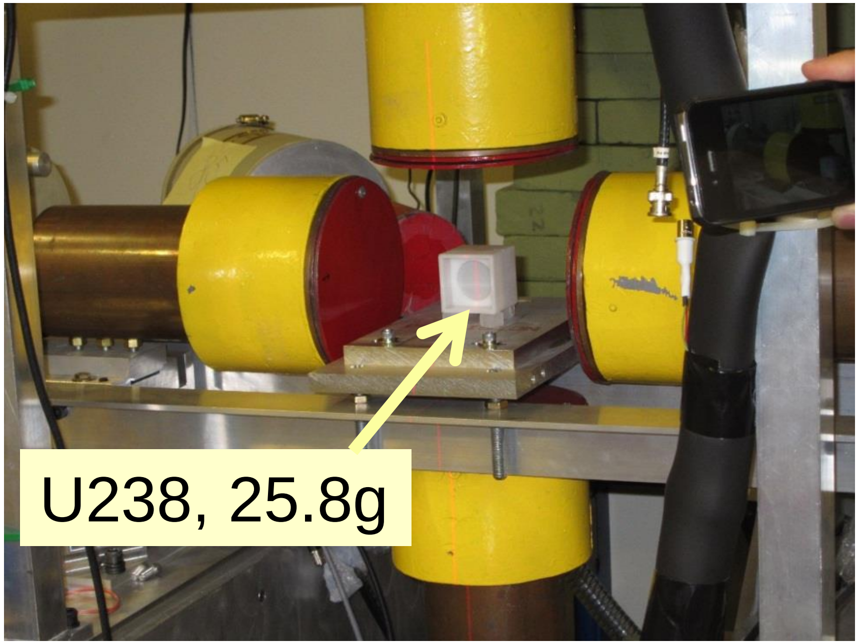

Ge detector and U-238 target with iron shields

- Four Ge detectors with relative efficiencies of 60% placed at 90 degrees.
- Covered with Pb sheets
- Pb and Cu absorbers attached in front of the Ge detectors

View from the downstream

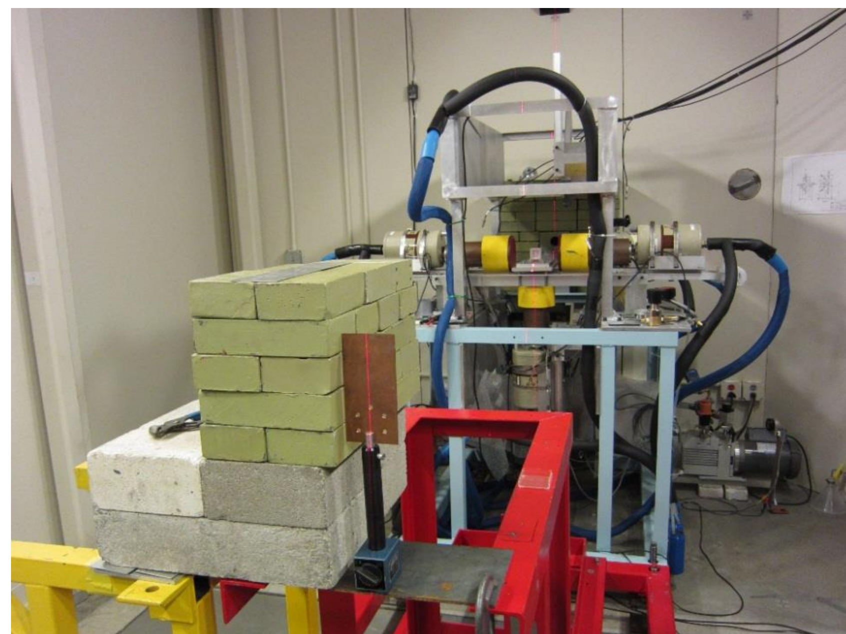

Experimental Results

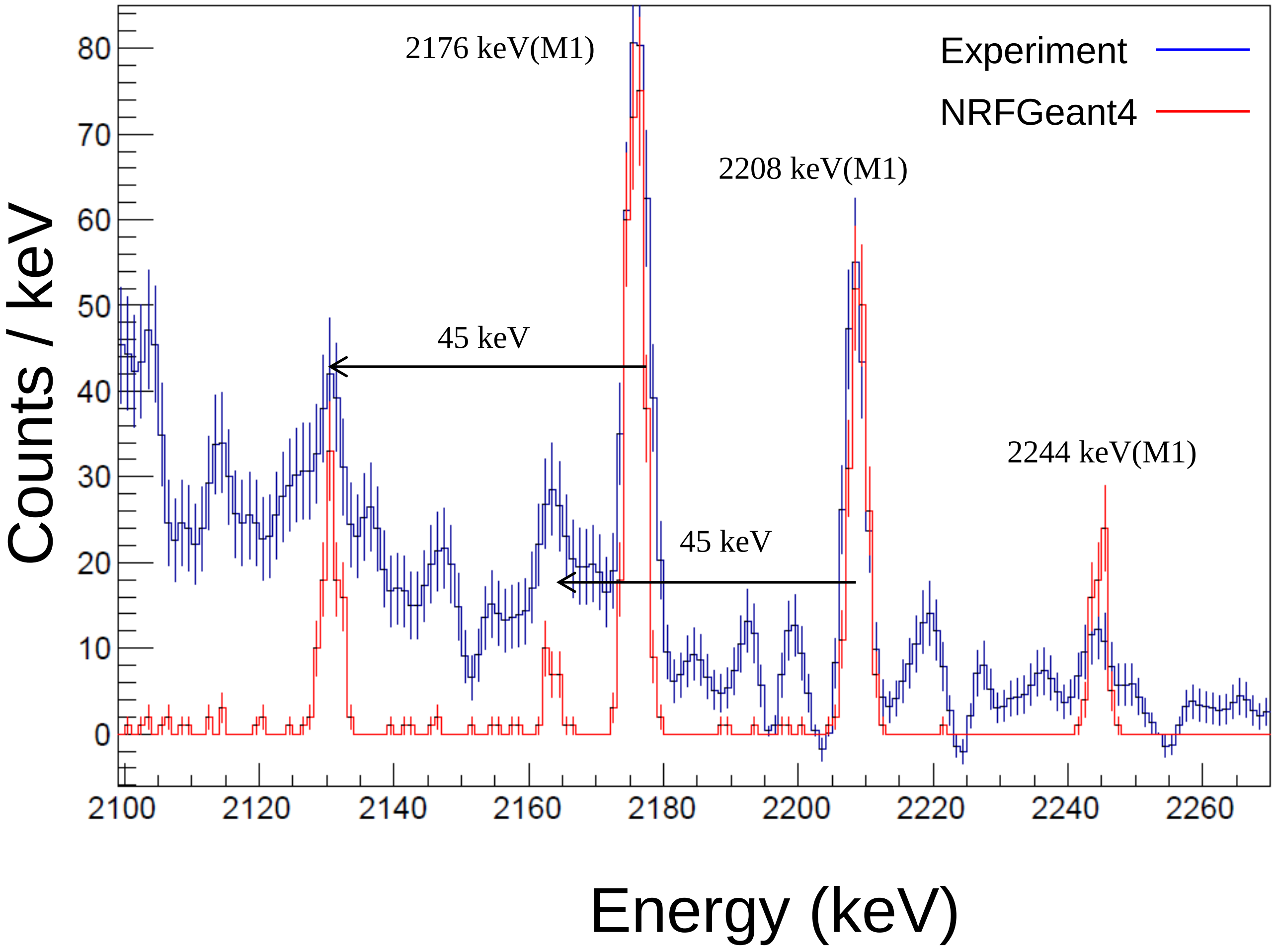

Transmission Measurement for Pu-239

Experimental setup

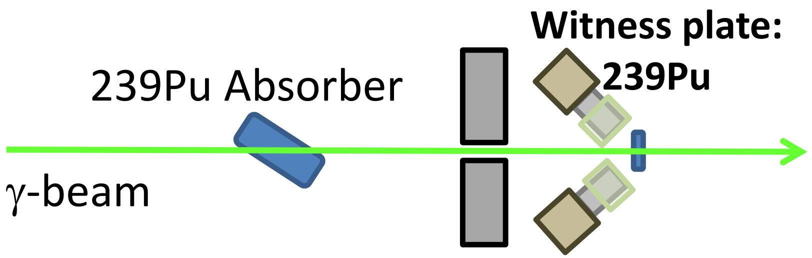

LCS γ-ray beam: E∼2.2 MeV, ΔE/E∼4%,
I_γ∼10^6 photons/sec

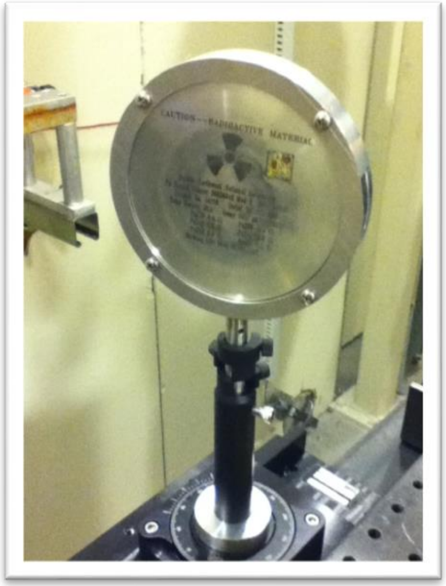

183 g ^{239}Pu
35.62 Curies total (1.3 TBq)

NRF energy spectrum

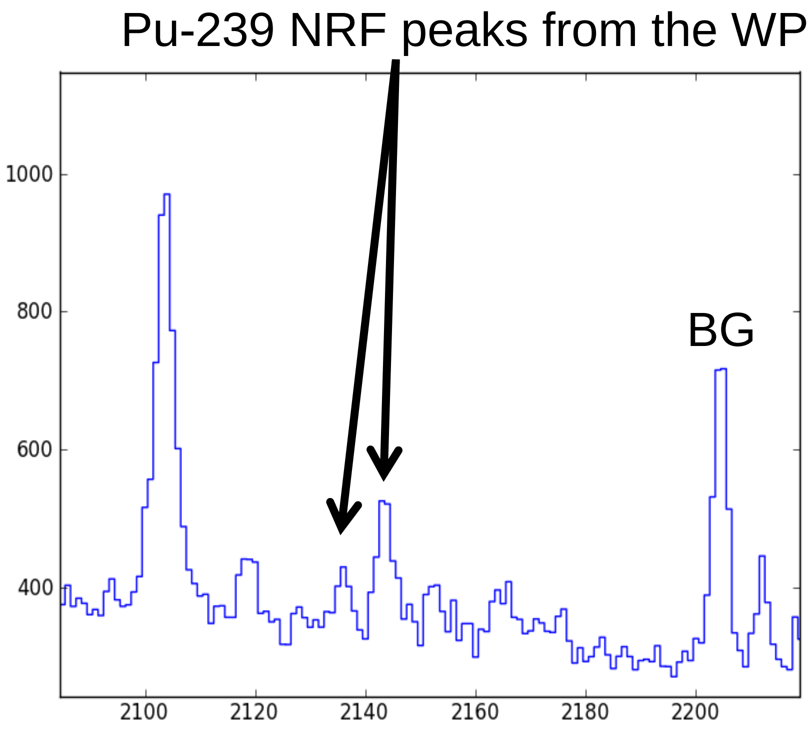

C.T. Angell, et al., proceedings of "Nuclear Physics and gamma-ray sources for nuclear security and nonproliferation", World Scientific, P.133 (2014).

Transmission Measurement for Al-27

LCS γ-ray beam: E～2 MeV, $\Delta E/E$～4%,
I_γ～10^6 photons/sec

Absorption targets: Al, Pb, concrete, stainless
for a TMI canister simulant

Witness plate: Al

Material	Thickness (cm)
Aluminum	2.5
Concrete	10.9
Stainless Steel	2.5
Lead	3.2
Water	15.2

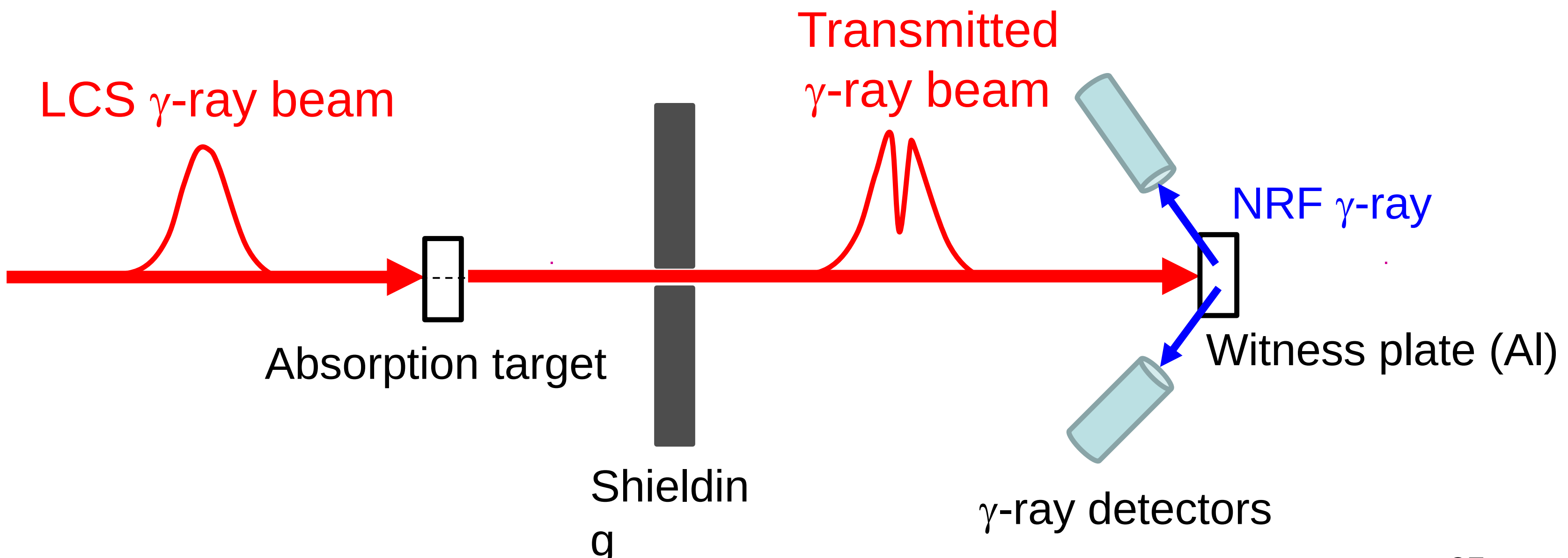

NRF γ-rays from the Al witness plate were measured by HPGe detectors.

Experimental Results

NRF γ-ray spectrum

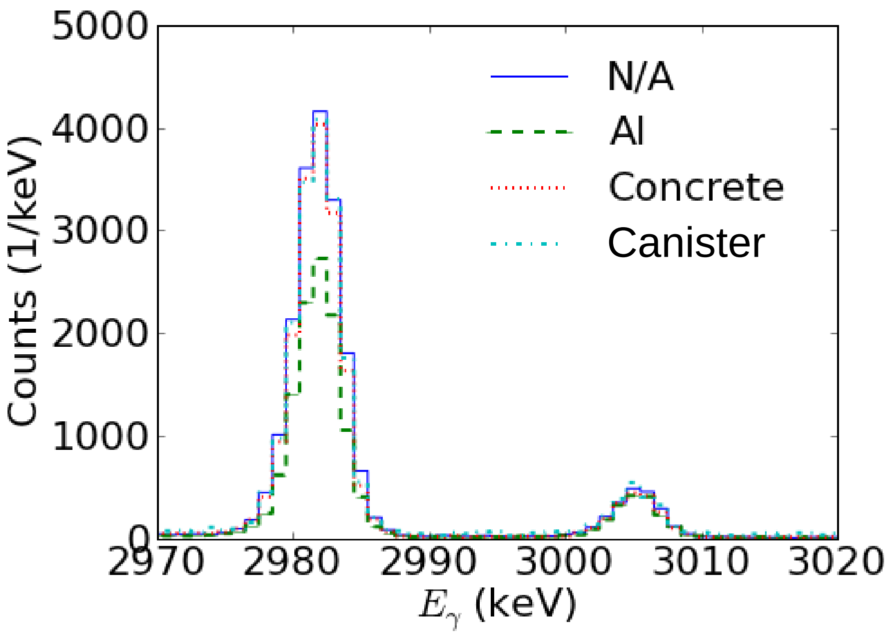

Compared with no absorber case (N/A),
•Decrease of the Al NRF γ-ray intensity verified for the Al absorption target
•Small difference verified for the concrete and canister absorption target

Measurement is unaffected by materials such as concrete and stainless.

C.Angell, et al., NIMB347,11 (2015).

Absorption amounts of the 2982 keV resonance

Absorber	Expected	Measured
Canister	0	0.01±0.01±0.03
Concrete	0.04±0.01	0.05±0.01±0.02
Alminum	0.345±0.006	0.358±0.005±0.02

2.5. NRF Data in Actinides

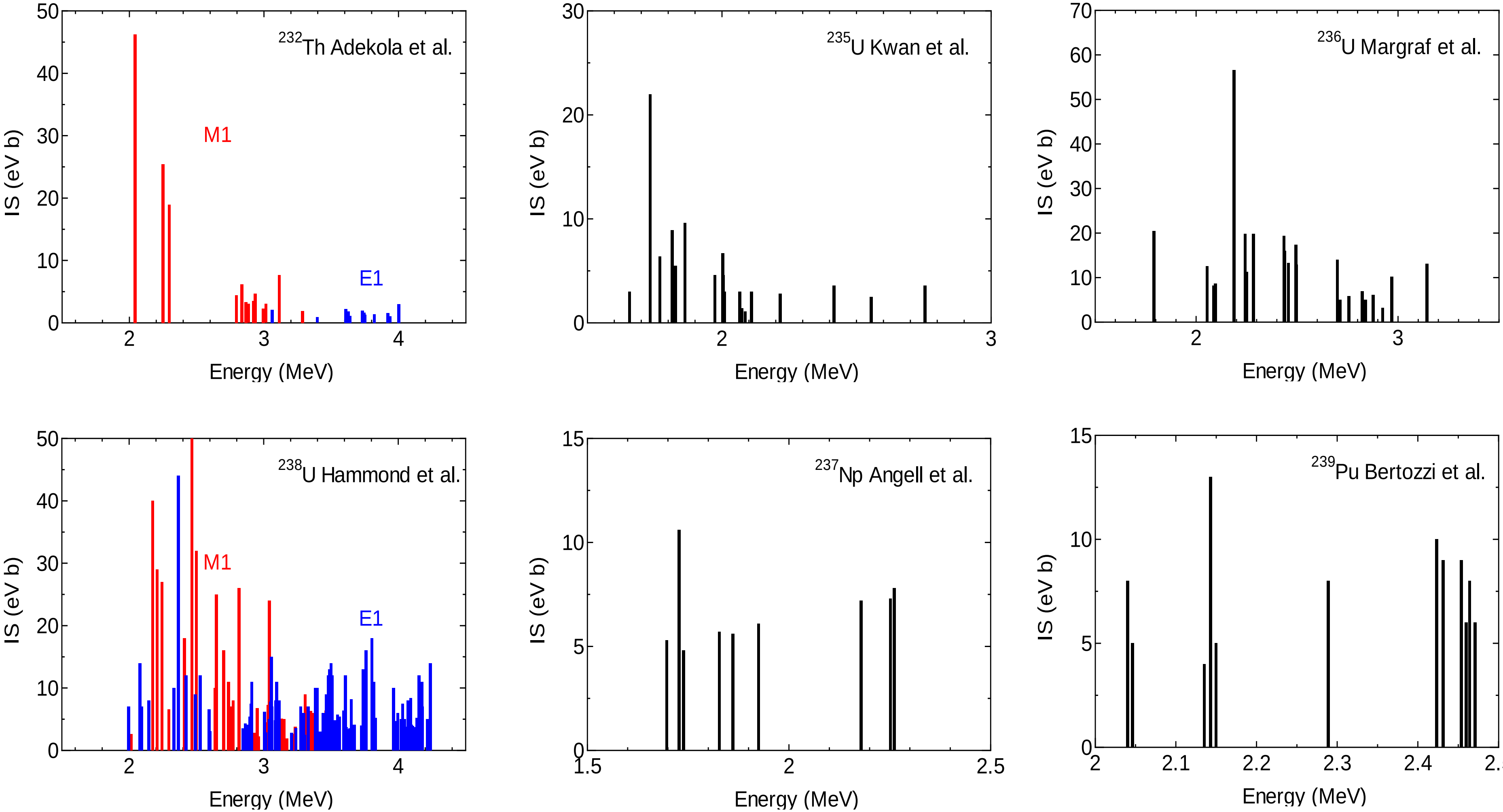

Systematic observation of M1 resonances (scissors mode) with integrated cross sections of 10 to 50 eV barn at excitation energies between 2 and 2.5 MeV.

Compilation of NRF data in EXFOR

A.Makinaga, Hokkaido Univ.

Compilation of the Nuclear Resonance Fluorescence (NRF) in Actinides

Proposer : S. P. Simakov, N. Otsuka (IAEA) IAEA NRDC WP2011-1, CP-D/703

- NRF – Excitation by photons of specific resonance in nucleus (E1 dipole, M1 scissor mode in deformed nuclei) and consequent decay by prompt g-ray emission to the ground or excited states => (g,g), (g,g')
- First time observed – in 238U and 232Th by R.D. Heil et al., NP A476(1988)39
- Practical importance- non-destructive assay of clandestine nuclear, toxic and explosive materials (safeguards of nuclear materials in IAEA mission)
- NRF is being added to ENDF photon library and MCNPX
- ~10 experiments performed with Bremsstrahlung and Laser-Compton Scattering

Target	Beam	E resonance MeV		Lab.	Author	ENTRY
U238	BRST	2.043	2.468	2GERIFS	R.D.Hel+	G0028.002
U236	BRST	1.791	3.143	2GERIFS	J.Margraf+	G0027.002
U238	BRST	1.782	1.846	2GERIFS	A.Zilges+	G0026.002
U235	BRST	1.687	1.862	2GERTHD	O.Yevetska+	G0026.003
U235	BRST	1.656	2.006	1USAMIT	W.Bertozzi+	L0139.002
Pu239	BRST	2.040	2.471	1USAMIT	W.Bertozzi+	L0139.003
Np237	BRST	1.689	2.506	1USAMIT	C.T.Angell+	L0155.002
Th232	LCS	2.044	4.002	1USATNL	A.S.Adekola+	L0159.002
U235	LCS	1.656	2.755	1USATNL	E.Kwan+	L

北海道大学

3.1. Photonuclear Reaction Data with Future Light Sources

ERL-based intense monoenergetic LCS photon source

Energy recovery electron linac (ERL)

Reuse of the electron power for acceleration

Laser enhancement cavity

Enhancement of the laser power inside cavity

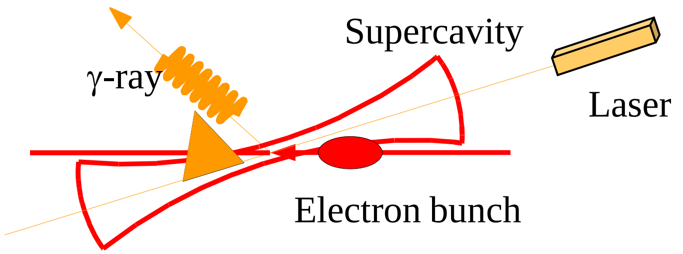

⇨ Increase the electron and laser densities at the collision

$E_\gamma \sim 2\text{MeV}$、$I \sim 10^{13}$ ph/s

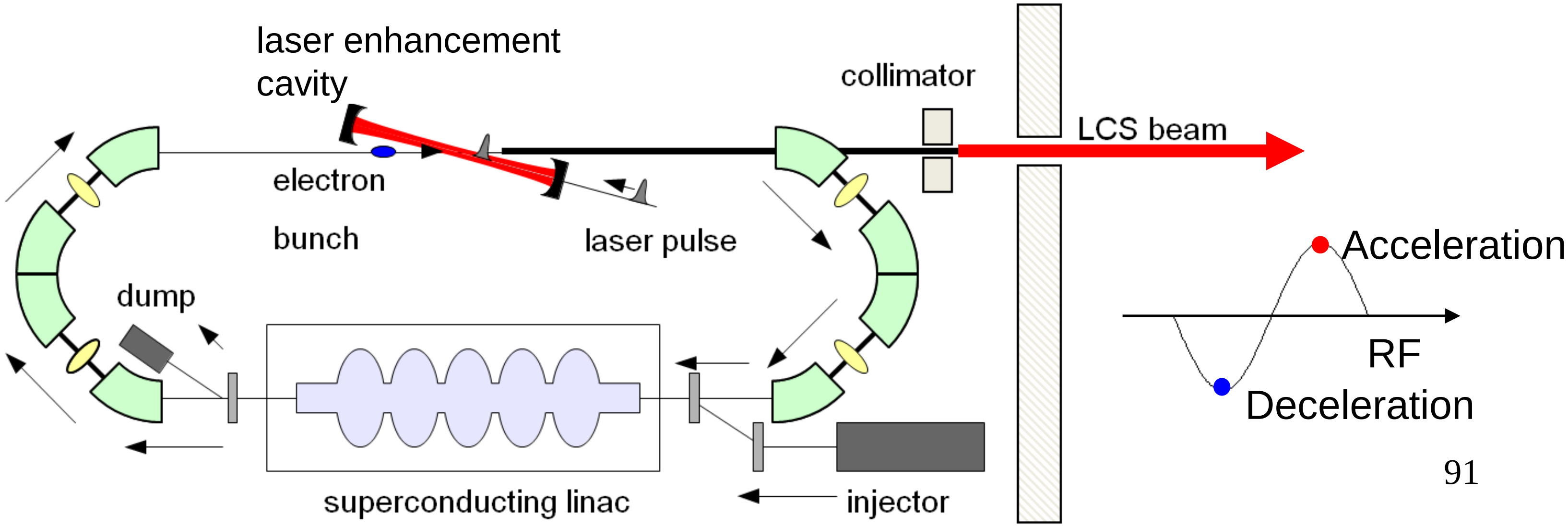

Demo-Experiment at cERL

cERL: Compact ERL at High Energy Accelerator Research Organization (KEK)

- Electron beam = 20 MeV, 10 mA
- Expected LCS γ: 7keV with ~10^{11} ph/s

Installation of accelerator components and 20-MeV electron recirculation were completed by 2013.

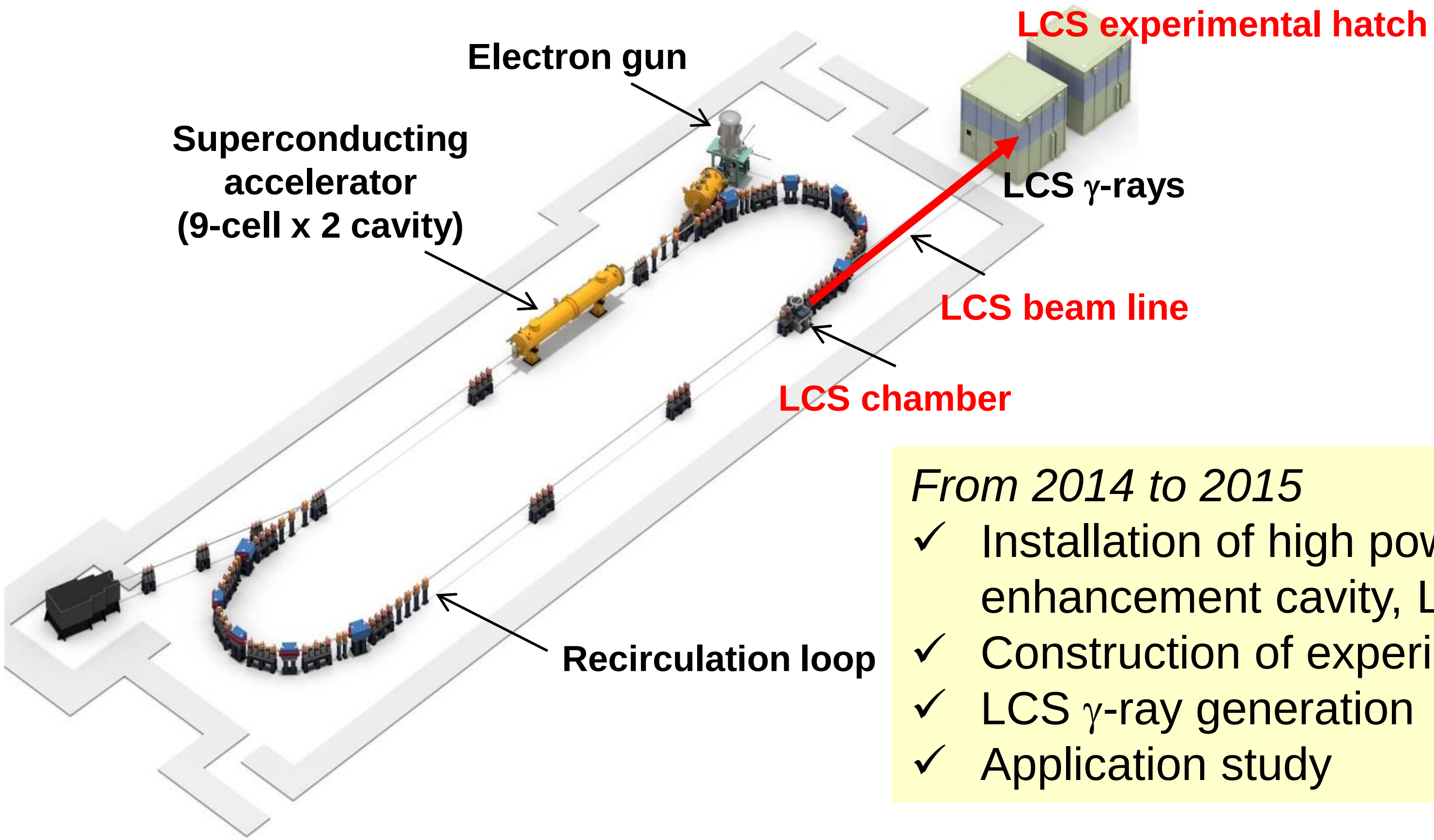

From 2014 to 2015

- ✓ Installation of high power laser, enhancement cavity, LCS beam line
- ✓ Construction of experimental hatch
- ✓ LCS γ-ray generation
- ✓ Application study

Equipment for LCS γ-Ray Generation

Electron Gun
(500kV,10mA)

Main SC Linac
(9 cell x 2 cavity)

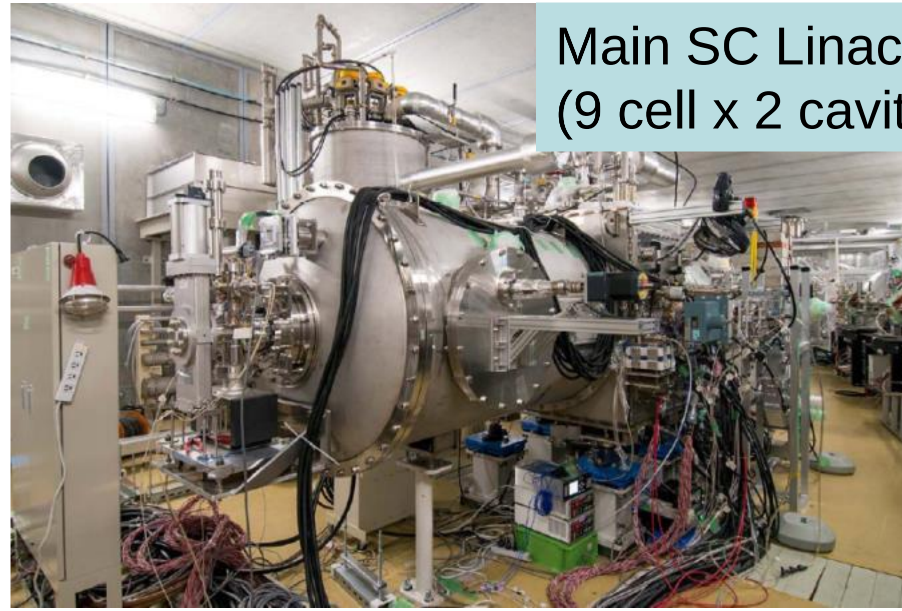

Enhancement
Cavity

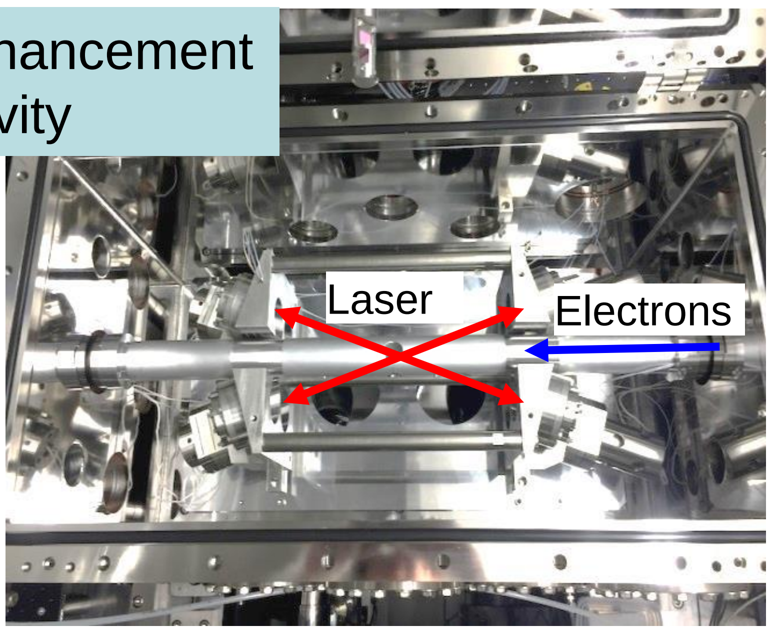

Experimental Hatch & Monitor Room

LCS Photon Beam Line

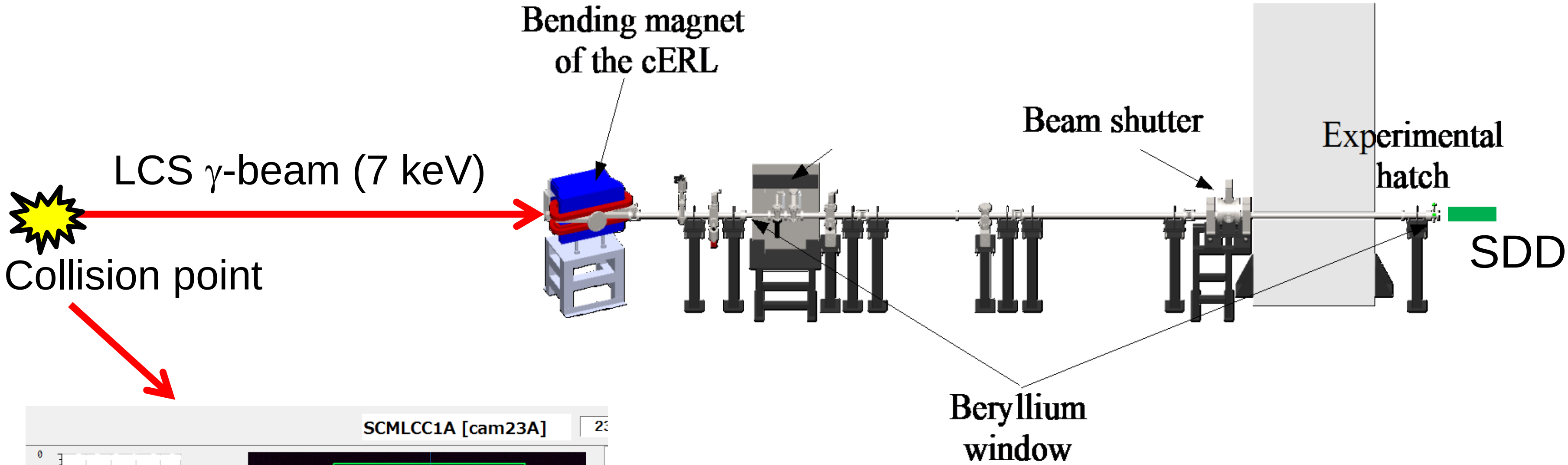

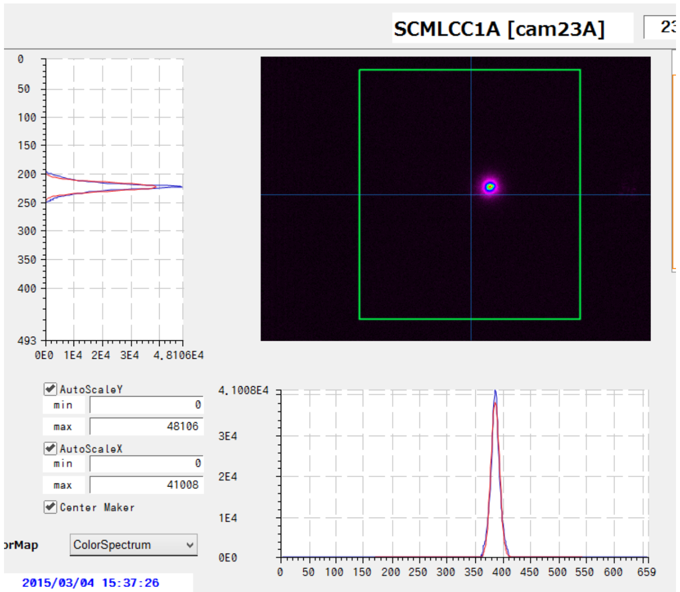

Electron beam spot at the collision point

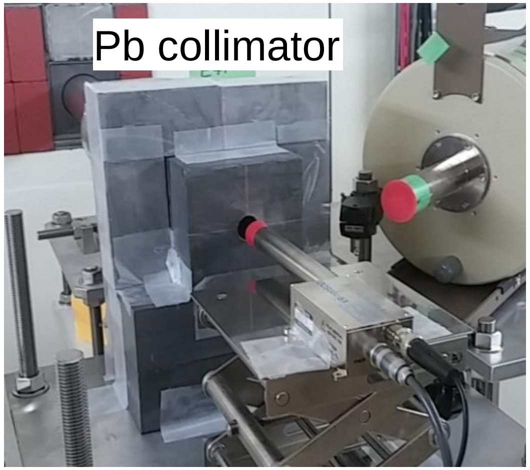

Silicon drift detector (SDD)

AMPTEK XR-100 SDD
Active diameter: 4.66mm
Ω=0.15mrad
Thickness: 500μm
Energy resolution:
125-140eV @5.9keV

LCS Photon Spectrum

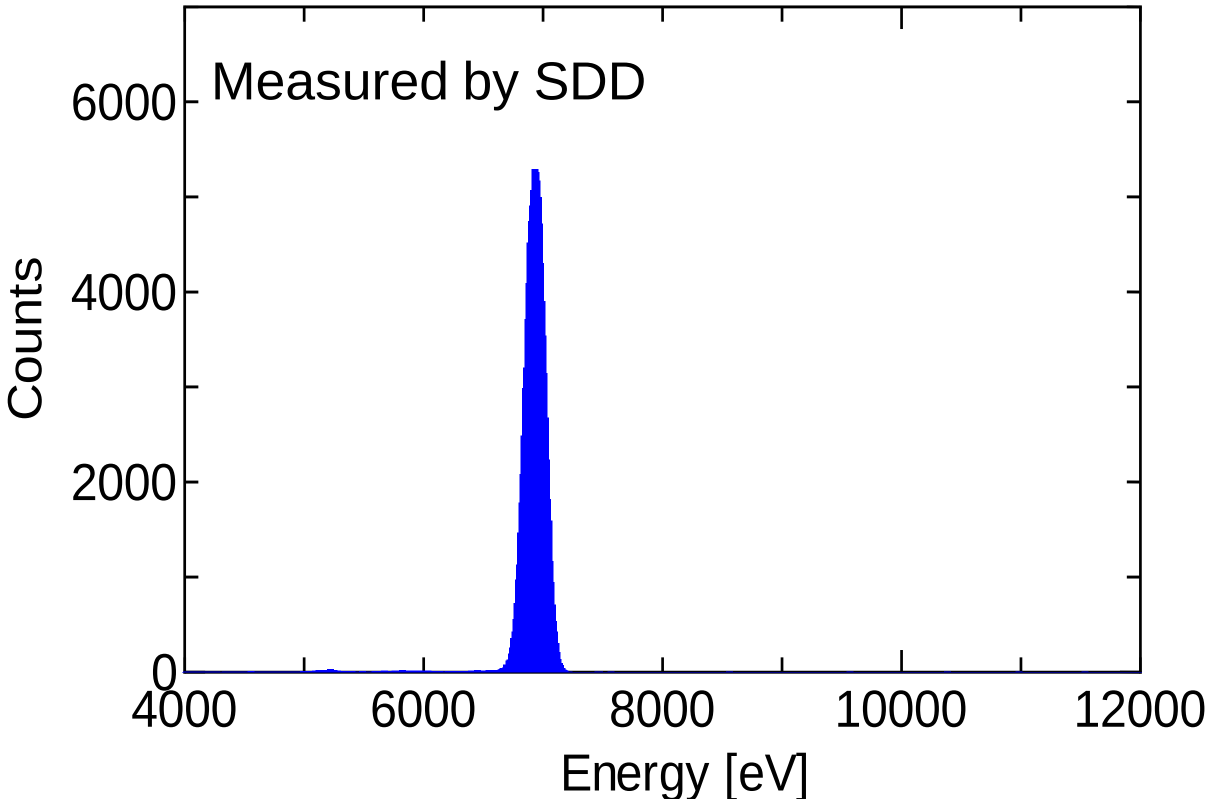

Electron
Energy: 20 MeV
Beam current: 58 μA
Bunch length: 2 ps
Spot size: 30 μm
Emittance: 0.4 mm mrad
Repetition rate: 162.5 MHz

Laser
Wave length: 1064 nm
Output power: 10 kW
Pulse length: 5.65 ps
Spot size: 30 μm
Collision angle: 18°
Repetition rate: 162.5 MHz

E = 6.9 keV
ΔE =173 eV (FWHM)
1200 cps @ ϕ4.66mm

LCS Photon Spectrum

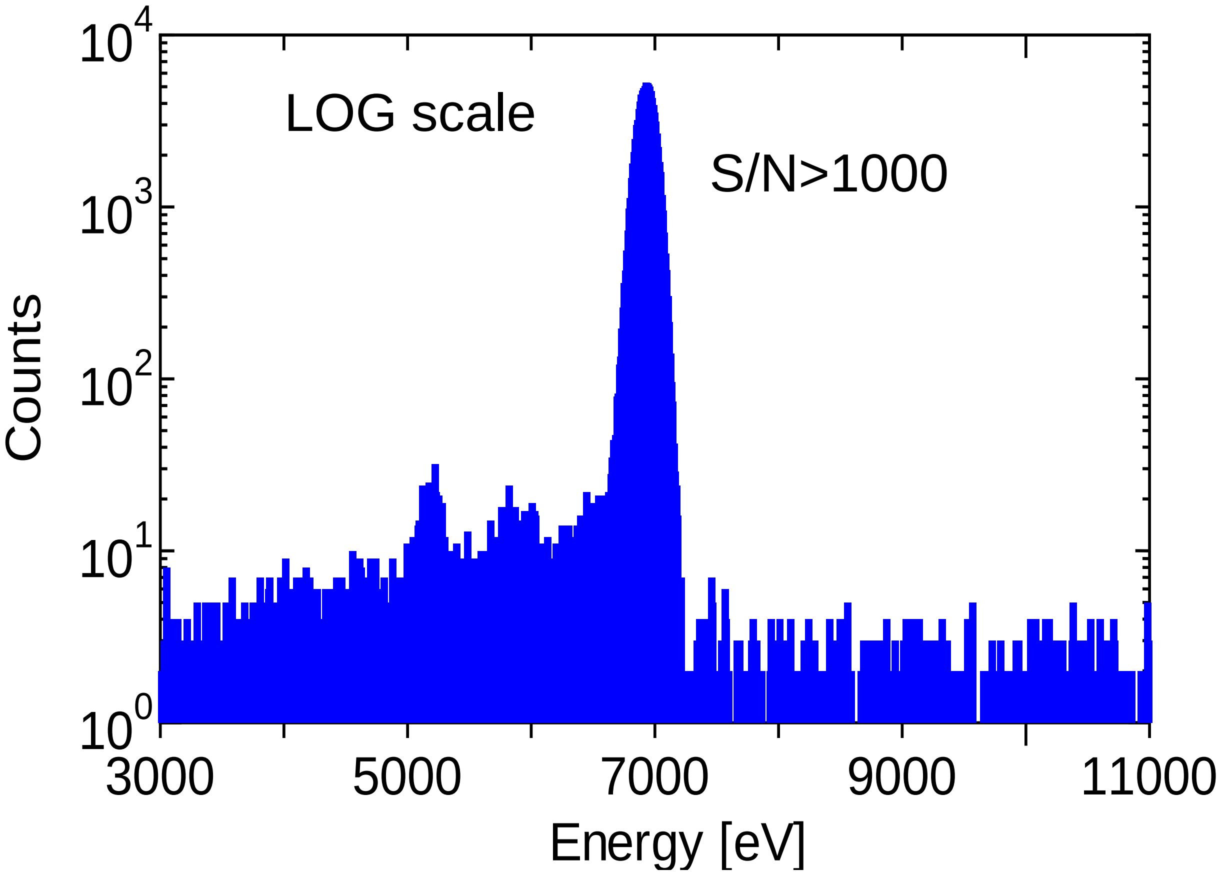

LCS photons
Peak energy: 6.9 keV
Flux at SDD: 1200 cps
Total flux: 4.25×10^7 ph/s

Estimated total flux for 10 mA electron and 100 kW laser operation:
7×10^{11} ph/s

Future Light Sources

	E_e(GeV)	E_γ(MeV)	$\Delta E_\gamma/E_\gamma$(%)	$\Delta\tau$(ps)	I_γ(/s)
AIST	0.5~0.8	4~20	5~10	$\sim 60\times10^3$	$\sim 10^6$
LASTI	1~1.5	1.7~80	5~10	$\sim 10\times10^3$	$\sim 10^6$
HIγS*	0.24~1.2	1~100	0.8~10		$10^4\sim10^8$

**H.R.Weller et al., Prog. in Part. and Nucl. Phys. 62(2009)257.*

	E_e(GeV)	E_γ(MeV)	$\Delta E_\gamma/E_\gamma$(%)	$\Delta\tau$(ps)	I_γ(/s)
ELI-NP[a]	0.6	0.5~13.2 or 19.5	0.1	2	$\sim 10^{12}$
HIγS2[b]	0.24~1.2	2~12	<0.5		$10^{11}\sim10^{12}$
ERL-LCS[c]	0.35	~2	<0.1		$\sim 10^{13}$

[a]*ELI-NP Research Activities Description, RA2 High-Brilliance Gamma Source.*
[b]*http://www.tunl.duke.edu/higs2.php*
[c]*R.Hajima, et al., J. Nucl. Sci. Tech. 45, 441 (2008).*

Photonuclear Reaction Data

•High intensity : Rare events/Rare isotopes (actinides, p-nuclei)

: Less amount of enriched target materials

•Small $\Delta E/E$: Fine measurements of excitation function

: Enhanced S/N ratios

•Even-even nuclei (31)

^{74}Se, ^{78}Kr, ^{84}Sr, ^{92,94}Mo, ^{96,98}Ru, ^{102}Pd, ^{106,108}Cd, ^{112,114}Sn, ^{120}Te, ^{124,126}Xe, ^{130,132}Ba, ^{136,138}Ce, ^{144}Sm, ^{152}Gd, ^{156,158}Dy, ^{162,164}Er, ^{168}Yb, ^{174}Hf, ^{180}W, ^{184}Os, ^{190}Pt, ^{196}Hg

•Odd-A nuclei (2)

^{113}In, ^{115}Sn

•Odd-Odd nuclei (2)

^{138}La (0.09%), ^{180}Ta (0.012%)